# Editorial corner – a personal view
## Chemically modified flame retardant polymers

*A. Toldy**

Department of Polymer Engineering, Faculty of Mechanical Engineering, Budapest University of Technology and Economics, Műegyetem rkp. 3., Budapest H-1111, Hungary

The increased attention to safety requirements has accelerated the investigation of flame retardant plastics, but the proportion of flame retarded types among commercial polymers is still lower than desirable. Nevertheless, certain segments of the industry started to recognize the importance of flame retardancy. According to a market study the annual consumption of flame retardants is currently over 1.8 million tonnes, which is the equivalent of a sales volume of approx. 3 billion €. The total flame retardant (FR) market will continue to increase with average annual growth rate of 3.7%, which is due in part to the fact that the use of plastics in the past few years has increased significantly. FRs are also of increasing importance due to the growing miniaturization of electronic and electrical equipment, which may imply high power density and areas with excessive heat. The heat concentration and fire threat associated with this miniaturization needs novel FR solutions.

There exist two main approaches to achieve flame retardancy: the additive and the reactive approach. Lately the reactive type was given much attention, especially in case of polycondensation or polyaddition type polymers, where monomers can be exchanged by components possessing both functionality and flame retardant moiety in the same molecule. The reactive FRs have numerous advantages: they provide more stable effect, as they are chemically incorporated into the polymer structure, so they do not migrate to the matrix surface either during high temperature processing or application.

Due to these reasons less FR is needed to achieve same level of flame retardancy, which leads to reduction of toxic gas emission compared to the additive approach. Moreover, as they perform properly in low percentage, they do not influence considerably the properties of the matrix, which is a great advantage compared to the traditional FRs, such as metal-hydroxides. In addition, reactive FRs can be cost-effectively integrated in the production process, simply by replacing the original non-FR component; which is essential nowadays.

The sustainable development concept applied to this field implies that FRs should involve a low impact on health and environment during the entire life cycle including recycling and disposal. The increasing focus on these issues has drawn the attention to halogen-free additives, especially to phosphorous reactive FRs. Phosphorus can act both in gas phase, mainly at the beginning of degradation, and later on principally in solid phase as intumescent FR, providing an outstanding FR effect supported by this combined mechanism.



Dr. Andrea Toldy
Member of Executive Editorial Board

*Corresponding author, e-mail: atoldy@mail.bme.hu

# Physicochemical and electrochemical characterization of battery separator prepared by radiation induced grafting of acrylic acid onto microporous polypropylene membranes

*N. K. Goel[1*], Y. K. Bhardwaj[1], R. Manoharan[2], Virendra Kumar[1], K. A. Dubey[1], C. V. Chaudhari[1], S. Sabharwal[1]*

[1]Radiation Technology Development Section Bhabha Atomic Research Centre, Trombay Mumbai-400 085, India
[2]High Energy Batteries (India) Ltd., Mathur, Pudukottai, India

**Abstract.** Mutual radiation grafting technique was used to graft acrylic acid on micrometer thick micro-porous polypropylene membrane using high-energy gamma radiation. Grafting could not be achieved in aqueous acrylic acid solution. The presence of Mohr's salt effectively retarded the homopolymerization of acrylic acid but did not lead to grafting enhancement. Mohr's salt in presence of acids was found to be effective in enhancing the grafting yield. Contact angle measurement studies of the grafted and radiation treated polypropylene showed that initial grafting as well as radiation treatment of poly(propylene) in aqueous medium and in presence of Mohr's salt enhances its affinity towards the grafting solution. The enhancement in the polar component of surface energy of treated polypropylene membrane is the primary cause of grafting enhancement. The membranes grafted to an extent of ~20% were found to perform comparably with the battery separator presently being used by battery industry.

*Keywords: polymer membranes, radiation grafting, acrylic acid, contact angle, charge-discharge*

## 1. Introduction

Separator materials for alkaline batteries have received a great deal of attention in last five decades. It is mainly due to the desire to develop high energy per unit weight and volume battery packages that materials are still searched for better separator properties [1]. However because of complexity of inventing new functional materials, the present trend is of modifying existing polymers. The modification of polymers through graft co-polymerization offers an attractive path for introducing desirable properties in existing polymer for various polymer applications [2, 3]. Radiation induced grafting offers some unique advantages over the conventional chemical grafting method

since it results in uniform grafting and it is room a temperature process [4]. Radiation grafted co-polymers have been tried for a wide spectrum of applications like surface modification [5], separation purposes [6], biotechnology [7], electrochemical applications such as electro-dialysis [8], battery separator [9] and solid polymer electrolyte in fuel cells [10]. Ion exchange membranes have been investigated for their suitability as battery separator because of their durability, long life, high charge density and appreciable ion exchange capacity at optimum water content, which is the most desirable property of the separator membranes [11]. Radiation induced grafting of various monomers onto poly(propylene) (PP) by pre irradiation as well as

---

post irradiation method has been investigated to improve/introduce certain desired properties. Grafting of hydrophilic monomers onto PP has been of particular interest because of good strength, low cost and easy availability in different forms [12, 13]. The grafted product possesses a hydrophilic surface and is of good strength. These grafted hydrophilic membranes have found promising application in form of a battery separator, since they fulfill basic requirements of a battery separator namely presence of spontaneous, uniform and permanent wettable surface in order to accommodate and fully retain the aqueous electrolyte solution. Also, the battery separator should be dimensionally stable and should not swell or shrink significantly on introduction of the electrolytic solution [14].

In the present work mutual radiation grafting technique has been used to graft acrylic acid onto micrometer thick polypropylene sheet to induce optimum wettability on its surface. Effect of various experimental variables on grafting yield has been studied. The grafted membranes were characterized for their wettability and surface energy by dynamic contact angle measurement. The developed membranes were tested for their performance as separator under actual battery conditions.

## 2. Materials and methods

### 2.1. Materials

The polypropylene (PP) micro-porous films (porosity 38%, pore dimensions 0.02–0.20 microns), thickness 2.5 μm in sheet form was supplied by M/s High Energy Batteries Ltd., India. Acrylic acid monomer (purity > 99%) from Fluka was used as received. Mohr's salt and all other chemicals used were of AnalaR (purity > 99%) grade. Doubly distilled water was used for preparation of all solutions and Millipore-Q water (conductivity 0.05 μS·cm$^{-1}$) was used for contact angle studies. Gamma chambers GC-5000 having Co$^{60}$ gamma radiation source, supplied by M/s BRIT, India having dose rate of 5 kGy·hr$^{-1}$ as measured by Fricke dosimetry were used for irradiation purpose with suitable lead/steel attenuators.

### 2.2. Grafting of acrylic acid onto polypropylene

Grafting of acrylic acid (AA) onto polypropylene (PP) films was carried out by mutual radiation grafting technique. PP film of known weight was immersed in grafting solution of known composition in glass-stoppered bottles for an hour. The bottles containing PP, immersed in grafting solution were then irradiated in gamma chambers for required radiation doses. The homopolymer was removed from the grafted samples using water as an extractant by Soxhlet extraction for 8 hours. The grafted samples were vacuum dried at 50°C and stored in desiccator for further use. Grafting yield (G.Y.) was determined gravimetrically using Equation (1):

$$G.Y.[\%] = \left( \frac{\text{Weight after grafting} - \text{Initial weight}}{\text{Initial weight}} \right) 100 \tag{1}$$

### 2.3. Characterization of grafted PP membrane

Fourier transformed infrared spectroscopy (FTIR) measurements were performed on a FTIR spectrophotometer from JASCO, model FT/IR-610. Samples were thoroughly ground at liquid nitrogen temperature and mixed with KBr to prepare discs by compression under vacuum. FTIR spectra were obtained in the range from 400 to 4000 cm$^{-1}$ with a resolution of 4 cm$^{-1}$ and averaged over 100 scans.
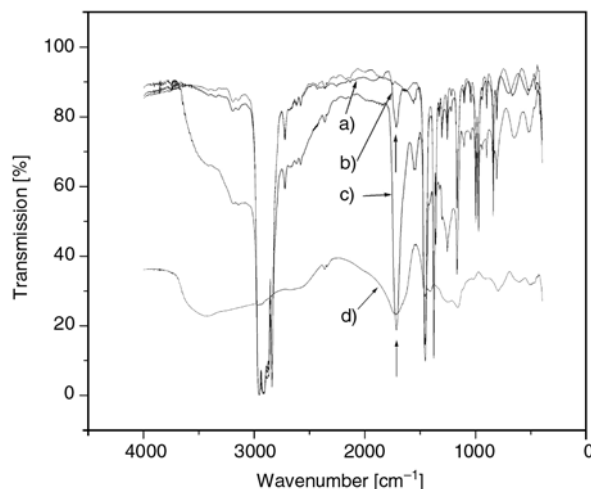


**Figure 1.** FTIR spectra of a) PP (b) PP grafted to an extent of 2% c) PP grafted to an extent of 8% d) polyacrylic acid

The absorption peaks corresponding to 2970, 2870, 1460, 1376 cm$^{-1}$ wave number were characteristic of –CH$_3$ and CH$_2$ groups in FTIR spectrum of PP as shown in Figure 1. The grafting of acrylic acid was established by well resolved absorption peak at 1760 cm$^{-1}$ which increased with extent of grafting (indicated by arrow in Figure 1)

The grafted PP films were characterized for their water uptake. The figures given in brackets on grafting profiles (to be described later in Figure 4) are the water uptake capacities at that grafting yield. The water uptake by grafted sheets was quite significant however there was a decrease in the water uptake capacity at higher grafting yield. The decrease in water uptake at higher grafting yield can be attributed to crosslinking of the grafted chains at higher radiation doses.

## 2.4. Wettability and surface energy analysis

The radiation-induced modification of surface was characterized by its wetting angle measurements. In this work, the Owens and Wendt method was used to determine the total surface energy and its resolution into polar and dispersive components [15], wherein the total solid surface tension γ was assumed to be of the general form as shown in Equation (2):

$$1 + \cos\theta = 2\sqrt{\gamma_s^d}\,\frac{\sqrt{\gamma_l^d}}{\gamma_l} + 2\sqrt{\gamma_s^p}\,\frac{\sqrt{\gamma_l^p}}{\gamma_l} \qquad (2)$$

In this equation, the subscripts *s* and *l* refer to the solid and liquid surface tension respectively; the superscripts *d* and *p* coincide with dispersive and polar components of total surface tension, where sum of these two values are equal to the total surface tension. The $\sqrt{\gamma_s^d}$ and $\sqrt{\gamma_s^p}$ are needed to be resolved. Therefore two independent contact angles were measured by two different liquids (water and diiodomethane) whose surface tension components are known.

The measurement of contact angles of the sample was carried out by sessile drop technique using image analysis software. A liquid droplet (1.5–2.5 µl) was allowed to fall on the samples to be studied from a software-controlled syringe. An image sequence was taken through a CCD camera of goniometer from GBX instruments, France which was connected to a PC computer and interfaced to image capture software (Windrop$^{++}$, GBX instruments).

## 3. Results and discussion

Radiation grafting is a function of many experimental variables such as dose, dose rate, ambient condition, monomer concentration, composition of grafting solution and properties of backbone material. Therefore, effect of various experimental parameters onto grafting yield was studied.

Initially grafting of acrylic acid (AA) on polypropylene (PP) was tried by irradiating PP film in presence of 15–100% AA [v/v] in aqueous medium. It was found that even at lowest concentration of 15% acrylic acid studied, the grafting solution turned to a soft, non-flowing gel at a dose of 2 kGy. The gel formation prevailed over the entire dose rate range 1.25–5 kGy·h$^{-1}$. Acrylic acid undergoes very fast homopolymerization and finally results in the formation of a crosslinked gel on irradiation in aqueous solution [16]. During homopolymer formation, some grafting would have taken place but it could not be determined as the PP film embedded in the gel got damaged during removal from the gel. In order to arrest the homopolymerization and enhance grafting yield, some established efficient homopolymer inhibitors in form of inorganic salts were tried. It has been reported that addition of certain metal salts to the reaction mixture suppresses the formation of homopolymer, thus leaving the monomer radicals free to take part in the grafting thereby reducing the homopolymer formation, increasing grafting and facilitating the retrieval of the resulting grafted copolymer [17, 18].

## 3.1. Radiation grafting in presence of homopolymerization inhibitor

Addition of certain inorganic salts suppresses the production of undesirable homopolymer during radiation induced grafting or redox grafting, thus leaving more monomer available for grafting and hence enhancing the grafting yield and facilitating easy retrieval of grafted product [19]. This has been attributed mainly to scavenging of OH radical (generated due to radiolysis of water in the bulk of the mixture) by metal ions (Equation (3)) thereby reducing the homopolymer formation in the bulk.
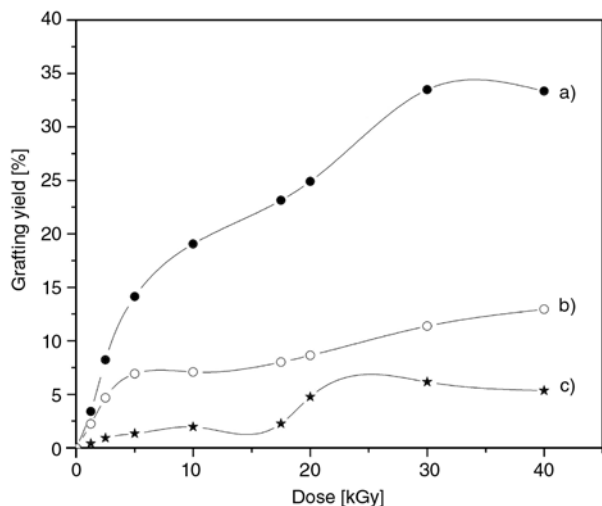
$$Fe^{2+} + {}^{\bullet}OH \rightarrow Fe^{3+} + OH^- \qquad (3)$$

**Figure 2.** Effect of homopolymer inhibitor salts on graft-
ing yield: salt concentration = 4% and acrylic
acid concentration = 20% in aqueous solution at
a dose rate of 5 kGy·h$^{-1}$
a) $FeSO_4 \cdot (NH_4)_2 SO_4 \cdot 6H_2O$ b) $CuSO_4$ c) $Cu_2SO_4$

In view of the works reported earlier, our grafting
was carried out initially in the presence of Ferrous
ammonium sulphate {$FeSO_4 \cdot (NH_4)_2 SO_4 \cdot 6H_2O$},
cupric sulphate ($CuSO_4$) and cuprous sulphate
($Cu_2SO_4$). Figure 2 shows effect of presence of
these salts as a function of irradiation dose. It is
clear from the results that Mohr's salt
{$FeSO_4 \cdot (NH_4)_2 SO_4 \cdot 6H_2O$} is most effective in
increasing the grafting. Therefore, further studies
were carried out at different concentrations of
Mohr's salt. Figure 3 shows the result of these stud-
ies. It was seen that grafting yield was maximum at
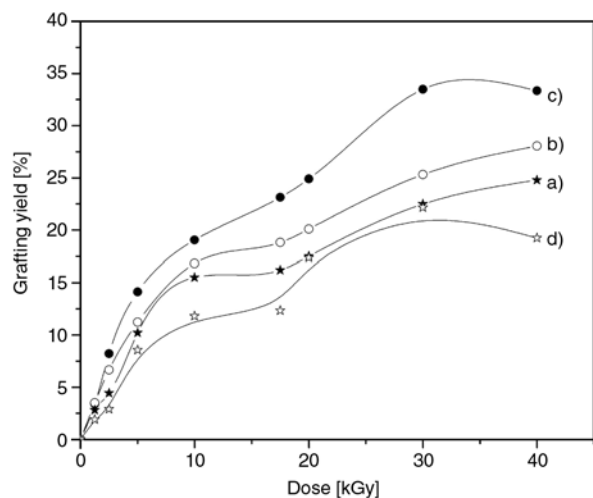salt concentration of 4%, at higher concentration

the grafting decreased. At Mohr's salt concentra-
tion > 4 grafting yield was low and there was no
significant change in the viscosity of the grafting
solution before and after irradiation indicating that
the homopolymerization as well as grafting was
severely hindered. It seems that the presence of
Mohr's salt in appropriate concentration decreases
homopolymerization reaction, which allows more
monomer to be available for grafting and hence
higher extent of grafting. Further grafting studies
were carried out at 4% Mohr's salt concentration.

## 3.2. Effect of dose rate on grafting

Figure 4 shows the grafting yield as a function of
radiation dose when the grafting was carried out in
20% AA + 4% $FeSO_4 \cdot (NH_4)_2 SO_4 \cdot 6H_2O$ aqueous
solution at different dose rates. The number of
grafted chains and chain lengths produced in
mutual grafting method is a function of total radia-
tion dose and the dose rate [20]. While the total
dose is a measure of total number of free radicals
generated on the trunk polymer, dose rate deter-
mines the rate of initiation of polymerization. As
expected, and shown in Figure 4, grafting yield
increased with radiation dose. However, it was
interesting to observe that the grafting yield
increased with dose rate also, unlike other grafting
systems reported [21, 22] where grafting has been
reported to decrease with the dose rate. Lower
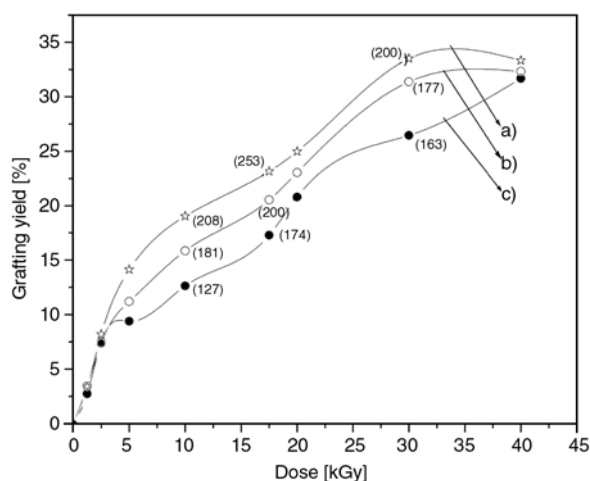grafting yields at higher dose rates have been attrib-



**Figure 3.** Effect of $FeSO_4 \cdot (NH_4)_2 SO_4 \cdot 6H_2O$ on grafting
yield in 20% AA solution at a dose rate of
5 kGy·h$^{-1}$ a) 0.5% b) 2% c) 4% d) 5%



**Figure 4.** Effect of dose rate on grafting yield when graft-
ing was carried out in 20% AA solution contain-
ing 4% $FeSO_4 \cdot (NH_4)_2 SO_4 \cdot 6H_2O$ a) 5 kGy·h$^{-1}$
b) 2.5 kGy·h$^{-1}$ c) 1.25 kGy·h$^{-1}$. Digits in brack-
ets: water uptake%.

uted earlier to energy deposition taking place predominantly in bulk of the solution, favoring homopolymerization of the monomer. The homopolymerization suppresses the grafting yields in two ways (i) the increased bulk viscosity restricts the diffusion of monomer from bulk to the reactive site thereby making the growing of chains at trunk polymer difficult (ii) due to the consumption of monomer in homopolymer formation, less monomer would be available for grafting reaction. Since here grafting was carried out in presence of homopolymerization inhibitor, there was no significant increase in the bulk viscosity therefore detrimental effect due to reason (i) above was not observed. Also, due to decrease in homopolymer formation more monomer was available to be grafted.

### 3.3. Effect of monomer concentration

The concentration of monomer to be grafted can be an important variable in extent of grafting. Therefore grafting was studied at three different concentrations. The results of these studies are shown in Figure 5. The grafting yield showed an increase when the concentration was increased from 10 to 20% of monomer. However there was no significant difference between 20 and 30% monomer concentration. Higher grafting yields are expected with increase in monomer concentration as, at any instant radicals generated on the backbone are able to interact with more monomer molecules. How-
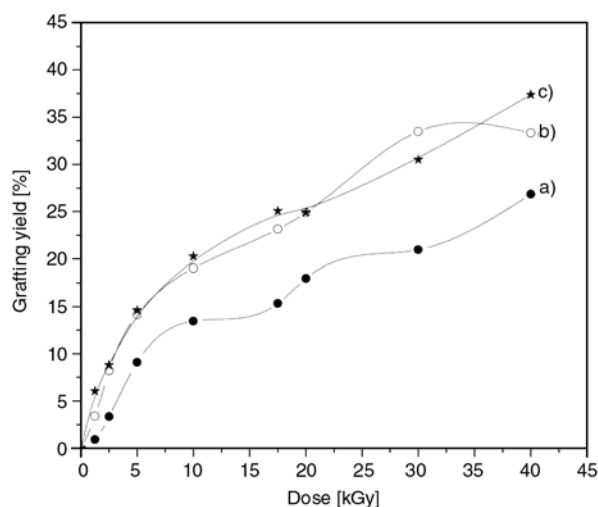


**Figure 5.** Effect of monomer concentration on grafting yield in 4% Mohr's salt solution a) 10% AA b) 20% AA c) 30% AA; 5 kGy·h$^{-1}$

ever, beyond certain monomer concentration, it seems that homopolymerization due to radicals generated in the bulk becomes predominant process and hence there is no significant increase in the grafting. Therefore, for further studies, concentration of monomer was fixed at 20% [v/v] to achieve high grafting levels and low homopolymer formation.

### 3.4. Effect of acid on grafting

Presence of additive like inorganic acid has been reported to enhance grafting by two ways [23, 24]. The presence of acid converts the radiolytically generated $e_{aq}^-$ into H, radical, which abstracts other H atoms from the backbone to generate more grafting sites on the polymer backbone as shown in Equations (4) and (5):

$$H^+ + e_{aq}^- \rightarrow {}^\bullet H \tag{4}$$

$$P{-}H + {}^\bullet H \rightarrow P^\bullet + H_2 \tag{5}$$

It has been postulated that the presence of acid improves the partition coefficient of the monomer between the polymer film and the bulk leading to an increase in local monomer concentration around the grafted growing chain thus increasing the grafting yield. Initially the grafting was studied in presence of acids without any Mohr's salt. This resulted in formation of soft cross-linked gel at a very low dose of 0.6 kGy and the grafted film could not be retrieved. This indicated that the polymerization of AA in aqueous solution was much faster in presence of acid. Further effect of acid on grafting was studied in presence of 4% Mohr's salt. Figure 6 shows the effect of presence of different acids on grafting yield. The grafting studies were tried in presence of HNO$_3$ also, however in presence of HNO$_3$ the grafting solution turned to crosslinked soft mass within few minutes of irradiation and grafting yield could not be determined. It is clear from Figure 6 that H$_2$SO$_4$ was most effective in improving the grafting yield, therefore further studies were carried out in presence of H$_2$SO$_4$. As shown in Figure 7, grafting increased with H$_2$SO$_4$ concentration in the concentration range studied. Therefore for further studies H$_2$SO$_4$ concentration of 0.5 mol·dm$^{-3}$ was fixed. In order to investigate the reason for increase in grafting yield in presence of acid, the uptake of grafting solution by backbone PP in presence of different acids was studied. It was
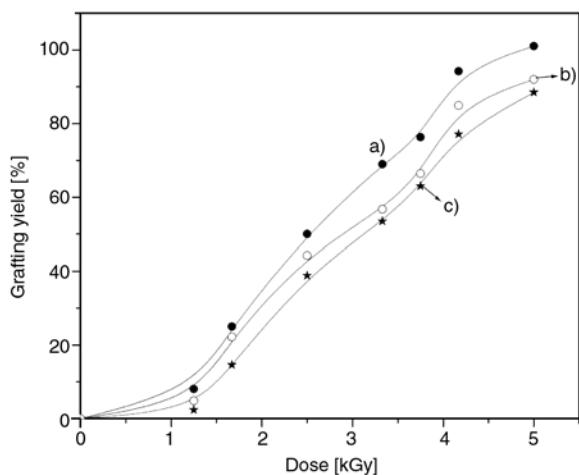
**Figure 6.** Effect of different acids on grafting yield in 20% AA solution in presence of 4% FeSO$_4$·(NH$_4$)$_2$SO$_4$·6H$_2$O at a dose rate of 5 kGy·h$^{-1}$ a) 0.5 mol·dm$^{-3}$ H$_2$SO$_4$ b) 0.5 mol·dm$^{-3}$ HClO$_4$ c) 0.5 mol·dm$^{-3}$ HCl
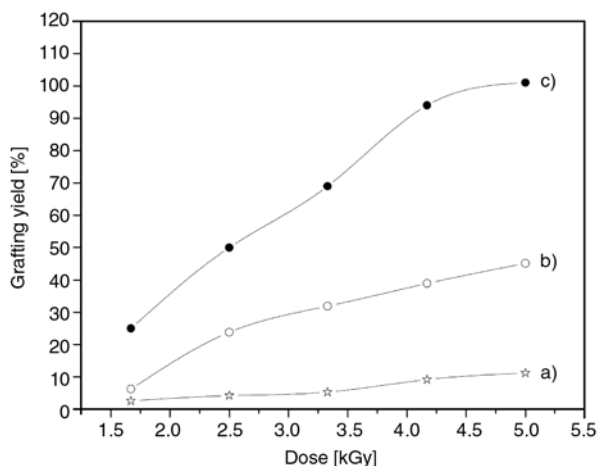


**Figure 7.** Effect of H$_2$SO$_4$ on grafting yield in 20% AA solution in presence of 4% FeSO$_4$·(NH$_4$)$_2$SO$_4$·6H$_2$O at a dose rate of 5 kGy·h$^{-1}$ a) 0.01 mol·dm$^{-3}$ H$_2$SO$_4$ b) 0.1 mol·dm$^{-3}$ H$_2$SO$_4$ c) 0.5 mol·dm$^{-3}$ H$_2$SO$_4$

seen that the backbone PP film did not swell in presence of acid even up to 2 mol·dm$^{-3}$ concentration of acid. This clearly indicated that as reported for other grafting systems [21, 22] where grafting enhancement was attributed to swelling of backbone in presence of solvent, enhancement in grafting in this study could not be any way assigned to swelling of PP due to grafting solution. Also, no swelling was observed for PP in 20% AA solution, 20% AA + 4% FeSO$_4$·(NH$_4$)$_2$SO$_4$·6H$_2$O solution and 20% AA + 4% FeSO$_4$·(NH$_4$)$_2$SO$_4$·6H$_2$O + 0.5 mol·dm$^{-3}$ solution.

## 3.5. Effect of ambience on grafting in presence and absence of acid

In order to study the effect of ambient on the grafting, grafting was carried out in 20% AA + 4% Mohr's salt solutions under three different ambient conditions (N$_2$ purged, aerated and O$_2$ saturated), at a dose rate of 3.2 kGy·h$^{-1}$. Results of this study, shown in Figure 8, indicate that effect of ambience on grafting yield was not significant. However when the grafting was carried out in presence of 0.5 mol·dm$^{-3}$ H$_2$SO$_4$ (all other conditions remaining the same) there was drastic effect of
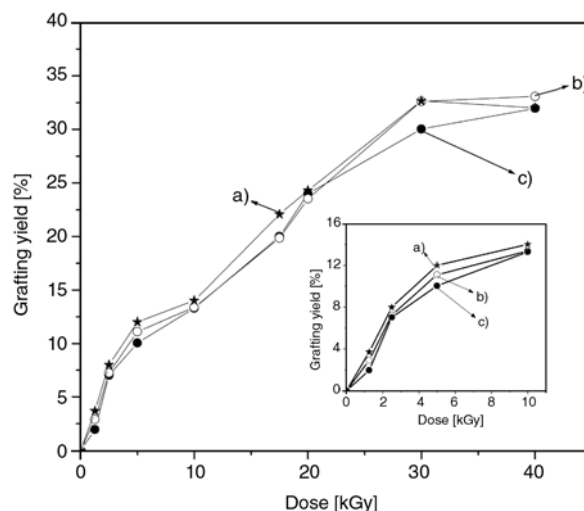


**Figure 8.** Effect of ambience on grafting yield in 20% AA + 4% Mohr's salt solution. Dose rate = 3.2 kGy·h$^{-1}$ a) de-aerated, b) aerated c) O$_2$ saturated. Inset: grafting yield at lower doses a) de-aerated b) aerated c) O$_2$ saturated.
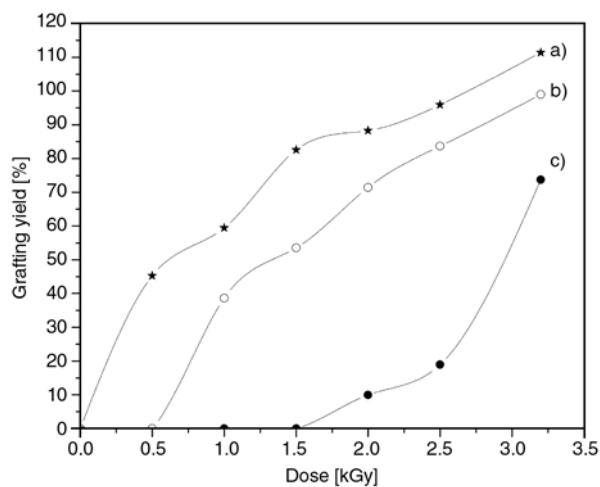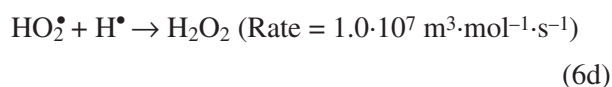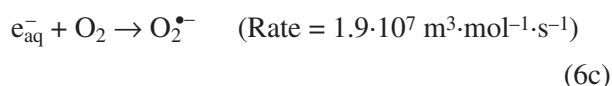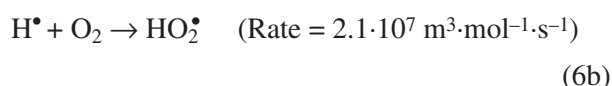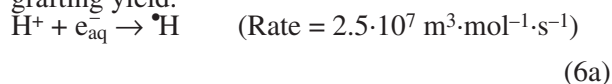


**Figure 9.** Effect of ambience on grafting yield in 20% AA + 4% Mohr's salt + 0.5 mol·dm$^{-3}$ H$_2$SO$_4$. Dose rate = 3.2 kGy·h$^{-1}$ a) de-aerated b) aerated c) O$_2$ saturated.

ambience as shown in Figure 9. We may suppose that in presence of acid all available $e_{aq}^-$ are converted to H radical in accordance with Equation (6a). Under aerated/oxygenated condition the H radicals efficiently react with available $O_2$ to form $HO_2^{\bullet}$ (Equation (6b)) whereas in absence of acid $e_{aq}^-$ reacts with $O_2$ to form superoxide anion ($O_2^{\bullet-}$) (Equation (6c)). $HO_2$ radical is known to undergo abstraction reaction with organic molecules (Equation (6d)) [25]. Thus $HO_2^{\bullet}$ through H abstraction reaction with backbone may generate grafting sites on backbone thereby contributing to increase in grafting yield. On the other hand the superoxide anion (Equation (6e)) is known to undergo very slow abstraction reaction and hence may not contribute significantly to increase in grafting yield.

$$H^+ + e_{aq}^- \rightarrow {}^{\bullet}H \qquad (\text{Rate} = 2.5 \cdot 10^7 \text{ m}^3 \cdot \text{mol}^{-1} \cdot \text{s}^{-1})$$
(6a)

$$H^{\bullet} + O_2 \rightarrow HO_2^{\bullet} \qquad (\text{Rate} = 2.1 \cdot 10^7 \text{ m}^3 \cdot \text{mol}^{-1} \cdot \text{s}^{-1})$$
(6b)

$$e_{aq}^- + O_2 \rightarrow O_2^{\bullet-} \qquad (\text{Rate} = 1.9 \cdot 10^7 \text{ m}^3 \cdot \text{mol}^{-1} \cdot \text{s}^{-1})$$
(6c)

$$HO_2^{\bullet} + H^{\bullet} \rightarrow H_2O_2 \, (\text{Rate} = 1.0 \cdot 10^7 \text{ m}^3 \cdot \text{mol}^{-1} \cdot \text{s}^{-1})$$
(6d)

$$O_2^{\bullet-} + H^{\bullet} \rightarrow \qquad (\text{Rate} \sim \text{very slow})$$
(6e)

## 3.6. Surface wettability studies of grafted surfaces

From the studies discussed above two important observations were made (i) The presence of Mohr's salt does not allow the viscosity of the bulk solution to increase and (ii) changes in the composition of grafting solutions had little effect on swelling of PP. Thus it would be worth investigating whether the availability of more monomer during grafting process was the sole reason for grafting enhancement, or did the affinity of PP increased for grafting solution as the grafting process progressed. To address this question affinity of PP for grafting solution was investigated by contact angle measurement. PP irradiated under different conditions namely in water, in 4% $FeSO_4 \cdot (NH_4)_2SO_4 \cdot 6H_2O$, in 0.5 mol·dm$^{-3}$ $H_2SO_4$, in 4% $FeSO_4 \cdot (NH_4)_2SO_4 \cdot 6H_2O$ + 0.5 mol·dm$^{-3}$ $H_2SO_4$ and grafted to different extent with AA were examined for their wettability against the grafting solution (20% AA +

4% $FeSO_4 \cdot (NH_4)_2SO_4 \cdot 6H_2O$ + 0.5 mol·dm$^{-3}$ $H_2SO_4$ in aqueous medium). Figure 10 shows the photographs recorded immediately after drops of solution were allowed to fall on PP. Figure 11 shows the change in contact angle with time. It is clearly visible from the photographs that contact angle decreases as the extent of grafting increase in the range 0–26.2% (Figures 10a–10c). Even at grafting yield as low as 0.99% of AA there was significant decrease in contact angle from 72 to 52°. Poly(acrylic acid) is insoluble in its monomer acrylic acid [23] but is soluble in water. It seems the covalently grafted and growing poly(acrylic acid) chains are more easily able to interact with the acrylic acid around when they are in extended, opened up state in grafting mixture due to their affinity for water and contribute to grafting enhancement. Similar increase in grafting yield in presence of suitable common solvent for polymer and monomer has been reported for other systems by us earlier [24, 26]. It is well known that irradiation of polymers under aerated conditions leads to generation of several functional groups on the surface which alter the surface energy and hence the wettability [27]. In order to probe any enhancement
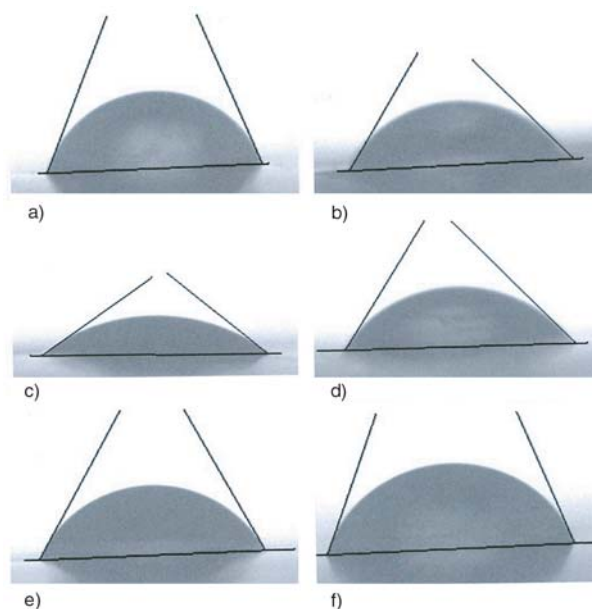


**Figure 10.** Initial contact angle of different PP surfaces for grafting solution (20% AA + 4% $FeSO_4 \cdot (NH_4)_2SO_4 \cdot 6H_2O$ + 0.5 mol·dm$^{-3}$ $H_2SO_4$) a) un-grafted PP b) PP grafted to an extent of 0.99% c) PP grafted to an extent of 26.2% d) PP irradiated in aqueous medium e) PP irradiated in 4% Mohr's salt f) PP irradiated in 0.5 mol·dm$^{-3}$ $H_2SO_4$
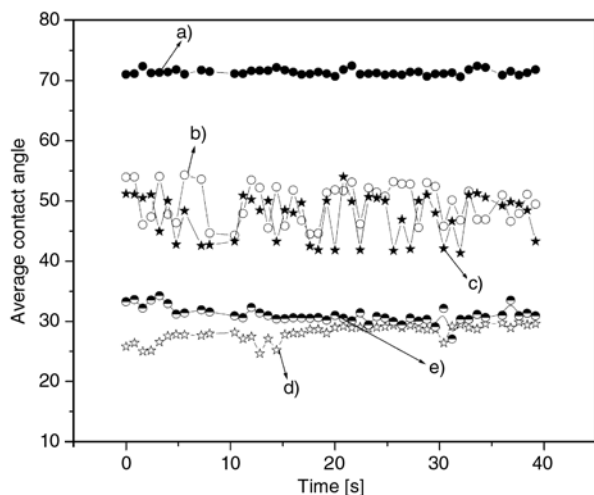
**Figure 11.** Change in contact angle with time against the grafting solution (20% AA + 4% FeSO$_4$·(NH$_4$)$_2$SO$_4$·6H$_2$O + 0.5 mol·dm$^{-3}$ H$_2$SO$_4$) for PP grafted to different extents a) un-grafted PP b) PP grafted to an extent of 0.99% c) PP grafted to an extent of 8% d) PP grafted to an extent of 16.6% e) PP grafted to an extent of 26.2%

of grafting due to irradiation in water, FeSO$_4$·(NH$_4$)$_2$SO$_4$·6H$_2$O, H$_2$SO$_4$ or FeSO$_4$·(NH$_4$)$_2$SO$_4$·6H$_2$O + H$_2$SO$_4$ the PP was irradiated in these separately for same dose as for grafting. The PP irradiated under different conditions (total dose = 0.8 kGy) was studied for its contact angle analysis against the grafting solution. Fig-
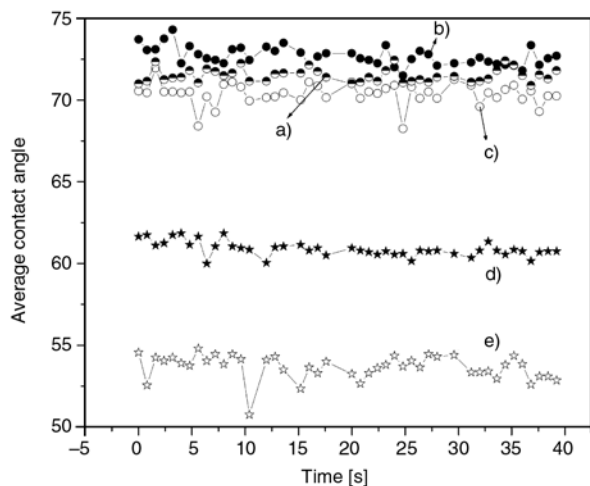


**Figure 12.** Change in contact angle with time against the grafting solution (20% AA + 4% FeSO$_4$·(NH$_4$)$_2$SO$_4$·6H$_2$O + 0.5 mol·dm$^{-3}$ H$_2$SO$_4$) for PP initially irradiated (total dose = 0.8 kGy) under different conditions a) un-grafted PP b) 0.5 mol·dm$^{-3}$ H$_2$SO$_4$ c) 4% FeSO$_4$·(NH$_4$)$_2$SO$_4$·6H$_2$O + 0.5 mol·dm$^{-3}$ H$_2$SO$_4$ d) 4% FeSO$_4$·(NH$_4$)$_2$SO$_4$·6H$_2$O e) water

ures 11 and 12 show the results of these studies. Comparing Figures 10a–10e and Figure 12 it is clear that irradiation in presence of water and other additives enhance the affinity for grafting solution to different extents. However in presence of acid alone or in combination with Mohr's salt there is no enhanced affinity for the grafting solution i.e. presence of sulphuric acid in the medium does not as such contribute to affinity of PP for grafting solution. Though the presence of acid may enhance grafting in accordance with Equation (4) or some way in which presence of AA in protonated state favours grafting in comparison to it being in deprotonated state. In order to substantiate our explanation given above the grafting of pre-grafted and pre-treated PP was studied at very low doses. Figure 13 shows results of these studies. As is clear from the figure the pre-treatment prior to grafting contributed significantly to grafting enhancement. However at present it is difficult to explain the grafting enhancement even for PP initially irradiated in sulphuric acid, as these membranes did not show any decrease in contact angle i.e. enhance affinity for grafting solution.

The increase in polar component of the similar polymer surfaces on plasma or conventional grafting of suitable monomers has been reported earlier [28, 29]. Efforts were made to estimate the change in the surface energy and resolve different components of surface energy of PP on grafting and also after irradiating PP under different conditions.
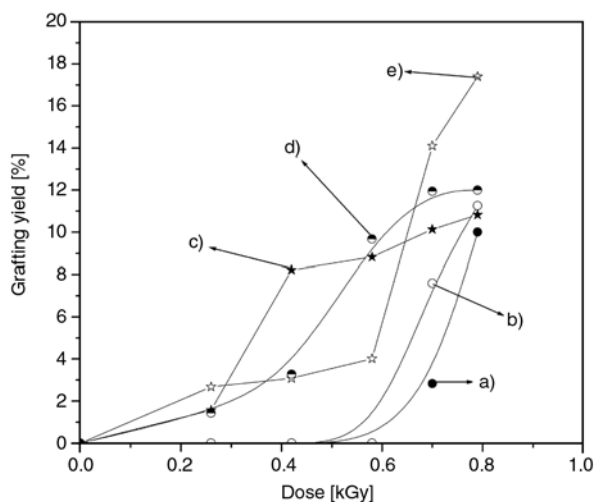


**Figure 13.** Grafting of PP treated initially under different conditions a) untreated b) grafted to an extent of 0.99% c) irradiated in water d) irradiated in 0.5 mol·dm$^{-3}$ H$_2$SO$_4$ e) irradiated in 4% Mohr's salt. Dose rate = 3.2 kGy·h$^{-1}$.

**Table 1.** The properties of liquids used for surface energy determination at 20°C

| Liquid | Surface tension [mN/m] | | |
|---|---|---|---|
| | $\gamma_1$ | $\gamma_1^d$ | $\gamma_1^p$ |
| Water | 68.9 | 18.6 | 50.3 |
| Diiodomethane | 49.7 | 48.0 | 1.7 |

Water and diiodomethane were used as test liquids for determination of surface energy of the samples. Tables 1 and 2 give the properties of the liquid used and the surface energy estimated for different samples. It is clear from the values in Table 2 that the grafting of AA enhances the total energy with substantial increase in the polar component. Slight increase in the polar component was also seen for the PP samples initially irradiated in different solutions. It is clear from these surface energy estimation and the results of Figure 13 that grafting enhancement under certain conditions is due to *in-situ* increase in the polar component of surface energy during irradiation. The increase of the polar component contributes to the enhanced affinity for the grafting solutions, which is reflected in decrease in the contact angle and enhanced grafting.

## 3.7. Performance of grafted PP membranes under actual battery conditions

The developed AA grafted PP sheet was tested for its performance under actual battery conditions related to the battery separator membrane presently used by Indian battery industry. For testing the grafted samples, the samples grafted to different extent were put in one Ni/2Cd electrode cells and soaked with KOH electrolyte. All the cells were subject to C/5 charging and 1C rate discharging. Those samples, which enabled the cells to pass 60 minutes of discharging, were considered to be working satisfactorily. Samples grafted to different extents were tested. Figures 14 and 15 show the results of some of the samples. It was seen that
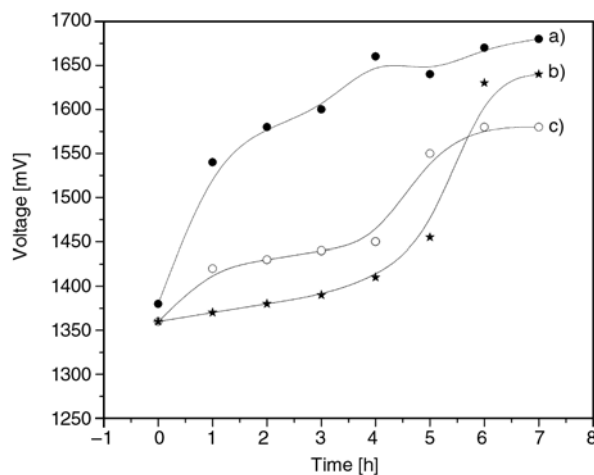


**Figure 14.** Performance of grafted membranes during charging a) PP grafted to an extent of 20% b) presently being used commercial membrane c) PP grafted to an extent of 10%
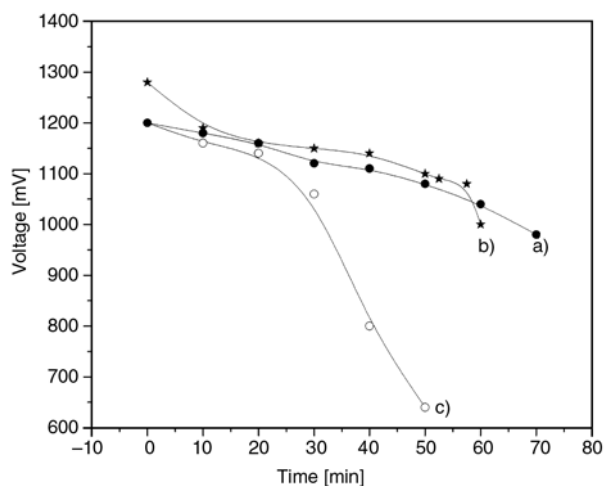


**Figure 15.** Performance of grafted membranes during discharging (a) PP grafted to an extent of 20% b) presently being used commercial membrane c) PP grafted to an extent of 10%

samples grafted to extent of 10% did not give satisfactory results. The samples grafted to extent >20% only gave satisfactory results. The sample grafted to an extent of 21% was also used for a fuel cell consisting of 17 Ni and 16 Cd electrodes. The performance was comparable with the cell assembled

**Table 2.** Surface energy of samples

| Sample | Surface energy [mJ/m²] | | |
|---|---|---|---|
| | Total energy | Polar component | Dispersive component |
| Ungrafted PP | 33.7 | 2.8 | 30.9 |
| PP grafted to an extent of 0.99% | 48.9 | 15.0 | 33.9 |
| PP grafted to an extent of 26.2% | 45.9 | 14.1 | 31.8 |
| PP irradiated in 4% Mohr's salt solution | 29.1 | 4.7 | 24.4 |
| PP irradiated in water | 33.5 | 3.3 | 30.2 |
| PP irradiated in 0.5 mol·dm⁻³ H₂SO₄ | 34.2 | 7.0 | 27.2 |

using battery separator presently used by the industry. The actual testing results indicated that grafting not only converts the hydrophobic PP into battery active hydrophilic state but also helps to retain the hydrophilic state over longer storage period, which is a necessity for Ni-Cd batteries.

## 4. Conclusions

AA grafted PP micrometer thick, micro-porous membrane has been successfully prepared by mutual radiation grafting technique. The grafting yield was found to be a function of experimental variables like dose, dose rate, ambience of grafting and the composition of grafting solution. The presence of acid in the grafting solution was found to enhance the grafting yield by many folds. The contact angle analysis of grafted product established that initial grafting enhances the wettability of the PP membrane and thus helps in grafting at latter stages. The prior radiation treatment of PP under suitable conditions also contributed to enhanced grafting. The membrane having grafting yield of 20% was found to perform comparably with the separator presently being employed by the industry with an added advantage of retaining the hydrophilic state over longer storage period.

## Acknowledgements

## References

[1] Arora P., Zhang Z.: Battery separators. Chemical Reviews, **104**, 4419–4462 (2004).
DOI: 10.1021/cr020738u

[2] Guthrie J. T.: Development in radiation induced graft polymerization to cellulosics. Polymer, **16**, 134–150 (1975).
DOI: 10.1016/0032-3861(75)90142-1

[3] Kabanov V. Y., Aliev R. E., Kudriayatsev V. N.: Present status and development trends of radiation induced graft polymerization. Radiation Physics and Chemistry, **37**, 175–192 (1991).

[4] Garnett J. L.: Grafting. Radiation Physics and Chemistry, **14**, 79–99 (1979).
DOI: 10.1016/0146-5724(79)90014-1

[5] Khan M. S., Lehmann D., Heinrich G.: Modification of PTFE nanopowder by controlled electron beam irradiation: A useful approach for development of PTFE coupled EPDM compounds. Express Polymer Letters, **2**, 284–293 (2008).
DOI: 10.3144/expresspolymlett.2008.34

[6] Matsumoto H., Koyama Y., Taniaoka A.: Interaction of proteins with weak amphoteric charged membrane surfaces: Effect of pH. Journal of Colloid and Interface Science, **264**, 82–88 (2003).
DOI: 10.1016/S0021-9797(03)00417-X

[7] Gupta B., Anjum N.: Preparation of ion-exchange membranes by the hydrolysis of radiation-grafted polyethylene-g-polyacrylamide films: Properties and metal-ion separation. Journal of Applied Polymer Science, **90**, 3747–3752 (2003).
DOI: 10.1002/app.12940

[8] El-Boohy H. A., Badr G.: Radiation grafting of 4-vinylpyridine onto poly-tetrafluoroethylene-perfluorovinylether (TFA) and poly-tetrafluoroethylene-polyethylene (ET) films. Journal of Radioanalytical and Nuclear Chemistry, **230**, 121–127 (1998).
DOI: 10.1007/BF02387457

[9] Kritzer P., Cook J. A.: Nonwovens as separators for alkaline batteries. Journal of the Electrochemical Society, **154**, A481–A494 (2007).
DOI: 10.1149/1.2711064

[10] Villaluenga J., Seoane B., Barragán V., Ruiz Banzá C.: Permeation of electrolyte water-methanol solutions through a Nafion membrane. Journal of Colloid and Interface Science, **268**, 476–481 (2003).
DOI: 10.1016/S0021-9797(03)00585-X

[11] Gupta B., Anjum N., Jain R., Revagade N., Singh H.: Development of membranes by radiation-induced graft polymerization of monomers onto polyethylene films. Journal of Macromolecular Science Part C, Polymer Review, **44**, 275–309 (2004).
DOI: 10.1081/MC-200029334

[12] Mazzei R., Tadey D., Smolko E., Rocco C.: Radiation grafting of different monomers onto PP foils irradiated with a 25 MeV proton beam. Nuclear Instruments and Methods in Physics Research Section B: Beam Interactions with Materials and Atoms, **208**, 411–415 (2003).
DOI: 10.1016/S0168-583X(03)00621-9

[13] Fasce L. A., Costamagna V., Pettarin V., Strumia M., Frontini P. M.: Poly(acrylic acid) surface grafted polypropylene films: Near surface and bulk mechanical response. Express Polymer Letters, **2**, 779–790, (2008).
DOI: 10.3144/expresspolymlett.2008.91

[14] Zhang S. S.: A review on the separators of liquid electrolyte Li-ion batteries. Journal of Power Sources, **164**, 351–364 (2007).
DOI: 10.1016/j.jpowsour.2006.10.065

[15] Thomas S. P., Thomas S., Abraham R., Bandyopadhyay S.: Polystyrene/calcium phosphate nanocomposites: Contact angle studies based on water and methylene iodide. Express Polymer Letters, **2**, 528–538 (2008).
DOI: 10.3144/expresspolymlett.2008.63

[16] Bhardwaj Y. K., Sabharwal S., Majali A. B.: Dynamic swelling kinetics of radiation polymerised poly(2-hydroxy ethyl methacrylate) and 2-hydroxy ethyl methacrylate-co-ionic hydrogels- Part I: Swelling in aqueous solution. Journal of Polymer Materials, **17**, 239–248 252 (2000).

[17] Gargan K., Kronfli E., Lovell K. V.: Pre-irradiation grafting of hydrophilic monomers onto polyethylene-1. The influence of homopolymerization inhibitors. Radiation Physics and Chemistry, **36**, 757–761 (1990).
DOI: 10.1016/1359-0197(90)90174-G

[18] Grushevskaya L. N., Aliev R. E., Kabanov V. Y.: Radiation-induced graft polymerization of acrylamide and acrylic acid onto polyethylene. Radiation Physics and Chemistry, **36**, 475–479 (1990).
DOI: 10.1016/1359-0197(90)90036-H

[19] O'Nell T.: Grafting of acrylic acid onto radiation-peroxidised polypropylene film in the presence of ferrous ions. Journal of Polymer Science Part A-1: Polymer Chemistry, **10**, 569–580 (1972).
DOI: 10.1002/pol.1972.150100221

[20] Chapiro A.: Radiation chemistry of polymeric systems. John Wiley and Sons, New York (1962).

[21] Chaudhari C. V., Bhardwaj Y. K., Sabharwal S.: Radiation grafting of methyl methacrylate on radiation crosslinked natural rubber film: Part I: Grafting conditions and grafting yield. Journal of Radioanalytical and Nuclear Chemistry, **267**, 113–119 (2006).
DOI: 10.1007/s10967-006-0016-x

[22] Virendra Kumar, Bhardwaj Y. K., Rawat K. P., Sabharwal S.: Radiation induced grafting of vinylbenzyltrimethylammmonium chloride (VBT) onto cotton fabric and study of its anti-bacterial activities. Radiation Physics and Chemistry, **73**, 175–182 (2005).
DOI: 10.1016/j.radphyschem.2004.08.011

[23] Gowariker V. R., Viswanathan N. V., Sreedhar J.: Polymer science. New Age International Publishers, New Delhi (2001).

[24] Chaudhari C. V., Dubey K. A., Bhardwaj Y. K., Virendra Kumar, Goel N. K., Sabharwal S.: Radiation grafting of acrylonitrile on ethylene-propylene diene terpolymer rubber: Optimization of grafting parameters and oil resistance properties. Journal of Radioanalytical and Nuclear Chemistry, **278**, 47–53 (2008).
DOI: 10.1007/s10967-007-7152-9

[25] Spinks J. W. T., Woods R. J.: Ion, excited molecules and free radicals. in 'An introduction to radiation chemistry' (eds. Spinks J. W. T., Woods R. J.) Wiley, New York, 280–282 (1990).

[26] Virendra Kumar, Bhardwaj Y. K., Dubey K. A., Chaudhari C. V., Goel N. K., Biswal J., Sabharwal S., Tirumalesh K.: Electron beam grafted polymer adsorbent for removal of heavy metal ion from aqueous solution. Separation Science and Technology, **41**, 3123–3140 (2006).
DOI: 10.1080/01496390600851673

[27] Ruiyu W., Ha H., Wang Y., Zhao W., Sha Y., Jin C., Wang G., Wu J.: Study on oxidation of polymers treated by high LET radiation. Radiation Physics and Chemistry, **52**, 251–256 (1998).
DOI: 10.1016/S0969-806X(98)00150-9

[28] Bhattacharya A., Mishra B. N.: Grafting: A versatile means to modify polymers: Techniques, factors and applications. Progress in Polymer Science, **29**, 767–814 (2004).
DOI: 10.1016/j.progpolymsci.2004.05.002

[29] Elvira C., Yi F., Azevedo M. C., Rebouta L., Cunha A. M., Román J. S., Reis R. L.: Plasma and chemical-induced graft polymerization on the surface of starch-based biomaterials aimed at improving cell adhesion and proliferation. Journal of Material Science: Materials in Medicine, **14**, 187–194 (2003).

# Synthesis of porous poly(acrylamide) hydrogels using calcium carbonate and its application for slow release of potassium nitrate

*G. R. Mahdavinia[1*], S. B. Mousavi[2], F. Karimi[3], G. B. Marandi[4], H. Garabaghi[1], S. Shahabvand[3]*

[1]Department of Chemistry, Faculty of Science, University of Maragheh, P.O. Box 55181-83111, Maragheh, Iran
[2]Department of Soil Science, Faculty of Agriculture, University of Maragheh, P.O. Box 55181-83111, Maragheh eh, Iran
[3]Department of Biotechnology, Faculty of Science, University of Maragheh, P.O. Box 55181-83111, Maragheh eh, Iran
[4]Department of Chemistry, Islamic Azad University, Karaj Branch, P. O. Box 31485-313, Karaj, Iran

**Abstract.** Porous poly(acrylamide) was synthesized using calcium carbonate microparticles and subsequent acid treatment to remove the calcium carbonate. Methylenebisacrylamide and ammonium persulfate/sodium metabisulfite were used as crosslinking agent and redox initiator, respectively. The porous structure of resulted hydrogels was confirmed using SEM micrographs. The effect of methylenebisacrylamide concentration and calcium carbonate amount on the swelling of the hydrogels was investigated. The results showed that the effect of methylenebisacrylamide and calcium carbonate variables on the swelling is reverse. The hydrogels were subsequently utilized for the loading of potassium nitrate. Potassium nitrate as active agent was loaded into hydrogels and subsequently the release of this active agent was investigated. In these series of investigation, the effect of content of loading, methylenebisacrylamide and calcium carbonate amount on the release of potassium nitrate from hydrogels was investigated.

*Keywords: polymer gels, porous polyacrylamide, swelling, slow release, potassium nitrate*

## 1. Introduction

Hydrogels are three-dimensional hydrophilic polymer networks capable of imbibing large amount of water [1]. For this reason they have been used widely in the field of drug delivery, immobilization of enzymes, dewatering of protein solutions, solute separation, baby diapers, soil for agriculture and horticulture, water-blocking tapes, absorbent pads, and numerous other applications [2–8]. High swelling rate is an important property of hydrogels. They mainly need several hours to reach maximum absorption capacity. The slow swelling of dried hydrogels is due to the slow diffusion of water into the glassy matrix of the dried hydrogels [9]. Chen and Park developed a new kind of superabsorbent

polymers, so called superporous hydrogels [10]. There are several well known methods to prepare porous hydrogels, including phase separation, foaming technique, emulsion-template synthesis, and particulate leaching and freeze-drying [11, 12]. Poly(acrylamide) (PAAm) is an important and hydrophilic polymer for preparation of hydrogels [13]. The common method to synthesis of PAAm hydrogels is the free radical crosslinking copolymerization of AAm monomer with multifunctional vinyl monomers [13]. PAAm hydrogels and their derivatives are the subject of many studies [14, 15]. PAAm hydrogels have proven capability of water absorption and biocompatibility with physiologic body fluids. The application of PAAm hydrogels in

---

*Corresponding author, e-mail: grmnia@mhec.ac.ir

controlled release of agrochemicals and bioactive have been investigated [16, 17]. Researchers have been reported porous PAAm hydrogels [18–20]. Synthesizing porous hydrogels using solution polymerization method in the presence of porogen (that produce gas bubbles from reaction of porogen with chemicals) is a difficult task, because produced gas bubbles from porogen leave the solution easily. The main aim of this work was to synthesize porous PAAm hydrogels through solution polymerization and its application to slow release of agrochemicals. To the best of our knowledge, there have been no previous reports on using the calcium carbonate for synthesis of porous PAAm hydrogel. The leaching of calcium carbonate and subsequently evolving of $CO_2$ gas from hydrogel matrix results in porous structure. Potassium nitrate, an agrochemical agent was loaded in the hydrogels and the release of this active agent in deionized water was studied.

## 2. Experimental

### 2.1. Materials

Acrylamide (AAm, Merck Co.) was used after crystallization from acetone. Methylenebisacrylamide (MBA, Fluka Co.), ammonium persulfate (APS, Fluka Co.), and sodium metabisulfite (SMBS, Fluka Co.) were used as received. Calcium carbonate (CCb ~3 µm, Fluka Co.), and other chemicals were used as received.

### 2.2. Synthesis of PAAm hydrogel

AAm solution was prepared in a one-liter reactor equipped with mechanical stirrer and gas inlet. AAm was dissolved in degassed distilled water. Reaction variables are given in Table 1. In general, AAm (3.0 g, 42 mmol) was dissolved in 30.0 ml of distilled degassed water. MBA as a crosslinker (0.050 g in 2 ml water, 0.32 mmol) was added to

the AAm solution and the mixture was continuously stirred under nitrogen gas. Various amounts of calcium carbonate powder (1.5, 3 and 6 g) were added to the reaction mixture and allowed to stir for 10 min. Then APS (0.05 g dissolved in 2 ml water, 0.22 mmol) and SMBS (0.05 g dissolved in 2 ml water, 0.26 mmol) as a redox initiator were added to the solution and stirred for 30 min. Obtained hydrogels in bulk state were cut in similar pieces (~2×2×2 mm). Subsequently, the calcium carbonate particles were dissolved in the aqueous 10% wt HCl solution by immersion of hydrogels for 24 h at ambient temperature. For removing the calcium chloride from dissolution of calcium carbonate and other remained substrates, the hydrogels were immersed in excess amount of deionized water for 6 days with daily refreshment of the water. In order to assure the complete removal of $Ca^{2+}$ and $Cl^-$ ions, $CO_3^{2-}$ and $Ag^+$ ions were used, respectively; in which lack of any precipitation was attributed to a complete removal. After this time, the hydrogels were poured to 300 ml ethanol. After dewatering for 24 h, the hardened hydrogel products were filtered, washed with fresh ethanol (2×50 ml) and dried at 50°C until obtaining a constant weight.

### 2.3. Bulk density measurement

Bulk density of dried hydrogels was determined by using picnometric method outlined in ASTM D792. In general, 1 g of dried hydrogels was placed in a 10 ml picnometer with known weight. Then the picnometer containing sample was filled with acetone as non-solvent and picnometer containing sample and acetone weighed to determine the density of sample according to standard method.

### 2.4. Swelling studies

Dried hydrogel pieces were used to determine the degree of swelling. The degree of swelling (*DS*)

**Table 1.** Amount of reaction parameters for synthesis of porous hydrogels ($H_2O$ 40 ml, APS/SMBS 0.22/0.26 mmol)

| Run | AAm [mmol] | MBA [mmol] | CaCO₃ [g] | DS [g/g] | loaded of PN [%] |
|------|-----------|-----------|-----------|----------|------------------|
| SP1 | 42 | 0.32 | 0.0 | 24 | 28.0 |
| SP2 | 42 | 0.32 | 1.5 | 28 | – |
| SP3 | 42 | 0.32 | 3.0 | 34 | 58.0 |
| SP4 | 42 | 0.32 | 6.0 | 44 | 78.0 |
| MBA1 | 42 | 0.16 | 3.0 | 41 | 61.7 |
| MBA2 | 42 | 0.32 | 3.0 | 34 | 56.1 |
| MBA3 | 42 | 0.65 | 3.0 | 17 | 30.0 |

was determined by immersing the hydrogels (0.1 g) in distilled water (100 ml) and was allowed to soak for 24 h at room temperature. After this time, they were removed from the water, blotted with filter paper to remove surface water, weighed and the *DS* was calculated using Equation (1):

$$DS = \frac{W_s - W_d}{W_d} \qquad (1)$$

where $W_s$ and $W_d$ are the weights of the samples swollen in water and in dry state, respectively. For studying the swelling kinetics of the hydrogels, a certain amount of samples (0.20 g) was poured into numbers of weighed tea bags and was immersed in 200 ml distilled water. At consecutive time intervals, the water absorbency of the hydrogels was measured according to the above method.

## 2.5. Loading/release of potassium nitrate

The potassium nitrate (PN) was dissolved in 25 ml deionized water with desired concentration (1% wt of PN for all samples, but in the series of effect of %loading on the release of PN, 0.5, 1 and 2% wt of PN solution was used). Pre-weighed dried and purified hydrogel pieces (0.1 g) were immersed in it for 24 h at room temperature. After withdrawing the loaded hydrogels, the volume of the remained PN solutions was filled to 25 ml and according to conductivity of these diluted solutions and calibration curve, the amount of loaded PN was calculated. Loaded hydrogels were filtered and dried in an oven at 40°C for constant weight. The milligram of loaded PN in hydrogels was calculated using calibration curve. The amounts of loaded PN in hydrogels were given in Table 1. For study the release of PN, deionized water was chosen as a release medium. In general, dried $KNO_3$ loaded hydrogels were immersed in 100 ml deionized water under un-stirred condition. At intervals, the amount of PN

released was evaluated using conductometer. The released PN was determined from the calibration curve.

## 2.6. Instruments

The surface morphology of the hydrogels was examined using scanning electron microscopy (SEM). The purified hydrogels were dewatered and dried at 40°C. The dried hydrogels were grinded and sieved to obtain 40–60 mesh. Dried hydrogel powder with 40–60 mesh size were coated with a thin layer of palladium gold alloy and imaged in a SEM instrument (Leo, 1455 VP). A conductivity meter (HANNAN, HI 8819N) was used to study of release of potassium nitrate.

## 3. Results and discussions

## 3.1. Synthesis and characterization

The aim of this study was to produce a porous crosslinked-PAAm hydrogel under solution polymerization. Porous hydrogel was successfully prepared by the incorporation of $CaCO_3$ microparticles. In the synthesized hydrogels, the porous structure can be formed in two ways: (a) acid treatment to leaching the $CaCO_3$ particles and (b) the hydrogel containing $CaCO_3$ particles has a pasty and jelly state that prevents removing the evolved $CO_2$ gas (from neutralization of $CaCO_3$ in the presence of acid) from the pasty and jelly state. So, the removed gas creates pores in the hydrogel. Figure 1 indicates SEM micrographs of hydrogels. The PAAm as a hydrogel component and $CaCO_3$ particles were observed in the hybrids, as shown in Figure 1b. After HCl treatment, the $CaCO_3$ particles have disappeared and pores could be clearly observed in the hydrogel, as shown in Figure 1c. On the other hand, pores were not observed in hydrogels prepared without the $CaCO_3$ particles, as shown in Fig-
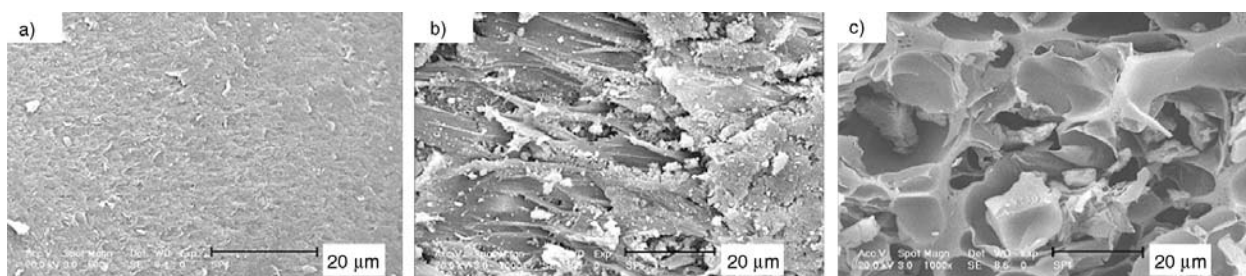


**Figure 1.** SEM micrographs (×1000, Scale bar: 20 μm) of a) non-porous PAAm, b) PAAm hydrogel containing $CaCO_3$ and c) porous hydrogel after removing of $CaCO_3$

ure 1a. These observations indicate that porous PAAm hydrogels were successfully prepared by the present technique.

## 3.2. Effect of CCb content on porosity

For all dried hydrogels, the bulk density of dried hydrogels was determined using picnometer. As shown in Table 2, the increase in $CaCO_3$ content has a big influence on the density of the hydrogels. The results reveal that the increase in $CaCO_3$ causes a decrease in the density of the hydrogels. Decrease in density can be attributed to the pores containing air [21]. Using the high content of $CaCO_3$ to synthesize of hydrogel causes the high number of produced pores, and subsequently the density will be decreased. So, the decrease in density can be attributed to the increase in porosity.

**Table 2.** Effect of $CaCO_3$ content on the bulk density ($\rho$) of dried hydrogels

| Sample | $CaCO_3$ [g] | $\rho$ [g/cm³] |
|--------|--------------|----------------|
| SP1 | 0.0 | 1.64 |
| SP2 | 1.5 | 1.23 |
| SP3 | 3.0 | 1.02 |
| SP4 | 6.0 | 0.85 |

## 3.3. Swelling study

### 3.3.1. Effect of $CaCO_3$ content on swelling

Figure 2 illustrates the equilibrium of water content and dynamic swelling behavior of hydrogels as a function of the $CaCO_3$ amount. As presented in this figure, by using the $CaCO_3$ in the feed mixture, the water absorbency of the hydrogels increases. This may be attributed to the fact that using $CaCO_3$ in
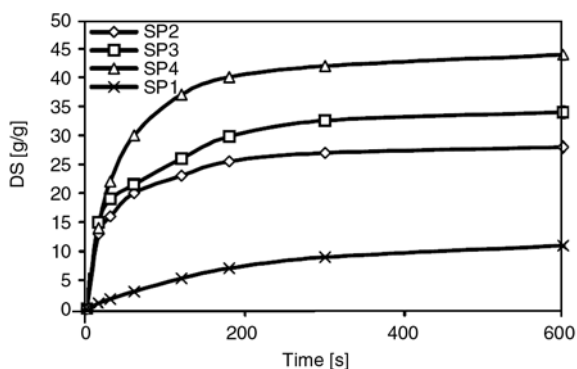


**Figure 2.** Water absorbing and dynamic swelling dependency of porous PAAm hydrogel as a function of amount of $CaCO_3$

the hydrogel makes pores in the hydrogel structure and results in a high water uptake. Also, hydrogels absorb higher amount of water with increasing $CaCO_3$ amount in reaction feed that may be due to increase in pore number. Also, the effect of $CaCO_3$ content on the swelling kinetic of the hydrogels was investigated. A preliminary study was conducted on the hydrogels swelling kinetics. The rate of water uptake in porous hydrogels is higher than that of non-porous hydrogel. Increase in the rate of absorption would be expected from the increase in surface area with increasing porosity of hydrogels. The swelling-time data can be fitted with the Equation (2) [22] to derive the power and rate parameters:

$$S_t = S_e(1 - e^{-t/\tau}) \qquad (2)$$

where $S_t$ is swelling at time $t$ [g/g], $S_e$ is equilibrium swelling ('power parameter', [g/g]), $t$ is time [sec] for swelling $S_t$, and $\tau$ stand for 'rate parameter' (time for $S_\tau$), [s]. The rate parameters for hydrogels prepared with using 0, 1.5, 3 and 6 g of $CaCO_3$ are 500, 128, 113, and 100 sec, respectively. The $\tau$ value for hydrogel with no-$CaCO_3$ is higher than those in the samples was synthesized using $CaCO_3$. This may simply be attributed to the fact that with using $CaCO_3$ in synthesis of hydrogel the porous structure is formed.

### 3.3.2. Effect of MBA concentration

Crosslinks are necessary to form a hydrogel in order to prevent dissolution of the hydrophilic polymer chains in an aqueous environment. To investigate the effect of MBA concentration on the water absorbency of the porous PAAm, the crosslinker concentration was chosen 0.13, 0.32 and 0.65 mmol. All the other parameters in these series of reaction were constant. As shown in Figure 3, as the concentration of the MBA was increased, the water absorbency of the hydrogel composite was decreased (41, 34 and 17 g/g for 0.13, 0.32 and 0.65 mmol of MBA, respectively). Clearly, a higher concentration of crosslinker produces a larger degree of polymer chains branching and generates an additional network. Thereby, with the crosslinker content increasing, the crosslinking density increases. As a result, the network space gets diminished, and less water enters the hydrogel [23].
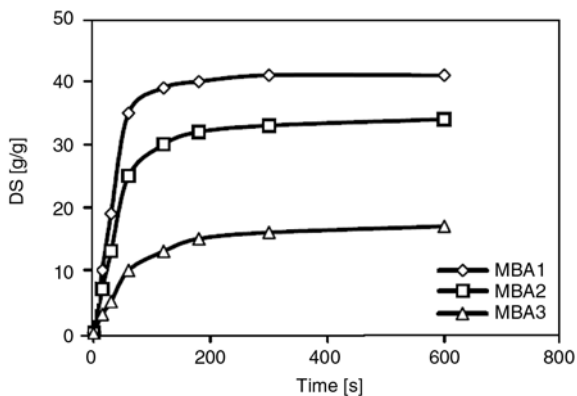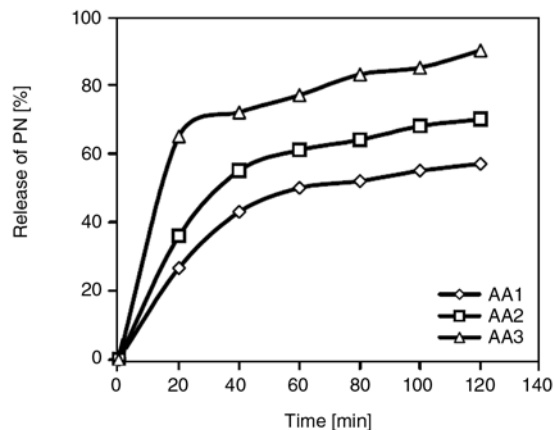
**Figure 3.** Effect of MBA concentration on the water absorbency and dynamic swelling of hydrogels



| Run | AA1 | AA2 | AA3 |
|---|---|---|---|
| Loading of PN [%] | 30 | 58 | 85 |

**Figure 4.** Effect of percentage of loading of PN (SP3 hydrogel) on the release of PN from hydrogel. AA1, AA2 and AA3 are PN loaded SP3 hydrogels containing 30, 58 and 85 of %loading, respectively.

## 3.4. Release of KNO₃ from PAAm hydrogel

The hydrogels have been evaluated as slow release matrix using potassium nitrate as model agrochemical. Potassium nitrate is used to improve production of crops. It is important to controlled release of agrochemical to diminish amount of active ingredient without reducing efficiency. The release of an active agent from hydrogel matrix may be affected by various parameters. Hydrogel composition and structure as well as %loading are important parameters. So, in this study we attempt to investigate the effect of MBA concentration and amount of $CaCO_3$ as well as the %loading on the release kinetic of $KNO_3$ from PAAm matrix. The release kinetic of active agent from loaded hydrogel is closely related to its water sorption kinetic [6, 16]. The % loading in various hydrogels was given in Table 1.

### 3.4.1. Effect of amount of loading on release of PN

The release profile of PN from the porous PAAm hydrogel loaded with various amounts of the PN was studied in deionized water. The results are shown in Figure 4. In this section of study, porous PAAm hydrogel, SP3, was immersed in PN solutions with various concentrations of PN (0.5, 1 and 2% wt of PN solution). The results show that the loading is increased with increasing the PN concentration in loading medium (%30 (AA1), %58 (AA2) and %85 (AA3) of loading for SP3 hydrogel in solution containing 0.5, 1 and 2% wt of PN, respectively). Then the dried and loaded hydrogels were immersed in deionized water to study the release profiles. The release profiles indicate that

the amount of released PN increases with increasing %loading of active agent. It is attributed to the larger amount of loading. The larger the initial load, the faster the movement of the solvent front penetrating the surface of the loaded hydrogel [6, 24].

### 3.4.2. Effect of MBA concentration on the release of PN

The release of $KNO_3$ from PAAm hydrogels was studied by varying MBA concentration. Figure 5 shows the effect of MBA concentration on the $KNO_3$ release behavior of the hydrogel. The results indicate that the release of active agent depends obviously on the crosslinker concentration. In the
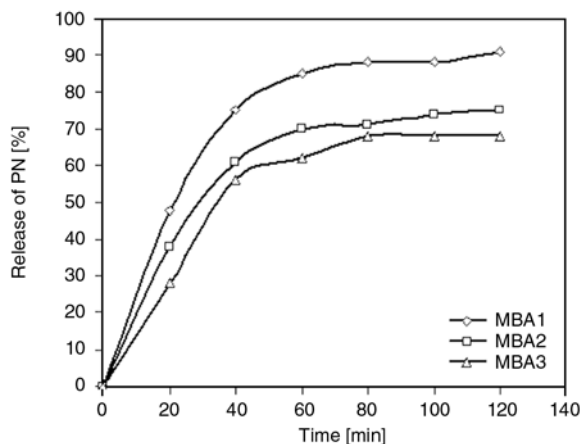


**Figure 5.** Effect of MBA concentration of the release of PN

first 40 min, 56, 61 and 75% of $KNO_3$ were released from MBA3, MBA2 and MBA1 hydrogels, respectively. The fast release of $KNO_3$ is due the higher swelling behavior of hydrogel with low concentration of MBA.

### 3.4.3. Effect of $CaCO_3$ amount of release of PN

The $KNO_3$ was entrapped inside the PAAm hydrogels in the swollen state. SP1, SP3 and SP4 were chosen for loading of potassium nitrate. Loading percentages were obtained to be 78, 58 and 28% as determined by conductivity method for SP4, SP3 and SP1, respectively. Figure 6 shows the effect of porosity on the $KNO_3$ release behavior of the hydrogels. The results indicate that the release of active agent depends obviously on the porosity. In the first 40 min, 76 (SP4) and 64 (SP3) percent of PN were released from porous hydrogels, while in non-porous hydrogel (SP1) the release amount is only 26 percent. The release kinetic of active agent from loaded hydrogel is closely related to its water sorption kinetic [25, 26]. The fast release of $KNO_3$ in porous hydrogels is due the fast swelling behavior of these polymers.

### 4. Conclusions

Porous PAAm hydrogels were synthesized by solution polymerization of acrylamide in the presence of calcium carbonate particles. Acid treatment of hydrogel-$CaCO_3$ hybrid results in a porous structure in the hydrogels. The porosity of the resulted hydrogels was confirmed using SEM micrographs. Dynamic swelling kinetics of the hydrogels shows that the rate of absorbency for porous hydrogels is
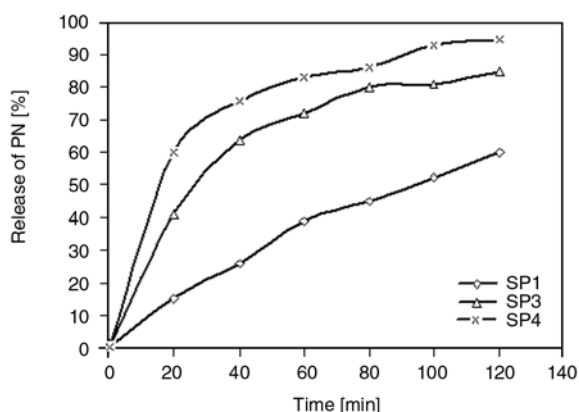
higher than that of non-porous hydrogel. The effect of MBA concentration and $CaCO_3$ amount showed that the water absorbency of the hydrogels is increased with increasing of $CaCO_3$ amount but decreased with increasing MBA concentration. Also, the results of release of PN from hydrogels showed that $CaCO_3$ amount, MBA concentration, and % loading affect the release of PN from hydrogels.

### Acknowledgements

**Figure 6.** Slow release dependency of hydrogels as a function of used $CaCO_3$

### References

[1] Pó R.: Water-absorbent polymers: A patent survey. Polymer Reviews, **34**, 607–662 (1994). DOI: 10.1080/15321799408014168

[2] Dayal U., Mehta S. K., Choudhary M., Jain R. C.: Synthesis of acrylic superabsorbents. Polymer Reviews, **39**, 507–525 (1999). DOI: 10.1081/MC-100101426

[3] Liu Q., Rauth A. M., Wu X. Y.: Immobilization and bioactivity of glucose oxidase in hydrogel microspheres formulated by an emulsification-internal gelation-adsorption-polyelectrolyte coating method. International Journal of Pharmaceutics, **339**, 148–156 (2007). DOI: 10.1016/j.ijpharm.2007.02.027

[4] Tonnesen H. H., Karlsen J.: Alginate in drug delivery systems. Drug Development and Industrial Pharmacy, **28**, 621–630 (2002). DOI: 10.1081/DDC-120003853

[5] Liu M., Liang R., Zhan F., Liu Z., Niu A.: Synthesis of a slow-release and superabsorbent nitrogen fertilizer and its properties. Polymers for Advanced Technologies, **17**, 430–438 (2006). DOI: 10.1002/pat.720

[6] Bajpai A. K., Giri A.: Swelling dynamics of a macromolecular hydrophilic network and evaluation of its potential for controlled release of agrochemicals. Reactive and Functional Polymers, **53**, 125–141 (2002). DOI: 10.1016/S1381-5148(02)00168-2

[7] Naganagouda N. K., Mulimani V. H.: Gelatin blends with alginate: Gel fibers for α-galactosidase immobilization and its application in reduction of nondigestible oligosaccharides in soymilk. Process Biochemistry, **41**, 1903–1907 (2006). DOI: 10.1016/j.procbio.2006.03.040

[8] Sheldon R. A: Enzyme immobilization: The quest for optimum performance. Advanced Synthesis and Catalysis, **349**, 1289–1307 (2007).
DOI: 10.1002/adsc.200700082

[9] Kabiri K., Omidian H., Hashemi S. A., Zohuriaan-Mehr M. J.: Synthesis of fast-swelling superabsorbent hydrogels: Effect of crosslinker type and concentration on porosity and absorption rate. European Polymer Journal, **39**, 1341–1348 (2003).
DOI: 10.1016/S0014-3057(02)00391-9

[10] Chen J., Park K.: Synthesis and characterization of superporous hydrogel composites. Journal of Controlled Release, **65**, 73–82 (2000).
DOI: 10.1016/S0168-3659(99)00238-2

[11] Omidian H., Rocca J. G., Park K.: Advances in superporous hydrogels. Journal of Controlled Release, **102**, 3–12 (2005).
DOI: 10.1016/j.jconrel.2004.09.028

[12] Serizawa T., Wakita K., Akashi M.: Rapid deswelling of porous poly(*N*-isopropylacrylamide) hydrogels prepared by incorporation of silica particles. Macromolecules, **35**, 10–12 (2002).
DOI: 10.1021/ma011362

[13] Thomas W. M., Wang D. W.: Acrylamide polymers. in 'Encyclopedia of Polymer Science and Engineering' (eds.: Mark H. F., Bikales N. M.) Vol 1, Wiley, New York, 169–211 (1964).

[14] Saraydin D., Karadag E., Öztop N., Güven O.: Adsorption of bovine serum albumin onto acrylamide-maleic acid hydrogels. Biomaterials, **15**, 917–920 (1994).
DOI: 10.1016/0142-9612(94)90117-1

[15] Saraydin D., Karadag E., Cetínkaya S., Güven O.: Preparation of acrylamide/maleic acid hydrogels and their biocompatibility with some biochemical parameters of human serum. Radiation Physics and Chemistry, **46**, 1049–1052 (1995).
DOI: 10.1016/0969-806X(95)00318-R

[16] Abd El-Rehim H. A.: Characterization and possible agricultural application of polyacrylamide/sodium alginate crosslinked hydrogels prepared by ionizing radiation. Journal of Applied Polymer Science, **101**, 3572–3580 (2006).
DOI: 10.1002/app.22487

[17] Abd El-Rehim H. A., Hegazi E. A., Abd El-Mohdy H. L.: Properties of polyacrylamide-based hydrogels prepared by electron beam irradiation for possible use as bioactive controlled delivery matrices. Journal of Applied Polymer Science, **98**, 1262–1270 (2005).
DOI: 10.1002/app.22167

[18] Lu G. D., Yan Q. Z., Ge C. H.: Preparation of porous polyacrylamide hydrogels by frontal polymerization. Polymer International, **56**, 1016–1020 (2007).
DOI: 10.1002/pi.2235

[19] Omidian H., Rocca J. G., Park K.: Elastic superporous hydrogel hybrid of polyacrylamide and sodium alginate. Macromolecular Bioscience, **6**, 703–710 (2006).
DOI: 10.1002/mabi.200600062

[20] Caykara T., Bulut M., Dilsiz N., Akyüz Y.: Macroporous poly(acrylamide) hydrogels: Swelling and shrinking behaviors. Journal of Macromolecular Science Part A: Pure and Applied Chemistry, **43**, 889–897 (2006).
DOI: 10.1080/10601320600653699

[21] Gemeinhart R. A., Park H., Park K.: Pore structure of superporous hydrogels. Polymers for Advanced Technologies, **11**, 617–625 (2000).
DOI: 10.1002/1099-1581(200008/12)11:8/12<617::AID-PAT12>3.0.CO;2-L

[22] Omidian H., Hashemi S. A., Sammes P. G., Meldrum I.: A model for the swelling of superabsorbent polymers. Polymer, **39**, 6697–6704 (1998).
DOI: 10.1016/S0032-3861(98)00095-0

[23] Wu J., Lin J., Zhou M., Wei C.: Synthesis and properties of starch-*graft*-polyacrylamide/clay superabsorbent composite. Macromolecular Rapid Communication, **21**, 1032–1034 (2000).
DOI: 10.1002/1521-3927(20001001)21:15<1032::AID-MARC1032>3.0.CO;2-N

[24] Kim S. W., Bae Y. H., Okano T.: Hydrogels: Swelling, drug loading, and release. Pharmaceutical Research, **9**, 283–290 (1992).
DOI: 10.1023/A:1015887213431

[25] Bajpai A. K., Giri A.: Water sorption behaviour of highly swelling (carboxy methylcellulose-g-polyacrylamide) hydrogels and release of potassium nitrate as agrochemical. Carbohydrate Polymers, **53**, 271–279 (2003).
DOI: 10.1016/S0144-8617(03)00071-7

[26] Colombo P., Bettini R., Peppas N. A.: Observation of swelling process and diffusion front position during swelling in hydroxypropyl methyl cellulose (HPMC) matrices containing a soluble drug. Journal of Controlled Release, **61**, 83–91 (1999).
DOI: 10.1016/S0168-3659(99)00104-2

# Influence of the composition of hydroxypropyl cellulose/maleic acid-*alt*-styrene copolymer blends on their properties as matrix for drug release

*G. G. Bumbu[1,3], B. S. Munteanu[2], J. Eckelt[3], C. Vasile[3*]*

[1]P. Poni Institute of Macromolecular Chemistry, Physical Chemistry of Polymer Laboratory, 41A Grigore Ghica Voda Alley, Ro 700487, Iasi, Romania
[2]'Al. I. Cuza' University, Faculty of Physics, 16 Carol I Blvd. Iasi, Romania
[3]University of Mainz, Institute of Physical Chemistry, 55099 Mainz, Germany

**Abstract.** Poly(carboxylic acid)-polysaccharide compositions have been found suitable for obtaining drug formulations with controlled release, most formulations being therapeutically efficacious, stable, and non-irritant. The influence of the characteristics of the aqueous solutions from which the polymer matrix is prepared (i.e. the total concentration of polymer in solutions and the mixing ratio between the partners, hydroxypropyl cellulose, HPC and maleic acid-*alternating*-styrene copolymer, MAc-*alt*-S) on the kinetics of some drugs release in acidic environment (pH = 2) has been followed by '*in vitro*' dissolution tests. It has been established that the kinetics of procaine hydrochloride release from HPC/MAc-*alt*-S matrix depends on its composition; the diffusion exponent, $n$ is close to 0.5 for matrices where one of the components is in large excess and $n \sim 0.02$ for middle composition range. The lower value of diffusion exponent for middle composition range could be caused by the so called 'burst effect', therefore the kinetic evaluation is difficult.

*Keywords:* biopolymers, interpolymeric association, maleic copolymer, drug release

## 1. Introduction

The design of interpolymeric complexes, which can be used for the immobilization of various drugs, hormones, enzymes, and proteins is of considerable interest because of the possibility of developing different controlled release systems.

Polysaccharides have several advantages as components in drug delivery systems. They are natural or semi-synthetic polymers showing a good biocompatibility with living cells. Blend of polysaccharides with synthetic water-soluble polymers lead to materials with improved physico-chemical and mechanical characteristics [1].

Several reports were devoted to the development of various drug dosage forms based on poly(carboxylic acid)-polysaccharide compositions indicating good results in the release of morphine sulfate [2], propranolol hydrochloride [3], carbamazepin [4], model peptide peroxidase [5], lidocaine [6] amoxillin and rifampicin, insulin [7], levomycetin [8, 9], proteins, lactate dehydrogenase [10], phenacetin [11], timolol maleate for ophthalmology application [12], antibacterial agent, ofloxacin [13] and many others. Most formulations were therapeutically efficacious, stable, and nonirritant [14]. The complexes based on poly(acrylic acid), PAA and methyl or hydroxypropyl methyl cellulose demonstrated very good ability to form capsules insoluble in acid media [15].

Satoh and co-workers [16] studied the bioadhesive properties of tablets consisting of hydroxypropyl cellulose (HPC) and carboxyvinyl polymer (CP) using mouse peritoneal membrane containing bleomycin hydrochloride, carboquone, and 5-fluorouracil and they found them favorable for the treatment of foci in the cervical canal.

In a previous work we showed that HPC and MAc-*alt*-S copolymer form interpolymeric complexes, IPC *via* hydrogen bonding interactions between the oxygen of the ether groups of HPC and the OH-groups of the carboxyl groups of MAc-*alt*-S [17, 18], IPC stabilized by hydrophobic interactions between the isopropyl side chain of HPC and the styrene groups of MAc-*alt*-S [19]. The stoichiometry of the interpolymeric complex was estimated to be HPC/MAc-*alt*-S = 40:60 [w/w] independent of the total polymer concentration in the system, $c_{pol}$. At $c_{pol} = 5$ mg·ml$^{-1}$, the mixtures with a content of HPC in the initial mixtures between 20 and 60 wt%, phase separate. At $c_{pol} = 10$ mg·ml$^{-1}$, depending on the mixing ratio between the partners, either a phase separation (in the mixtures with a prevailing content of one of the components) or a gelation (similar mixing ratio between components) occurs. The IR spectra indicated that there is a tendency of the MAc-*alt*-S, independent of the mixing ratio of the components, to accumulate in the gel until it reaches a concentration of around 60 wt%. The maximum concentration of the precipitate in the gel phase is also reached at a mixing ratio between HPC and MAc-*alt*-S of 40/60 that corresponds to the stoichiometry of the complex. At pH lower than 4.5 the HPC/MAc-*alt*-S, IPC becomes water-insoluble [18].

It is well known from membrane science that the morphology and therefore the permeability and transport characteristics highly depend on the way of preparation [20]. Also in mixtures that can form IPCs, it is expected that when one of the components is in large excess, the structure of the inter-polymer associations to be different to the mixtures where the ratio between the components is close to the stoichiometry, therefore a different morphology and release profile of the drug is expected.

In this work, it is investigated the influence of the characteristics of the aqueous solutions from which the polymer matrix is prepared, i.e. the total concentration of polymer in solutions and the mixing ratio between the partners, hydroxypropyl cellulose and maleic acid-*alternating*-styrene copolymer, on the kinetics of the various drugs released in acidic environment (pH = 2). Three drugs with different structure, molecular weight and solubility have been incorporated in the HPC/MAc-*alt*-S matrices, namely: procaine hydrochloride, vanillin and tannic acid.

Procaine hydrochloride, known also as novocaine, it is a local anaesthetic from the amino ester group, mainly used to reduce the pain of intramuscular infections, in stomatology, etc. It acts by constriction of blood vessels determining the bleeding reduction without generating a euphoric state or dependence. Procaine blocks the generation and transmission of the nervous impulses by lowering the membrane permeability to the ions, inhibiting the depolarization and so loosing of pain sensation. Procaine is also the main ingredient in the preparation of the Gerovital H3 known to slow down the aging effects. From theoretical point of view procaine is often used as model drug in many drug release experiments.

Vanillin (4-hydroxy-3-methoxybenzaldehyde) is efficacious for the treatment of chronic hypoacidic gastritis and chronic non-acid gastritis. As well as this receptor inhibition, in the central nervous system, vanillin also influences the craving to consume food. In this context it is supposed that the vanillin is able to increase the concentration of the neurotransmitter serotonin in the brain [21]. Increased brain serotonin concentration, however, leads demonstratively to a reduced craving to consume food.

Tannic acid can be used for medical purposes such as: anti-diarrhoea, hemostats and anti-piles compounds, while together with other related compounds as those containing galic and elagic acids (epigalitaninuri) are inhibitors in HIV replications. It has anti-bacterial properties and is a very beneficial anti-oxidant. In high quantities it slows down the absorption of iron and possibly other trace minerals. The use of tannic acid as an adjuvant therapy for burn wounds has regained interest in present times. In particular, some preclinical and clinical studies indicate that highly purified tannic acids can provide a valuable tool to improve wound healing and to reduce scar tissue formation, it induces a durable, supple crust that did not obstruct the regular outgrowth of epithelium. The assumed hepatotoxicity of tannic acid is questioned [22].

## 2. Experimental
## 2.1. Materials
Hydroxypropyl cellulose LF, Klucel™, a food grade polymer, offered by courtesy of Aqualon Company, Hopewell, Virginia has been used. According to the producer specifications, HPC LF has a molecular mass of approximately 100 000 g·mol$^{-1}$ and a 3.4 moles of substitution [23]. The main chain of HPC consists of glucopyranosyl units linked in $(1 \rightarrow 4)$ β position. The side substituents are formed by short chains containing from one up to six hydroxypropyl units.

Maleic acid-*alternating*-styrene copolymer (MAc-*alt*-S) was prepared by the hydrolysis of maleic anhydride-*alternating*-styrene copolymer (MA-*alt*-S) in pure water, at 80°C for 4 h. MA-*alt*-S has been synthesized by free radical copolymerizations, in toluene, at 80°C (the detailed synthesis has been

described in ref. [24]). The molecular mass of the MAc-*alt*-S copolymer was calculated based on the molecular mass of the MA-*alt*-S copolymer as being 130 000 g·mol$^{-1}$, considering that there are no changes in chain length during hydrolysis. The MAc-*alt*-S copolymer is totally water-soluble.
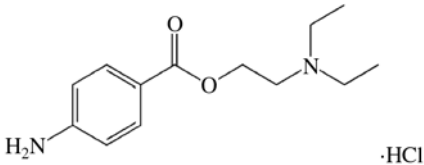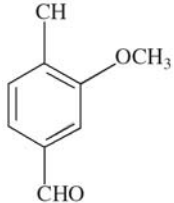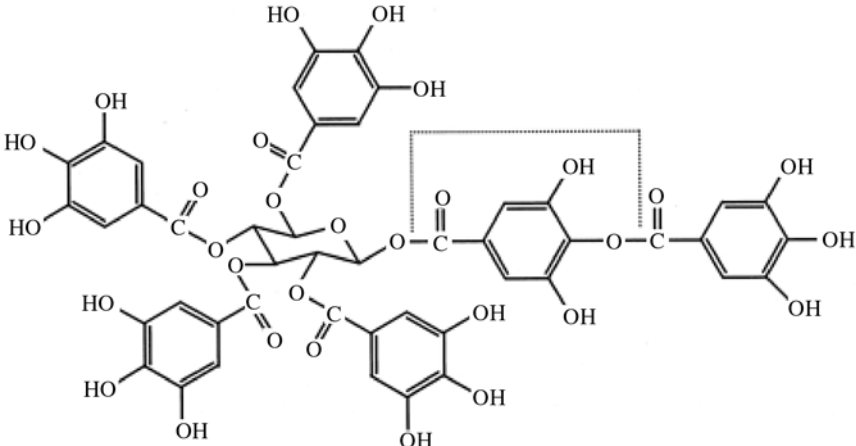
Both samples (HPC and MAc-*alt*-S copolymer) were carefully purified before study by dialysis against water and then freeze dried.

The structure and the water solubility of the used drugs are summarized in Table 1.

Twice-distilled water was used as solvent for all measurements. The pH of the solutions was adjusted at value 2 with diluted HCl solution in twice-distilled water.

Procaine hydrochloride, vanillin and tannic acid were purchased from Sigma Aldrich and used as received.

**Table 1.** Characteristics of the used drugs

| Drug | Structure | Water solubility [mg/l] |
|---|---|---|
| Procaine hydrochloride |  | 9450 Easily soluble in cold water* |
| Vanillin |  | 10000 Soluble in 125 parts water** |
| Tannic acid |  | Completely soluble: 1 g/0.35 ml water*** |

*Science Laboratories, http://www.sciencelab.com/xMSDS-Procaine_hydrochloride-9924715;
 Mallinckrodt Baker Inc. Materials safety data sheet
**http://www.jtbaker.com/msds/englishhtml/v2775.htm
***http://www.jtbaker.com/msds/englishhtml/t0065.htm

## 2.2. Preparation of the IPC/drug systems

The drugs were incorporated in the polymeric matrix of HPC, MAc-*alt*-S or their mixtures at different mixing ratios, at a weight ratio between matrix and drug of 4 to 1. As MAc-*alt*-S forms a precipitate with procaine hydrochloride, the samples were prepared as followed: the corresponding amount of drug was previously dissolved in the aqueous solution of HPC and then the HPC-drug solution was mixed with the aqueous solution of the MAc-*alt*-S in different mixing ratios. The obtained samples were frozen at –50°C and freeze-dried.

The polymer matrix was prepared at the following weight mixing ratios between HPC and MAc-*alt*-S: 10/90, 40/60, 50/50, 80/20 at two different total polymer concentrations $c_{pol}$ = 5 mg/ml and $c_{pol}$ = 10 mg/ml.

For comparison reasons the same preparation procedure was used to incorporate vanillin and tanic acid in the 40 wt% HPC/60 wt% MAc-*alt*-S matrix at $c_{pol}$ = 10 mg/ml.

## 2.3. Sample characterization

A Leitz Wetslar microscope, Germany was used to investigate the fluorescence behaviour of the samples at a magnification of 250×.

*In vitro* release studies have been conducted in a standard dissolution set-up. [25] Aliquots of the medium of 1 ml were withdrawn periodically at predetermined time intervals and analyzed using a Hewlett Packard 8540A spectrophotometer. In order to maintain the solution concentration the sample is reintroduced in the circuit after analyzing. The concentrations of the drug were calculated based on previously measured calibration curves for each drug at their specific maximum absorption wavelengths using solutions of known concentrations in the range of loaded drug. The maximum absorption wavelengths at pH = 2 are for procaine hydrochloride at $\lambda_{max}$ = 292 nm, vanillin at $\lambda_{max}$ = 229 nm and tannic acid at $\lambda_{max}$ = 212 nm.

A simple, semi-empirical equation using Higuchi model was used to analyze kinetically the data regarding the drug release from HPC/MAc-*alt*-S system at the initial stages (approximately 60% fractional release) [26–32] (Equation (1)):

$$\frac{M_t}{M_\infty} = k_H t^n \qquad (1)$$

where $M_t/M_\infty$ is the fractional drug release; $M_t$ and $M_\infty$ are the absolute cumulative amounts of drug released at time $t$ and at infinite time (in this case maximum release amount in the experimental conditions used, at the plateau of the release curves), respectively; $k_H$ is the Higuchi dissolution constant that incorporates the characteristics of the macromolecular network system and the drug, and $n$ is the diffusional exponent, which is an indicative of the transport mechanism.

It has been established that for $n = 0.5$, the release mechanism follows the Fick's law diffusion. A value of $n = 1$, it means that the drug release is independent of time, while when $n$ lies between 0.5 and 1 an anomalous transport is involved [27, 33].

## 3. Results and discussion

The matrices do not exhibit fluorescence or it is very weak for the MAc-*alt*-S copolymer. In fluorescence microscopy the colour depends on the drug type being brown-to-green for procaine hydrochloride (Figure 1a) transparent-to-light green for vanillin (Figure 1b) and dark-brown-to-dark blue (Figure 1c) for tannic acid and the aspect (Figures 1a to 1c) indicates a homogenous distribution of the drugs in the matrix.

### 3.1. Influence of the drug type

The release profile of the three drugs, procaine hydrochloride, vanillin, and tannic acid, with different solubility or size from a HPC/MAc-*alt*-S interpolymeric associations matrix was investigated at pH = 2 and $T$ = 37°C, an environment that simulate the physiological conditions in the stomach, Figure 2. The matrix has a composition of 40HPC/60MAc-*alt*-S and it was prepared form a solutions with $c_{pol}$ = 5 and 10 mg/ml. The maximum released quantity at pH = 2 is lower (~38%) when concentration was 5 wt% in respect with the case when concentration was 10% (~58%), while the release time decreased with increasing concentration. These values depend on the composition of HPC/MAc-*alt*-S. The kinetic values are evaluated for approximately 60% of drug released.
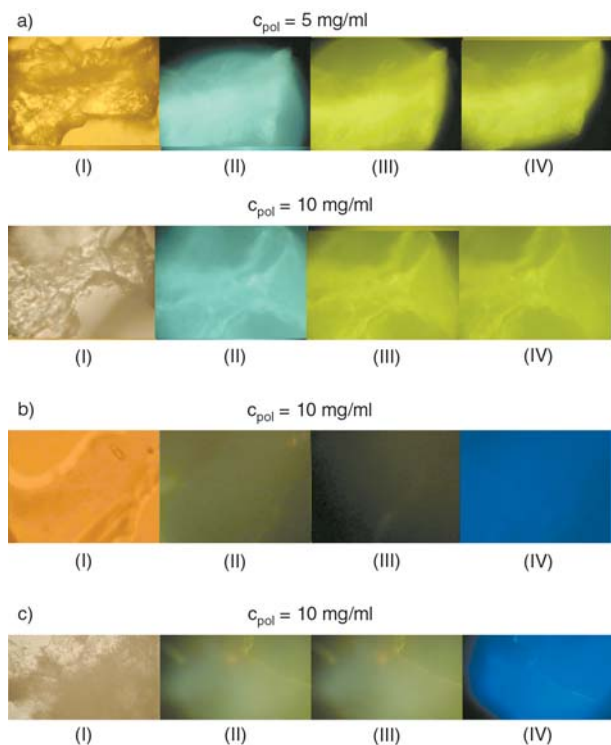
**Figure 1.** a) Microscopical aspects of the 40HPC/60MAc-
*alt*-S/procaine hydrochloride system prepared
form both a solution with a $c_{pol}$ = 5 mg/ml and
$c_{pol}$ = 10 mg/ml in fluorescence light at various
wavelengths of excitation: (I) white light,
(II) 380 nm, (III) 410 nm and (IV) 440 nm.
b) Microscopical aspects of the 40HPC/60MAc-
*alt*-S/vanillin system prepared form a solution
with a $c_{pol}$ = 10 mg/ml in fluorescence light at
various wavelengths of excitation: (I) white
light, (II) 380 nm, (III) 410 nm and (IV) 440 nm.
c) Microscopical aspects of the 40HPC/60MAc-
*alt*-S/tannic acid system prepared form a solu-
tion with a $c_{pol}$ = 10 mg/ml in fluorescence light
at various wavelengths of excitation: (I) white
light, (II) 380 nm, (III) 410 nm and (IV) 440 nm

One can notice that procaine hydrochloride is
released the fastest from the matrix, while the
vanillin was the slowest. The equilibrium values of
the fractional release are reached after only 14 min-
utes for procaine hydrochloride while for tannic
acid this value is reached after ca. 47 minutes, and
vanillin needs about 190 minutes.
The kinetic data obtained by analysing the drug
release profile according to Equation (1) are col-
lected in Table 2.
Tannic acid and vanillin have similar release order,
therefore similar transport mechanisms. The data
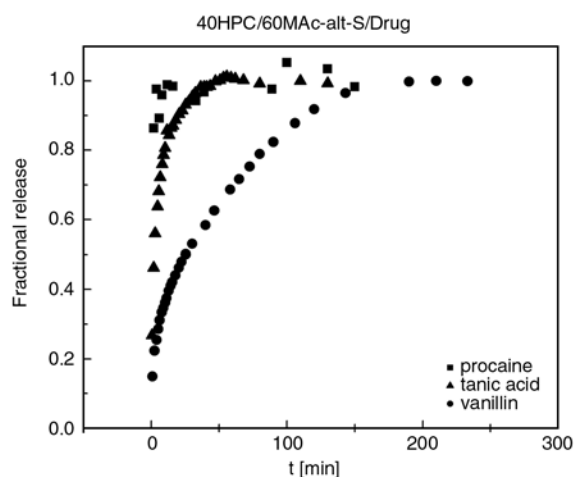for procaine hydrochloride are difficult to analyse,



**Figure 2.** Release profiles of procaine hydrochloride, tan-
nic acid, and vanillin from a 40HPC/60MAc-
*alt*-S matrix at pH = 2 and $T$ = 37°C

**Table 2.** Values of $n$ and $k_H$ for various drugs released from
a 40HPC/60MAc-*alt*-S matrix at pH = 2 and
$T$ = 37°C

| Drug | n | $k_H$ [min$^{-n}$] |
|---|---|---|
| Tannic acid | 0.326 ± 0.008 | 0.384 ± 0.006 |
| Procaine hydrochloride | 0.018 ± 0.007 | 0.920 ± 0.020 |
| Vanillin | 0.351 ± 0.003 | 0.160 ± 0.001 |

as the release of the drug is very fast. It is character-
ized by a pronounced 'burst effect'.

## 3.2. Influence of matrix composition on the release profile

The fractional release of procaine hydrochloride
from matrices with different ratios between HPC
and MAc-*alt*-S is shown in Figures 3a and 3b
The release profile of the drug depends both on the
ratio between the HPC and MA-*alt*-S and on the
total polymer concentration of the solutions used
for the preparation of matrix. For example for the
matrix containing 80HPC/20MAc-*alt*-S the release
time decreases from 175 minutes when the system
is prepared from a solution with $c_{pol}$ = 5 mg/ml to
100 minutes when it is obtained form $c_{pol}$ =
10 mg/ml, while for the matrix 50HPC/50MAc-
*alt*-S, these values are 60 and 20 min, respectively.
Procaine hydrochloride releases much faster from
matrices with a composition close to the stoichiom-
etry of the IPC than from matrices where one of the
components are in excess. For example for the
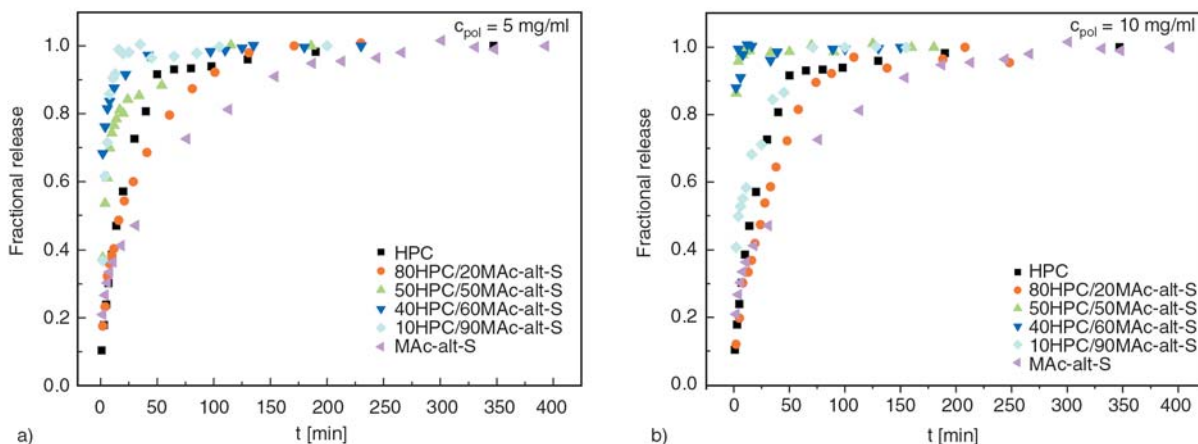matrix containing 40HPC/60MAc-*alt*-S the plateau

**Figure 3.** Release profiles of procaine hydrochloride from HPC/MAc-*alt*-S matrix for various ratio between components and different total polymer concentration in the initial solution: (a) $c_{pol}$ = 5 mg/ml and (b) $c_{pol}$ = 10 mg/ml

is reached after about 50 minutes while for 80HPC/20MAc-*alt*-S it takes about 175 minutes.

The similar values for the release time have been obtained by other authors from different non-covalent hydrogen bonding or polyionic interpolymeric complexes. For example using poly(vinyl alcohol)/poly(acrylic acid), PAA interpolymer complexes release time of mucosal drug delivery was max. 60 or 30 min [23], PAA/Chitosan (100 min) [34], Chitosan/polyethyleneoxide-maleic acid copolymer films (max. 50 min) [32]. In the last case for the polyelectrolyte complex films derived from polyethyleneoxide-maleic acid copolymer, Leong *et al.*, found a release time of ibuprofen of maximum 30 min [31]. When entering into intestine, where pH ~7.4 the H-bonding associations between polymer components and those between drug and polymer matrix are destroyed due to the basic pH and release rate and amount of the drug released will be faster and respectively higher [35–37].

The derivatives of the release profile curves, proportional with the rate of drug release, are shown in Figure 4. All show an exponential decrease with time up to 75 min then level off.

In the first 30 minutes, the release rate is very fast for all studied systems, they present the 'burst effect' and then a plateau value is reached for the entire investigated duration of the release study. One can notice that the slowest release rates is given by 10HPC/ 90MAc-*alt*-S matrix, when the mixture is prepared form a solution with a $c_{pol}$ = 5 mg/ml and 80HPC/ 20MAc-*alt*-S matrix, respectively when this is prepared from a solution with a concentration of $c_{pol}$ = 10 mg/ml.
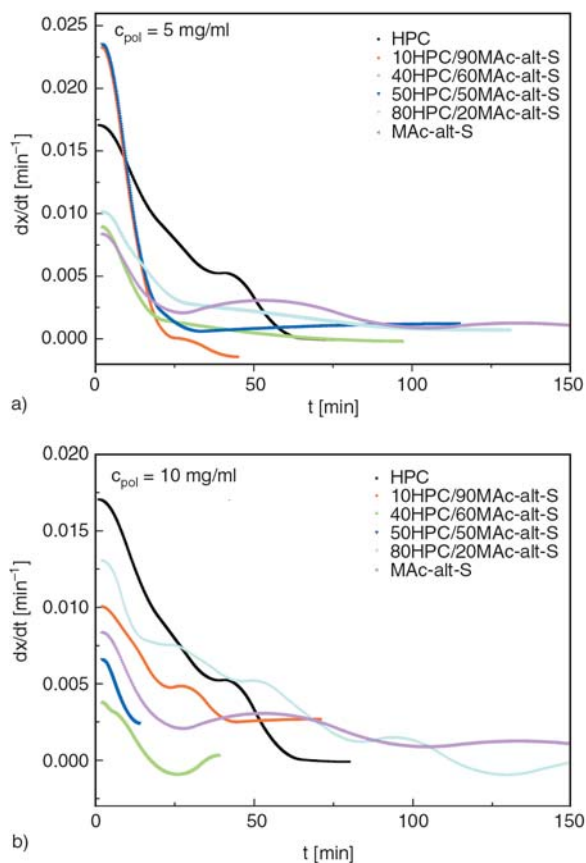


**Figure 4.** Derivative curves of the release profiles of procaine hydrochloride from HPC/MAc-*alt*-S matrix: a) $c_{pol}$ = 5 mg/ml and b) $c_{pol}$ = 10 mg/ml

Kinetic analysis of our data is presented in Figures 5a and 5b and obtained values are given in Table 3.

The kinetics of procaine hydrochloride release from HPC/MAc-*alt*-S matrices depends on their composition; the diffusion exponent, *n* is close to
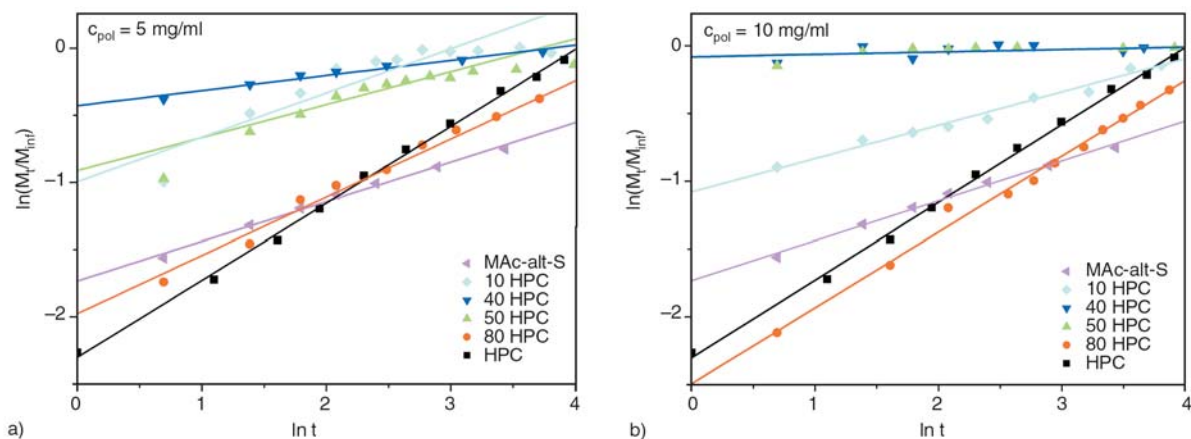
**Figure 5.** Graph for the evaluation of the release order: a) $c_{pol} = 5$ mg/ml and b) $c_{pol} = 10$ mg/ml

**Table 3.** Values of $n$ and $k_H$ for various studied cases

| Sample | n | $k_H$ [min$^{-n}$] |
|---|---|---|
| $c_{pol} = 5$ mg/ml | | |
| MAc-*alt*-S | 0.290 ± 0.010 | 0.177 ± 0.005 |
| 80HPC/20MAc-*alt*-S | 0.430 ± 0.010 | 0.139 ± 0.006 |
| 50HPC/50MAc-*alt*-S | 0.250 ± 0.030 | 0.400 ± 0.030 |
| 40HPC/60MAc-*alt*-S | 0.113 ± 0.009 | 0.650 ± 0.010 |
| 10HPC/90MAc-*alt*-S | 0.330 ± 0.050 | 0.370 ± 0.050 |
| HPC | 0.570 ± 0.010 | 0.100 ± 0.003 |
| $c_{pol} = 10$ mg/ml | | |
| MAc-*alt*-S | 0.290 ± 0.010 | 0.177 ± 0.005 |
| 80HPC/20MAc-*alt*-S | 0.560 ± 0.020 | 0.083 ± 0.004 |
| 50HPC/50MAc-*alt*-S | 0.019 ± 0.006 | 0.920 ± 0.020 |
| 40HPC/60MAc-*alt*-S | 0.018 ± 0.007 | 0.920 ± 0.020 |
| 10HPC/90MAc-*alt*-S | 0.340 ± 0.010 | 0.250 ± 0.010 |
| HPC | 0.570 ± 0.010 | 0.100 ± 0.030 |

0.5 for matrix where one of the components is in large excess and $n \sim 0.02$ for middle composition range. An exception is the diffusional exponent for the release from pure MAc-*alt*-S. As it has been above mentioned, in this case the components form an insoluble complex.

## 4. Conclusions

The release profile of the drugs from a system that can form interpolymer association is influenced by the mixing ratio between the components and the total polymer concentration the matrix is prepared from. For compositions close to the stoichiometry of the IPC, the release drug rate is faster, while for pure MAc-*alt*-S it takes the longest to reach the plateau. The total polymer concentration of the HPC/MAc-*alt*-S solutions influences the procaine delivery release profile especially for mixture

where one of the components is in excess. The delivery rate slows down after around 30–40 minutes.

## References

[1] Kamel S., Ali N., Jahangir K., Shah S. M., El-Gendy A. A.: Pharmaceutical significance of cellulose: A review. Express Polymer Letters, **2**, 758–778 (2008). DOI: 10.3144/expresspolymlett.2008.90

[2] Anlar S., Çapan Y., Güven O., Gögüş A., Dalkara T., Hincal A. A.: Formulation and *in vitro-in vivo* evaluation of buccoadhesive morphine sulfate tablets. Pharmaceutical Research, **11**, 231–236 (1994). DOI: 10.1023/A:1018951323522

[3] Taylan B., Çapan Y., Güven O., Kes S., Hincal A. A.: Design and evaluation of sustained-release and buccal adhesive propranolol hydrochloride tablets. Journal of Controlled Release, **38**, 11–20 (1996). DOI: 10.1016/0168-3659(95)00094-1

[4] Ikinci G., Çapan Y., Senel S., Alaaddinoglu E., Dalkara T., Hincal A. A.: In vitro/in vivo studies on a buccal bioadhesive tablet formulation of carbamazepine. Pharmazie, **55**, 762–765 (2000).

[5] Clausen A. E., Bernkop-Schnürch A.: Direct compressible polymethacrylic acid-starch compositions for site specific drug delivery. Journal of Controlled Release, **75**, 93–102 (2001). DOI: 10.1016/S0168-3659(01)00366-2

[6] Ishida M., Machida Y., Nambu N., Nagai T.: New mucosal dosage form of insulin. Chemical and Pharmaceutical Bulletin, **29**, 810–816 (1981).

[7] Callens C., Remon J. P.: Evaluation of starch-maltodextrin-Carbopol® 974P mixtures for the nasal administration. Journal of Controlled Release, **66**, 215–220 (2000).
DOI: 10.1016/S0168-3659(99)00271-0

[8] Nurkeeva Z. S., Khutoryanskiy V. V., Mun G. A., Sherbakova M. V., Ivaschenko A. T., Aitkhozhina N. A.: Polycomplexes of poly(acrylic acid) with streptomycin sulfate and their antibacterial activity. European Journal of Pharmaceutics and Biopharmaceutics, **57**, 245–249 (2004).
DOI: 10.1016/S0939-6411(03)00149-8

[9] Nurkeeva Z. S., Mun G. A., Khutoryanskiy V. V.: Interpolymer complexes of water-soluble nonionic polysaccharides with polycarboxylic acids and their applications. Macromolecular Bioscience, **3**, 283–295 (2003).
DOI: 10.1002/mabi.200390037

[10] Callens C., Adriaens E., Dierckens K., Remon J. P.: Toxicological evaluation of a bioadhesive nasal powder containing a starch and Carbopol® 974 P on rabbit nasal mucosa and slug mucosa. Journal of Controlled Release, **76**, 81–91(2001).
DOI: 10.1016/S0168-3659(01)00419-9

[11] Ozeki T., Yuasa H. and Okada H.: Controlled release of drug via methylcellulose-carboxyvinylpolymer interpolymer complex solid dispersion. AAPS PharmSciTech, **6**, E231–E236 (2005).
DOI: 10.1208/pt060233

[12] Kumar S., Himmelstein K. J.: Modification of in situ gelling behavior of carbopol solutions by hydroxypropyl methylcellulose. Journal of Pharmaceutical Sciences, **84**, 344–348 (1995).
DOI: 10.1002/jps.2600840315

[13] Srividya B., Cardoza R. M., Amin P. D.: Sustained ophthalmic delivery of ofloxacin from pH triggered in situ gelling system. Journal of Controlled Release, **73**, 205–211 (2001).
DOI: 10.1016/S0168-3659(01)00279-6

[14] Nurkeeva Z. S., Mun G. A., Khutoryanskiy V. V.: Interpolymer complexes of water-soluble non-ionic polysaccharides with polycarboxylic acids and their applications. Macromolecular Bioscience, **3**, 283–295 (2003).
DOI: 10.1002/mabi.200390037

[15] Khutoryanskiy V. V., Cascone M. G., Lazzeri L., Nurkeeva Z. S., Mun G. A., Mangazbaeva R. A.: Phase behavior of methylcellulose-poly(acrylic acid) blends and preparation of related hydrophilic films. Polymer International, **52**, 62–67 (2003).
DOI: 10.1002/pi.1004

[16] Satoh K., Takayama K., Machida Y., Suzuki Y., Nakagaki M., Nagai T.: Factors affecting the bioadhesive property of tablets consisting of hydroxypropyl cellulose and carboxyvinyl polymer. Chemical and Pharmaceutical Bulletin, **37**, 1366–1368 (1989).

[17] Bumbu G-G., Eckelt J., Vasile C., Wolf B. A.: Interpolymer complex between hydroxypropyl cellulose and maleic acid-styrene copolymer: Phase behavior of semi-dilute solutions. Macromolecular Bioscience, **5**, 936–940 (2005).
DOI: 10.1002/mabi.200500070

[18] Bumbu G. G., Vasile C., Eckelt J., Wolf B. A.: Investigation of the interpolymer complex between hydroxypropyl cellulose and maleic acid-styrene copolymer, I. Dilute solutions studies. Macromolecular Chemistry and Physics, **205**, 1869–1876 (2004).
DOI: 10.1002/macp.200400253

[19] Bumbu G. G., Vasile C., Chitanu G. C., Staikos G.: Interpolymer complexes between hydroxypropylcellulose and copolymers of maleic acid: A comparative study. Macromolecular Chemistry and Physics, **206**, 540–546 (2005).
DOI: 10.1002/macp.200400489

[20] Baker R. W.: Membrane technology and applications. McGraw-Hill, New York (2000).

[21] Schloss P., Williams C. D.: The serotonin transporter: A primary target for antidepressant drugs. Journal of Psychopharmacology, **12**, 115–121 (1998).
DOI: 10.1177/026988119801200201

[22] Halkes S. B. A.. Van den Berg A. J. J., Hoekstra M. J., Du Point J. S., Kreis R. W.: The use of tannic acid in the local treatment of burn wounds: Intriguing old and new perspectives. Wounds, **13**, 144–158, (2001).

[23] Technical Bulletin. Aqualon, a Division of Hercules Inc (1990).

[24] Chitanu G. C., Bumbu G. G., Carpov A., Vasile C.: Analysis and characterisation of maleic anhydride copolymers. II. Some aspects of thermo-oxidative decomposition. International Journal of Polymer Analysis and Characterization, **4**, 479–500 (1998).
DOI: 10.1080/10236669808009730

[25] Oh J-M., Cho C-S., Choi H-K.: A mucoadhesive polymer prepared by template polymerization of acrylic acid in the presence of poly(vinyl alcohol) for mucosal drug delivery. Journal of Applied Polymer Science, **94**, 327–331 (2004).
DOI: 10.1002/app.20911

[26] Higuchi T.: Rate of release of medicaments from ointment bases containing drugs in suspension. Journal of Pharmaceutical Sciences, **50**, 874–875 (1961).
DOI: 10.1002/jps.2600501018

[27] Gohel M. C., Panchal M. K., Jogani V. V.: Novel mathematical method for quantitative expression of deviation from Higuchi model. AAPS PharmSciTech, **1**, 43–48 (2000).
DOI: 10.1208/pt010431

[28] Ritger P. L., Peppas N. A.: A Simple equation for description of solute. Release I. Fickian and anomalous release from non-swellable devices in the form of slabs, spheres, cylinders or discs. Journal of Controlled Release, **5**, 23–36 (1987).
DOI: 10.1016/0168-3659(87)90034-4

[29] Chen J., Sun J., Yang L., Zhang Q., Zhu H., Wu H., Hoffman A. S., Kaetsu I.: Preparation and characterization of a novel IPN hydrogel memberane of poly(*N*-isopropylacrylamide)/carboxymethyl chitosan (PNIPAAM/CMCS). Radiation Physics and Chemistry, **76**, 1425–1429 (2007).
DOI: 10.1016/j.radphyschem.2007.02.045

[30] Peppas N. A.: Analysis of Fickian and non-Fickian drug release from polymers. Pharmaceutica Acta Helvetiae, **60**, 110–111 (1985).

[31] Peppas N. A.: Hydrogels in medicine and pharmacy. CRC Press, Boca Raton (1986).

[32] Peppas N. A., Sahlin J. J.: A simple equation for the description of solute release. III. Coupling of diffusion and relaxation. International Journal of Pharmaceutics, **57**, 169–172 (1989).
DOI: 10.1016/0378-5173(89)90306-2

[33] Shin-Ya Y., Tsurushima H., Tsurumi T., Kajiuchi T., Leong K. W.: Polyelectrolyte complex films derived from polyethyleneoxide-maleic acid copolymer and chitosan: Preparation and characterization. Macromolecular Bioscience, **4**, 526–531 (2004).
DOI: 10.1002/mabi.200300110

[34] de la Torre P. M., Torrado S., Torrado S.: Interpolymer complexes of poly(acrylic acid) and chitosan: Influence of the ionic hydrogel-forming medium. Biomaterials, **24**, 1459–1468 (2003).
DOI: 10.1016/S0142-9612(02)00541-0

[35] Peh K-K., Yuen K-H.: Development and in vitro evaluation of a novel multiparticulate matrix controlled release formulation of theophylline. Drug Development and Industrial Pharmacy, **21**, 1545–1555 (1995).
DOI: 10.3109/03639049509069244

[36] Korsmeyer R. W., Gurny R., Doelker E., Buri P., Peppas N. A.: Mechanisms of solute release from porous hydrophilic polymers. International Journal of Pharmaceutics, **15**, 25–35 (1983).
DOI: 10.1016/0378-5173(83)90064-9

[37] Kubo W., Miyazaki S., Attwood D.: Oral sustained delivery of paracetamol from in situ-gelling gellan and sodium alginate formulations. International Journal of Pharmaceutics, **258**, 55–64 (2003).
DOI: 10.1016/S0378-5173(03)00163-7

# The effect of pyrolytic carbon black prepared from junked tires on the properties of ethylene-propylene-diene copolymers (EPDM)

*A. Du[1*], Z. Zhang[2], M. Wu[1]*

[1]Key Laboratory of Rubber-plastics, Ministry of Education, Qingdao University of Science & Technology, Qingdao 266042, China
[2]Xuzhou College of Industrial Technology, Xuzhou 221140, China

**Abstract.** Pyrolytic carbon black (PCB) made from used tires was used in ethylene-propylene-diene copolymers (EPDM). The microstructure of PCB was characterized by scanning electron microscopy (SEM). PCB was compounded with EPDM to prepare EPDM vulcanizates. The effects of PCB on the processing properties of EPDM compounds and the mechanical properties of vulcanizates were investigated and compared with other traditional fillers such as semi-reinforcing furnace black (N774), light calcium carbonate (CaCO$_3$) and thermal black (N990). At the same time, the rheological behavior of EPDM compounds filled with different fillers was characterized by capillary rheometrics. The SEM photos showed that the particle shape was quiet different from that of CaCO$_3$ and N990, it was similar to that of N774. The primary particle size was smaller than that of N774, but the aggregate size of PCB was larger than that of N774. The effect of PCB on the processing properties of EPDM compounds was similar to that of other fillers. Among the four fillers, PCB imparted EPDM compounds with higher Mooney viscosity. With the increase of filler content, the scorch time and optimum curing time of EPDM compounds changed little. The reinforcing effect of PCB was similar to that of N990, but inferior to that of N774. With the increase of PCB content, tensile strength, tear strength, and modulus at 100% elongation of EPDM vulcanizates increased significantly. When EPDM was filled with 50 phr PCB, the tear strength of EPDM vulcanizates increased by 3 times, compared with that of EPDM gum vulcanizates. The appearance of EPDM extrudate filled with PCB was coarser than that of other fillers.

*Keywords: mechanical properties, rubber, reinforcements, pyrolytic carbon black, ethylene-propylene-diene copolymer*

## 1. Introduction

The demand for tires is increasing rapidly with the development of the car industry. At the same time, the amount of used tires is also increasing rapidly. The disposal of used tires has become an important issue worldwide and represents a major environmental problem. At present there are three kinds of methods for the reclamation of used tires; they are retreading, recycling and pyrolysis [1]. The former two methods are not the final disposal of the used tires. Pyrolysis processing of used tires is consid-

ered to be an environmentally acceptable and promising disposal method with its high-energy recovery and low pollution emission.

The main pyrolytic products of used tires are pyrolytic oil, pyrolytic gas and pyrolytic carbon black (PCB). Many scholars [2–8] home and abroad have studied the pyrolysis technology and characterized the properties of PCB. Many researchers [9–11] investigated the specific surface area and porosity of PCB. PCB can be used as fuel or as fillers in asphalt and rubbers [12–14]. There

are few reports about PCB used in rubbers. In recent years, Peng and Xiao [15] investigated the superfine grinding and surface chemical modification of PCB, and studied the effect of modified PCB on the properties of NR (natural rubber) vulcanizates. Our previous work investigated the basic characteristics of PCB and the effects of PCB on the properties of SBR (stryene butadiene rubber) [16]. In this paper, we compare the microstructure of PCB, N774, N990 and $CaCO_3$, and focus our efforts on the application of PCB in EPDM. As EPDM is a non-self-reinforcing rubber, the tensile strength of gum vulcanizates was very low. It is widely used for extruding products, such as hose and sealing strip. Various fillers showed obvious reinforcement for it. The effect of PCB on the processing properties of EPDM compounds and the mechanical properties of EPDM vulcanizates were systematically studied and compared with that of traditional carbon black and inorganic fillers.

## 2. Experimental

### 2.1. Materials

Ethylene-propylene-diene rubber (EPDM 2340A) was supplied by DSM, semi-reinforcing furnace carbon black (N774), was product of Qingdao Degussa Chem. Co. Ltd, China; thermal carbon black (N990), was product of Cabot Co., pyrolytic carbon black prepared from used tires (PCB) was supplied by Jinan Wanda New Energy Source Co. Ltd. (China), other agents were all industrial grades.

### 2.2. Morphology observation of PCB

PCB powder and other fillers were coated with a thin gold layer and examined with a JSM 6700F scanning electron microscope (SEM).

### 2.3. Compounding and sample preparation

The mixtures of rubber and all kinds of additives were prepared on a two-roller mill at room temperature. All the samples were based on 100 parts by weight of rubber. At first, activating agents (zinc oxide and stearic acid) were added into rubbers. After dispersion, fillers (N990, N774, PCB or $CaCO_3$) were added into the compounds. At last, the dicumyl peroxide (DCP) and triallyl isocyanu-

rate (TAIC) were added. The compounds were press-cured to a 2 mm thick sheet at 170°C according to the curing time predicted by the vulkameter (UCAN EK-2000P from Taiwan).

### 2.4. Rheological behavior

Mooney viscosity ($ML_{1+4}$ at 100°C) of the compounds was determined on an automated Mooney viscometer (UCAN EK-2000M from Taiwan) according to ISO 289-1. Curing characteristics were measured at 170°C using a moving-die rheometer (UCAN EK-2000P from Taiwan) according to ISO 3417.

Rheological behavior was characterized by capillary rheometry (Model RH2000, from Bohlin Company of England). Slenderness ratios of capillary are 16:1 and 0.4:1, respectively. The appearance of extrudate was observed by optical microscope (Model BX 51, from Olympus Company of Japan).

### 2.5. Measurement of mechanical properties

Tensile properties were measured with dumbbell specimens. The length of specimen was 75 mm and the cross section were 4 mm (width) × 2 mm (thickness) according to ASTM D412. Tear strength was tested according to ASTM D624 using an unnotched 90° angle test piece. Both tensile and tear tests were performed on an GT-AI-7000S (Guangzhou, China) material tester at a crosshead speed of 500 mm/min. Shore A hardness was determined using a hand-held Shore A Durometer according to ASTM D2240. All tests were carried out at 23°C.

## 3. Results and discussion

### 3.1. SEM photos of fillers

Figures 1a to 1d are SEM photos of N774 and PCB respectively. Seen from Figure 1, the particle shape of PCB is similar to that of N774, but quite different from that of N990 and $CaCO_3$. The particles of N990 are round and uniform, while the microstructure of $CaCO_3$ is flaky. The aggregation size of PCB (~10 μm) is obviously larger than that of N774 (~2 μm). At the same time, the size of N774 particle aggregation is uniform and the size distribution is narrow. Seen from Figures 1c and 1d, the basic fundamental particles of PCB are smaller
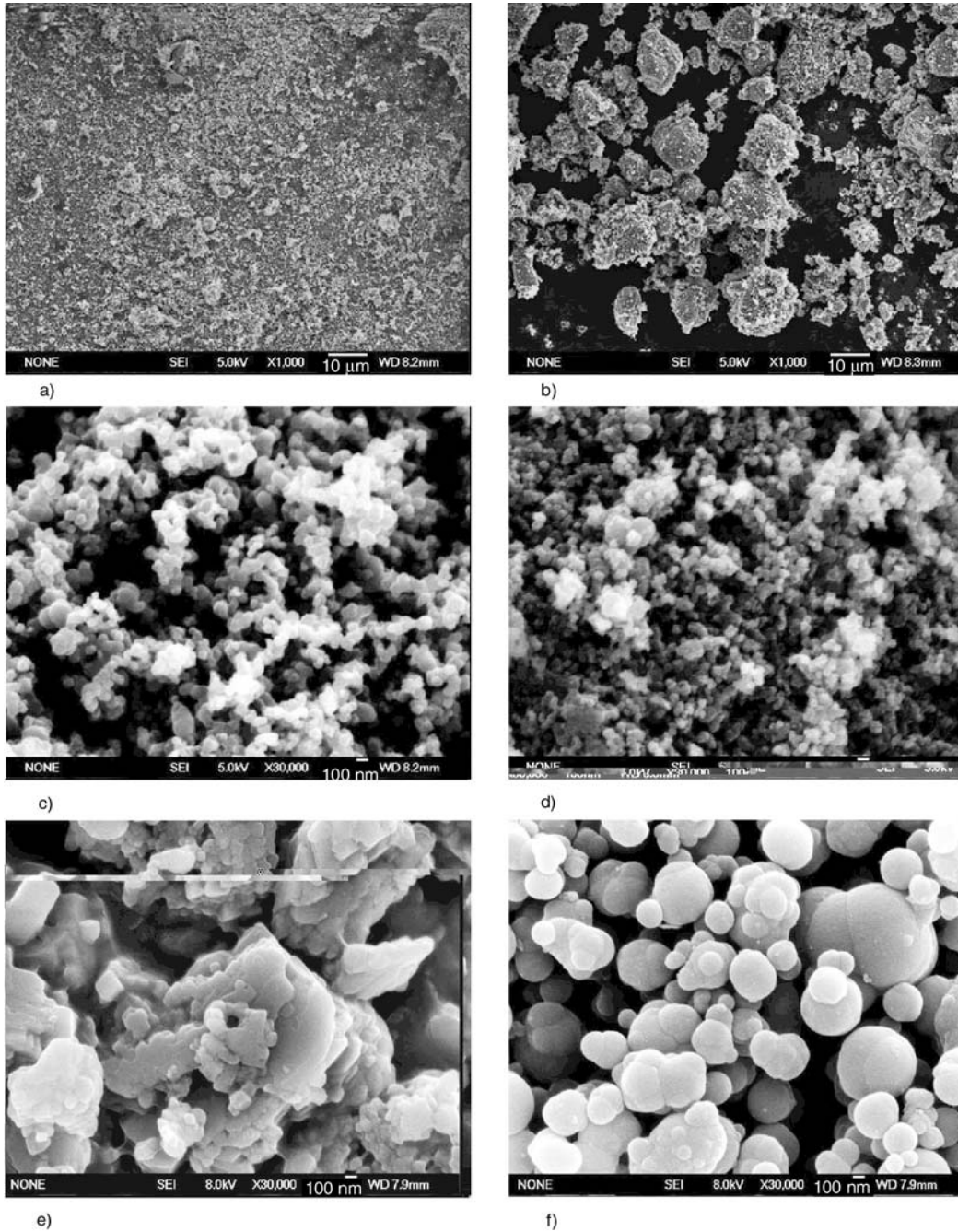
**Figure 1.** The microstructure of fillers a) N774 (×1 000); b) PCB (×1 000); c) N774 (×30 000); d) PCB (×30 000); e) CaCO$_3$ (×30 000); f) N990 (×30 000)

than that of N774, but the size distribution of PCB is wider than that of N774. Compared with the particles of CaCO$_3$ and N990, the particle size of PCB is much smaller.

## 3.2. The application of PCB in EPDM

As is well known, commercial carbon blacks show obvious reinforcing effects for rubbers. PCB is sim-ilar to commercial carbon blacks in the constitution and structure, although the ash content of PCB is more than that of other carbon blacks [16]. Here we investigate the effect of PCB on the processing and mechanical properties of EPDM vulcanizate, and, at the same time compare it with commercial carbon blacks (such as N990 and N774) and inorganic filler (CaCO$_3$).

### 3.2.1. Effect of fillers on the curing characteristics and Mooney viscosity of EPDM compounds

The effects of different fillers on the Mooney viscosity of EPDM compounds are shown in Figure 2. The Mooney viscosities of EPDM compounds increase with the incorporation of all four kinds of fillers. The Mooney viscosities of EPDM compounds filled with PCB is obviously higher than those of EPDM compounds filled with $CaCO_3$, N990 and N774. The magnitude of Mooney viscosity of EPDM filled with different fillers is as follows: PCB>N774>N990>$CaCO_3$. As well known, the effect of the particle size of filler on the Mooney viscosity of compounds is more obvious than other factors such as structure and surface activity. As shown in Figure 1, the primary particle of PCB is smaller than that of N774, which leads to the higher Mooney viscosity of EPDM compounds. The effects of different fillers on the curing characteristics of EPDM compounds are shown in Table 1. With the incorporation of fillers into EPDM, the lowest torque ($M_L$) and highest torque ($M_H$) of EPDM compounds increase. In general, $M_H - M_L$ reflects the curing state of compounds and the reinforcing effect of fillers. Here the values of $M_H - M_L$ increase with the amount of fillers. It indicates that four fillers show obvious reinforcing effect for EPDM. Compared with gum compounds, the scorch time ($t_{s1}$) and the optimum curing time ($t_{c90}$) of EPDM compounds filled with different fillers shorten. Because the four kinds of fillers are weakly alkaline, they accelerate curing. But with the increase of filler content, the $t_{c90}$ of EPDM compounds filled with different fillers change little.
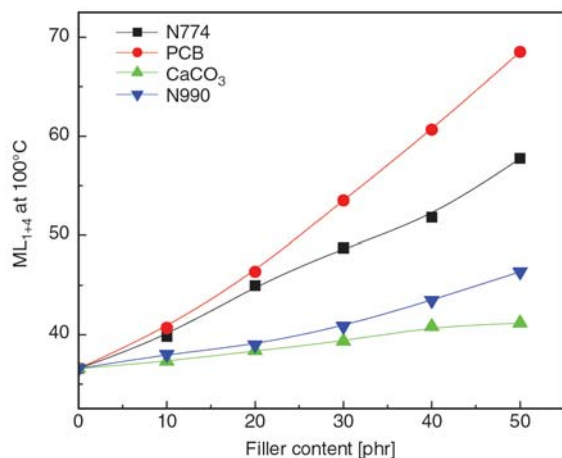
**Table 1.** The curing characteristics of EPDM compounds at 170°C

| Sample | $M_L$ [Ncm] | $M_H$ [Ncm] | $t_{c10}$ [min] | $t_{c90}$ [min] |
|---|---|---|---|---|
| 1 | 3.2 | 151.6 | 1.05 | 14.10 |
| 2 | 3.6 | 161.0 | 0.97 | 12.10 |
| 3 | 3.4 | 184.5 | 1.05 | 12.35 |
| 4 | 3.6 | 194.9 | 1.08 | 13.00 |
| 5 | 4.0 | 193.2 | 1.00 | 12.27 |
| 6 | 4.3 | 205.2 | 1.02 | 12.47 |
| 7 | 3.5 | 177.7 | 1.12 | 12.08 |
| 8 | 4.4 | 196.3 | 0.88 | 12.11 |
| 9 | 5.0 | 228.9 | 0.92 | 11.65 |
| 10 | 6.2 | 246.0 | 0.92 | 11.95 |
| 11 | 7.0 | 266.6 | 0.93 | 11.65 |
| 12 | 3.8 | 178.4 | 1.10 | 13.20 |
| 13 | 4.0 | 188.5 | 1.07 | 12.77 |
| 14 | 4.4 | 210.9 | 1.07 | 12.53 |
| 15 | 4.4 | 233.3 | 1.05 | 12.25 |
| 16 | 4.9 | 256.2 | 1.03 | 12.50 |
| 17 | 4.2 | 178.8 | 0.97 | 12.12 |
| 18 | 5.2 | 196.2 | 0.95 | 12.13 |
| 19 | 6.3 | 212.4 | 0.87 | 12.20 |
| 20 | 7.6 | 225.0 | 0.90 | 12.07 |
| 21 | 10.1 | 243.0 | 0.88 | 11.20 |

Note: 1[#]    represents the gum compounds (no filler);
2–6[#]    represent EPDM compounds filled with $CaCO_3$ (the amount of $CaCO_3$ 10–50 phr);
7–11[#]    represent EPDM compounds filled with N774 (the amount of N774 10–50 phr);
12–16[#]    represent EPDM compounds filled with N990 (the amount of N990 10–50 phr);
17–21[#]    represent EPDM compounds filled with PCB (the amount of PCB 10–50 phr)

### 3.2.2. Effect of fillers on the rheological behavior of EPDM compounds

*The viscous activation energy of EPDM compounds*

The variation in viscosity of polymer with temperature complies with the Arrhenius equation (Equation (1)):

$$\eta = A \cdot e^{\Delta E_\eta / RT} \tag{1}$$

where   $A$ – constant;   $\Delta E_\eta$ – viscous activation energy; $R$ – gas constant; $T$ – absolute temperature. The logarithmic format of Equation (1) is given in Equation (2):

$$\ln \eta = \ln A + \frac{\Delta E_\eta}{RT} \tag{2}$$

The $\ln\eta - T^{-1}$ plots of EPDM compounds filled with different fillers are shown in Figure 3. As seen from Figure 3, $\ln\eta$ is linear with $T^{-1}$. According to Equa-
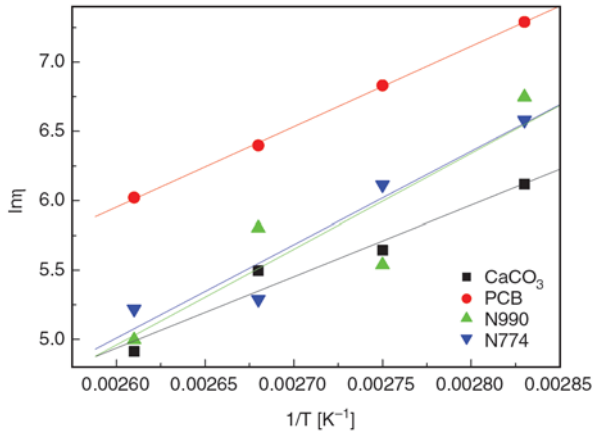


**Figure 2.** The effect of different fillers on the Mooney viscosity of EPDM compounds

**Figure 3.** The lnη–$T^{-1}$ plot of EPDM compounds filled with different fillers

**Table 2.** The viscous activation energy of EPDM compounds filled with different fillers

| Fillers | $\Delta E_\eta$ [kJ/mol] |
|---------|--------------------------|
| $CaCO_3$ | 42.86 |
| PCB | 48.32 |
| N990 | 57.45 |
| N774 | 55.97 |

force between molecules. $\Delta E_\eta$ of EPDM filled with PCB is less than that of EPDM filled with N990 and N774, but greater than that of EPDM filled with $CaCO_3$. It reveals that the reinforcing effect of PCB is inferior to that of N990 and N774, superior to that of $CaCO_3$.

tion (2), we can obtain the viscous activation energy of EPDM compounds, as shown in Table 2. $\Delta E_\eta$ reflects the minimum energy that the motion of macromolecule needs to overcome the interaction

### 3.2.3. The appearance of EPDM extrudate at different shearing rates

Figure 4 shows the appearance of EPDM extrudate at different shearing rates. As seen from Figure 4,
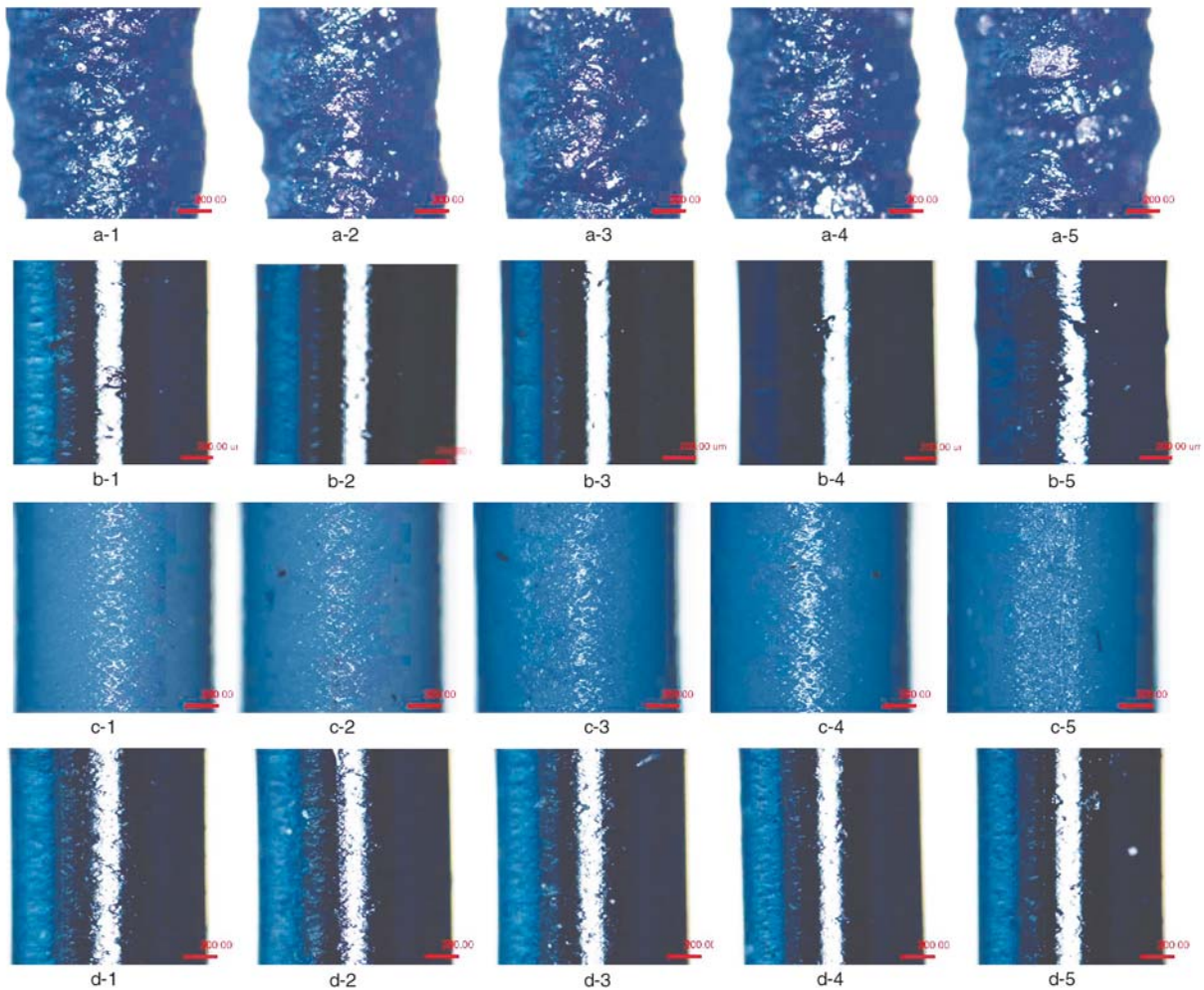


**Figure 4.** The surface appearance of EPDM compounds filled with different fillers at 110°C. a) EPDM/PCB compounds; b) EPDM/N990 compounds; c) EPDM/$CaCO_3$ compounds; d) EPDM/N774 compounds. Shearing rate/s: 1 – 23.06; 2 – 60.62; 3 – 163.92; 4 – 465.84; 5 – 1436.93.

the appearance of EPDM compounds filled with CaCO₃, N990, and N774 is smooth at low shearing rate. Even at high shearing rate, the appearance is still smooth. While the appearance of EPDM compound filled with PCB is coarse even at low shearing rate. The appearance of PCB filled EPDM compound is sausage-like. The poor appearance of PCB filled EPDM compound results from the higher Mooney viscosity of compounds. The higher the Mooney viscosity, the poorer the extruding performance.

### 3.2.4. Effect of different fillers on the mechanical properties of EPDM vulcanizates

The effects of different fillers on the mechanical properties of EPDM vulcanizates are shown in Figure 5. The four kinds of fillers showed different reinforcing effect for EPDM vulcanizates. With the increase of fillers content, the tensile strength of EPDM vulcanizates is gradually improved. Compared with the other kinds of carbon blacks (N990 and N774), the tensile strength of EPDM vulcanizates filled with PCB is lower than that of N774, and approaches to that of N990. Among the four kinds of fillers, CaCO₃ shows little reinforcing effect for EPDM vulcanizates. The tensile strength of EPDM vulcanizates change little with the incorporation of CaCO₃ into EPDM vulcanizates. The tear strength of EPDM vulcanizates is greatly improved with the increase of filler content, as shown in Figure 5b. The fillers show different effects on the tear strength of EPDM vulcanizates: N774>PCB>N990>CaCO₃. When the amount of PCB is 50 phr, the tear strength of EPDM vulcanizate is about 22 kN·m⁻¹, which is greater than that of N990 and CaCO₃, approaches to that of N774. Compared with that of gum vulcanizates, the tear strength of EPDM vulcanizates filled 50 phr PCB improved by 3 times. Although the primary particle size of PCB is smaller than that of N774, the reinforcing effect of PCB for EPDM is inferior to that of N774. It is attributed to the surface activity of filler. During the pyrolysis of used tires, the carbonaceous residue formed deposites on the surface of PCB, which covers the surface active sites of PCB [17].
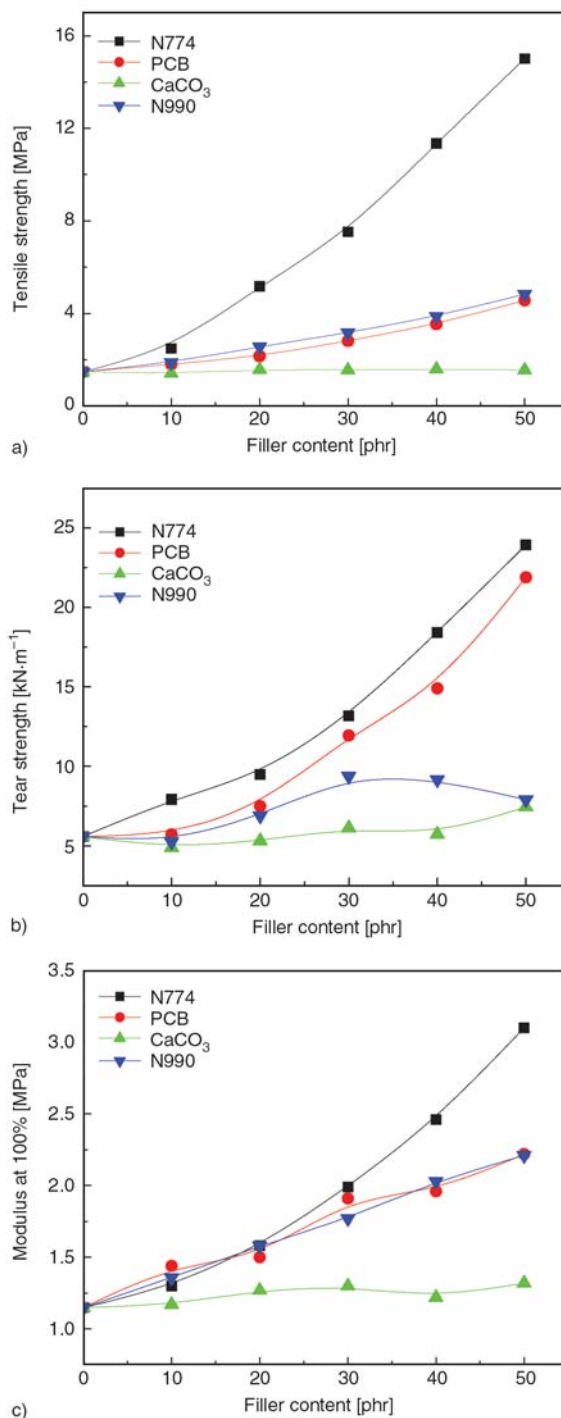


**Figure 5.** The effect of different fillers on the mechanical properties of EPDM vulcanizates

## 4. Conclusions

1) SEM photos indicate that the particle shape of PCB is quite different from that of N990 and CaCO₃, but similar to that of N774. The primary particle size of PCB is smaller than that of N774, but the aggregate size of PCB is larger than that of N774, and the size distribution is wider.

2) The effect of PCB on the processing properties of EPDM compounds is similar to that of other traditional carbon blacks. The variation of Mooney viscosity and curing characteristic of compounds with PCB content is similar to that of other general fillers (for example N990, N774 and CaCO$_3$). With the incorporation of fillers into EPDM, the scorch time and optimum curing time of EPDM compounds change little, while the Mooney viscosity increases.

3) With the increase of PCB content, the tensile strength, tear strength, modulus at 100% elongation of EPDM vulcanizates are greatly improved. With the increase of filler content, the tensile strength of EPDM vulcanizates filled with PCB approach to that of N990, while the tear strength of EPDM vulcanizates filled with PCB is superior to that of N990, and approach to that of N774. When the amount of PCB increases from 10 to 50 phr, the tear strength of EPDM vulcanizates increased by 3 times.

4) The appearance of EPDM compounds filled with PCB is sausage-like, and coarser than that of other fillers.

## References

[1] Fan R. D.: Integrate utilizing technology of scrap rubber (Chinese). Chemical Industry Press, Beijing, (1989).

[2] Olazar M., Araboiurrutia M., López G., Aguado R., Bilbao J.: Effect of acid catalysts on scrap tyre pyrolysis under fast heating conditions. Journal of Analytical and Applied Pyrolysis, **82**, 199–204 (2008).
DOI: 10.1016/j.jaap.2008.03.006

[3] Rofigul Islam M., Tushar M. S. H. K., Haniu H.: Production of liquid fuels and chemicals from pyrolysis of Bangladeshi bicycle/rickshaw tire wastes. Journal of Analytical and Applied Pyrolysis, **82**, 96–109 (2008).
DOI: 10.1016/j.jaap.2008.02.005

[4] Helleur R., Popovic N., Ikura M., Stanciulescu M., Liu D.: Characterization and potential applications of pyrolytic char from ablative pyrolysis of used tires. Journal of Analytical and Applied Pyrolysis, **58–59**, 813–824 (2001).
DOI: 10.1016/S0165-2370(00)00207-2

[5] Kaminsky W., Mennerich C.: Pyrolysis of synthetic tire rubber in a fluidized-bed reactor to yield 1,3-butadiene, styrene and carbon black. Journal of Analytical and Applied Pyrolysis, **58–59**, 803–811 (2001).
DOI: 10.1016/S0165-2370(00)00129-7

[6] Cunliffe A. M., Williams P. T.: Composition of oils derived from the batch pyrolysis of tires. Journal of Analytical and Applied Pyrolysis, **44**, 131–152 (1998).
DOI: 10.1016/S0165-2370(97)00085-5

[7] Teng H., Serio M. A., Wojtowicz M. A., Bassilakis R., Solomon P. R.: Reprocessing of used tires into activated carbon and other products. Industrial and Engineering Chemistry Research, **34**, 3102–3111 (1995).
DOI: 10.1021/ie00048a023

[8] Yang Y. R., Lü J., Chen B. C.: Surface characteristics of carbon black produced by pyrolysis of used tires (Chinese). Acta Scientiae Circumstantiae, **22**, 637–640 (2002).

[9] Ogasawaro S., Kuroda M., Wakai N.: Preparation of activated carbon by thermal decomposition of used automotive tires. Industrial and Engineering Chemistry Research, **26**, 2552–2556 (1987).
DOI: 10.1021/ie00072a030

[10] Merchant A. A., Petrich M. A.: Pyrolysis of scrap tires and conversion of chars to activated carbon. AIChE Journal, **39**, 1370–1376 (1993).
DOI: 10.1002/aic.690390814

[11] Miguel G. S., Fowler G. D., Dall'Orso M., Sollars C. J.: Porosity and surface characteristics of activated carbons produced from waste tire rubber. Journal of Chemical Technology and Biotechnology, **77**, 1–8 (2001).

[12] Yousefi A. A., Ait-Kadi A., Roy C.: Effect of used-tire-derived pyrolytic oil residue on the properties of polymer-modified asphalts. Fuel, **79**, 975–986 (2000)
DOI: 10.1016/S0016-2361(99)00216-1

[13] Leblanc J. L., Roy C., Mirmiran S., Benallal B., Schwerdtfeger A. E.: The plasticizing properties of heavy oils obtained from the vacuum pyrolysis of used tires. Kaustschuk Gummi Kunststoffe, **49**, 194–199 (1996).

[14] Roy C., Chaala A., Darmstadt H.: The vacuum pyrolysis of used tires end-uses for oil and carbon black products. Journal of Analytical and Applied Pyrolysis, **51**, 201–221 (1999).
DOI: 10.1016/S0165-2370(99)00017-0

[15] Peng X. Q., Xiao G. L.: Further processing and application of pyrolytic carbon black of used tires (Chinese). Polymer Materials: Science and Engineering, **20**, 142–144 (2004).

[16] Du A. H., Wu M. S., Su C. Y., Chen H.: The characterization of pyrolytic carbon black prepared from used tires and its application in styrene-butadiene rubber (SBR). Journal of Macromolecule Science, Part B Physics, **47**, 268-275 (2008).
DOI: 10.1080/00222340701748768

[17] Darmstadt H., Roy C., Kaliaguine S., Xu G., Auger M., Tuel A., Ramaswamy V.: Solid state $^{13}$C-NMR spectroscopy and XRD studies of commercial and pyrolytic carbon blacks. Carbon, **38**, 1279–1287 (2000).
DOI: 10.1016/S0008-6223(99)00259-6

# Synergistic effects of Na+-montmorillonite and multi-walled carbon nanotubes on mechanical properties of chitosan film

*J. P. Zhang*[1,2], *A. Q. Wang*[1*]

[1]Center of Eco-material and Green Chemistry, Lanzhou Institute of Chemical Physics, Chinese Academy of Sciences, Lanzhou, 730000, P.R. China
[2]Graduate University of the Chinese Academy of Sciences, Beijing, 100049, P.R. China

**Abstract.** Chitosan/Na+-montmorillonite/multi-walled carbon nanotubes (CTS/MMT/MWCNTs) nanocomposite films were prepared by a simple solution-evaporation method. The effects of MMT and MWCNTs on mechanical properties of the nanocomposite films were investigated. The results indicate that the simultaneously introduced MMT and MWCNTs into CTS film could greatly improve the mechanical properties. The Young's modulus of the CTS film is increased about 50% as 1.0 wt% MMT and 1.0 wt% MWCNTs are introduced. The MMT could compensate the negative effect of MWCNTs on elongation at break of the CTS film. The highest elongation at break is obtained when the contents of MMT and MWCNTs are 0.5 and 0.5 wt%, respectively. Formation of the MMT···CTS···MWCNTs subassembly may be responsible for the observed synergistic effect of MMT and MWCNTs on mechanical properties of the CTS film.

*Keywords: nanocomposites, chitosan, films, mechanical properties, multi-walled carbon nanotubes*

## 1. Introduction

Chitosan (CTS), a high molecular weight polysaccharide from chitin, is the most abundant biomass in the world. Because of unique structure (active $-NH_2$ and $-OH$) and properties (bioactive, biocompatibility, biodegradability, antibacterial activities, etc.), CTS is still intensively investigated now and has been widely applied in various fields including controlled drug delivery, food packaging film, artificial skin, water treatment, biosensor, and so on [1–3]. CTS is frequently used in the form of film because of its good film-forming character, high hydrophilicity and low density. Recently, various composite films based on CTS and nanoparticles have been explored focused on improving the low mechanical property and brittleness of the neat CTS films. The introduced functional nanoparticles (such as silica [4], montmorillonite [5] and organic

rectorite [6]) could endow the neat CTS film with novel properties including electronic conductivity and sterilization [5, 7].

Carbon nanotubes (CNTs) have been widely focused in nanoscience since their discovery in 1991 [8]. The preparation of nanocomposites based on CNTs is one of the hot topics in the CNTs field [9, 10] because of their unique properties such as high modulus, high intrinsic electrical conductivity, small size and high thermal conductivity [11, 12]. CNTs have been proved to be advanced multi-functional fillers in polymer-based nanocomposites [13, 14]. IR photoresponse of CNTs is dramatically enhanced by embedding CNTs into the polycarbonate matrix [15]. However, the strong cohesive nature and low stability of CNTs in solution discourage greatly their manipulation and widespread applications in many fields [16, 17]. Considerable

---

investigations have been done to overcome these problems by introducing appropriate solubilization groups (such as $-COO^-$, $-SO_3^-$ and $-NH_3^+$) either to the end or to the side wall of CNTs through a covalent or noncovalent way [18–20]. Various polymers, including peptides, amylase, DNA, poly(acrylic acid), CTS, etc., have been used to disperse CNTs through a noncovalent way and to keep the unique properties of CNTs [3]. Among them, the CTS/CNTs system is especially interesting because the introduced CTS endows CNTs with biocompatibility. Consequently, the CTS/CNTs system acquires electronic and optical properties and biocompatibility, which make the biological and medicinal applications of CNTs possible. The CTS/CNTs system has been used for the preparation of biosensors of cholesterol, glucose, DNA, etc. [21, 22]. Mechanical properties (including the tensile modulus and strength) of CTS film could be greatly improved by introducing only 0.8 wt% of CNTs [2]. However, the elongation at break of the neat CTS film decreased with the introduction of CNTs.

Polymer/layered silicate nanocomposites frequently exhibit remarkably improved mechanical and materials properties (such as a higher modulus, increased strength, decreased gas permeability and increased biodegradability of biodegradable polymers), and are attracting considerable interest in the polymeric materials field [23]. $Na^+$-montmorillonite (MMT) is one of the most important layered silicates used for the preparation of these organic-inorganic nanocomposites. MMT is composed of an aluminate sheet sandwiched between two silicate sheets stacked together by weak ionic and van der Waals forces which make MMT easily to be intercalated and/or exfoliated [24]. Swelling ratio and mechanical behavior of the poly(*N*-isopropylacrylamide) hydrogel were improved by the introduction of MMT [25]. The $-NH_2$ groups of CTS are protonated in acidic aqueous solution and could intercalate into layers of MMT to form the CTS/MMT nanocomposites [5]. The CTS/MMT nanocomposite film was seldom investigated until now although the CTS/MMT systems have been applied in many fields.

Considering the high performance and unique properties of CTS, CNTs and MMT, the combination of them may generate a novel material which holds great potential for pharmaceutical and bio-

logical applications. In the present work, the CTS/MMT/multi-walled carbon nanotubes (CTS/MMT/MWCNTs) nanocomposite films are prepared by introducing MMT and MWCNTs into neat CTS film through a simple solution-evaporation method, and the synergistic effects on the mechanical properties of nanocomposite films are investigated.

## 2. Experimental

### 2.1. Materials

CTS (the deacetylation degree is 0.85, average molecular weight is $90 \cdot 10^4$) was supplied by Zhejiang Yuhuan Ocean Biology Co. (Zhejiang, China). MMT with a cation-exchange capacity of 102.8 mmol/100 g was supplied by Longfeng Montmorillonite Co. (Shandong, China) and was milled through a 320-mesh screen before use. MWCNTs (purity > 95%, diameter = 20~40 nm) prepared using the chemical vapor deposition method were purchased from Shenzhen Nanotech Port Co., Ltd. (China). The catalyst in the MWCNTs was removed by concentrated nitric acid, and then filtered and washed with double-distilled water until pH > 5. All solutions were prepared with double-distilled water.

### 2.2. Preparation of the CTS/MMT/MWCNTs nanocomposite films

The CTS/MMT/MWCNTs nanocomposite films were prepared according to the following procedure. 7.0 g of CTS was dissolved in 273 ml of the aqueous solution of acetic acid (2% v/v) to form the aqueous solution of CTS (2.5 wt%). Appropriate amount of MMT and MWCNTs were suspended in 8.0 ml double-distilled water with sonication for 20 min at 25°C, 40 kHz and 100 W. Subsequently, 48.75 g of the above aqueous solution of CTS was charged into the MMT/MWCNTs mixture and mechanically stirred at 1000 rpm for 1h followed by 20 min at 12 000 rpm, and then sonicated for 20 min to facilitate the intercalation of MMT and the dispersion of MWCNTs. After that, the CTS/MMT/MWCNTs mixture was poured into a glass dish (7 cm×13 cm) and the water was evaporated at 50°C. The uniform nanocomposite films with an average thickness of 40 μm were then obtained and no further treatment was employed. The weight

ratio of MMT and MWCNTs ($m_{MMT}$:$m_{MWCNTs}$ = 1:1) to the total solid is kept at 0, 0.2, 0.5, 1.0, 2.0 and 5.0 wt%. The CTS/MMT and CTS/MWCNTs nanocomposite films were prepared according to the same procedure. The weight ratio of MMT or MWCNTs to the total solid is kept at 0, 0.2, 0.5, 1.0, 2.0 and 5.0 wt%.

## 2.3. Tensile test

The tensile tests were carried out using a New SANS universal material testing system (CMT 4304) at room temperature with gauge length of 10 mm and crosshead speed of 2 mm/min. Measurements were carried out in sextuple and the averaged results were shown.

## 2.4. Characterization

X-ray diffraction (XRD) analyses of the specimens were performed using an X-ray diffractometer with Cu anode (PAN alytical Co. X'pert PRO), running at 40 kV and 30 mA, scanning from 1 to 10° with a step size of 0.0167°. The micrographs of samples were taken using field emission scanning electron microscopy (FE-SEM, JSM-6701F, JEOL, Ltd). Before FE-SEM observation, all samples were fractured with liquid nitrogen, and then fixed on copper stubs and coated with gold.

## 3. Results and discussion

### 3.1. XRD analysis

XRD patterns of CTS, MMT and MWCNTs are shown in Figure 1a. As can be seen, the typical diffraction peak of MMT is observed at $2\theta = 6.94°$ corresponding to a basal spacing of 1.274 nm, whereas, CTS and MWCNTs show no diffraction peak in the $2\theta$ range investigated. The typical diffraction peak of MMT at $2\theta = 6.94°$ disappears after incorporated into CTS (CTS/MMT) or simultaneously incorporated into CTS with MWCNTs (CTS/MMT/MWCNTs) as shown in Figure 1b, which indicates that MMT is exfoliated by CTS and the exfoliated nanostructure is formed. The –$NH_2$ groups of CTS convert to positively charged –$NH_3^+$ groups under acidic medium. A part of –$NH_3^+$ groups could exchange with $Na^+$ ions between layers of MMT through a cation exchange process and intercalate into layers of MMT [26].
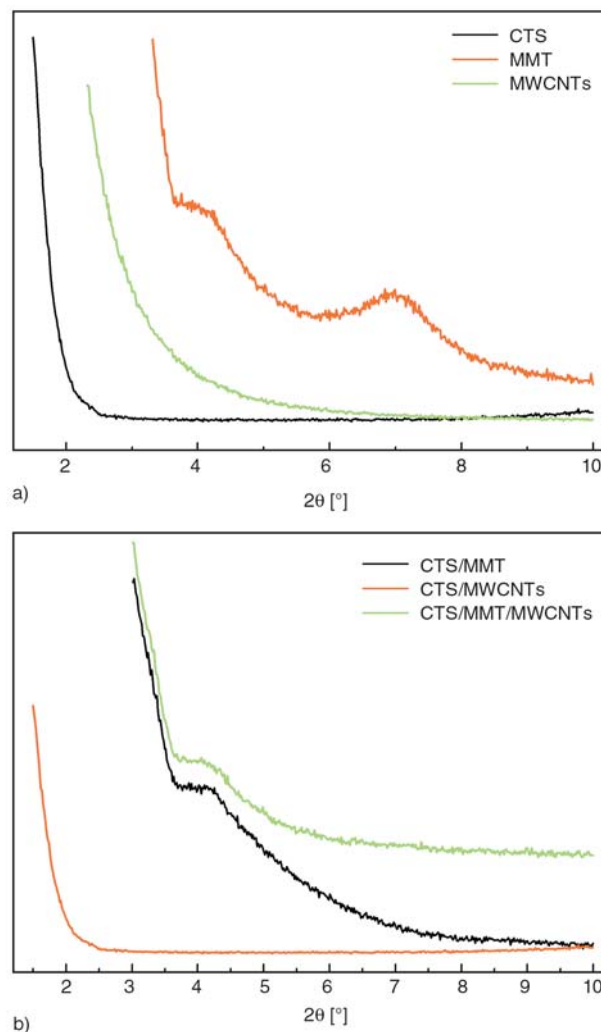


**Figure 1.** a) XRD patterns of CTS, MMT and MWCNTs and b) XRD patterns of the CTS/MMT (2.0 wt% MMT), CTS/MWCNTs (2.0 wt% MWCNTs) and CTS/MMT/MWCNTs (1.0 wt% MMT, 1.0 wt% MWCNTs) nanocomposite films

The –$NH_3^+$ groups of CTS could bind tightly to the negative sites of MMT [5]. In addition, the hydrogen bonding between –$NH_2$ and –OH groups of CTS and the layers of MMT also facilitates the intercalation of CTS chains. It also can be seen from Figure 1b that the introduced MWCNTs does not show obvious influence on the XRD patterns of CTS/MWCNTs and CTS/MMT/MWCNTs. This result indicates that the interaction between CTS and MWCNTs does not form any new crystalline structure or influence the intercalation of CTS into layers of MMT. Similar effect of MWCNTs on the XRD pattern of CTS has also been observed by Wang *et al*. [2]. It should be noted that factors like line broadening and MMT dilution may also contribute to the observed disappearance of diffraction peak of MMT according to Eckel *et al*. [27].

## 3.2. Morphology analysis

Figure 2 shows FE-SEM images of the fracture surfaces of the neat CTS film and the CTS/MMT/MWCNTs nanocomposite film. As shown in Figure 2a, the neat CTS film shows a smooth and tight fracture surface. An almost homogeneous dispersion of MMT (indicated with circles) and MWCNTs (indicated with rectangles) is observed throughout the CTS matrix as shown in Figure 2b except for some small aggregates of MMT on the top of the graph. Consequently, an effective three-dimensional network is constructed and the CTS/MMT/MWCNTs nanocomposite film is formed with MMT and MWCNTs as inorganic crosslinkers. It also can be seen from Figure 2b that there are some bubbles around the homogeneously dispersed MMT and MWCNTs, which may be attributed to their strong interfacial interaction with the CTS matrix. CTS has good film-forming character, however, the formed neat CTS film is mechanically
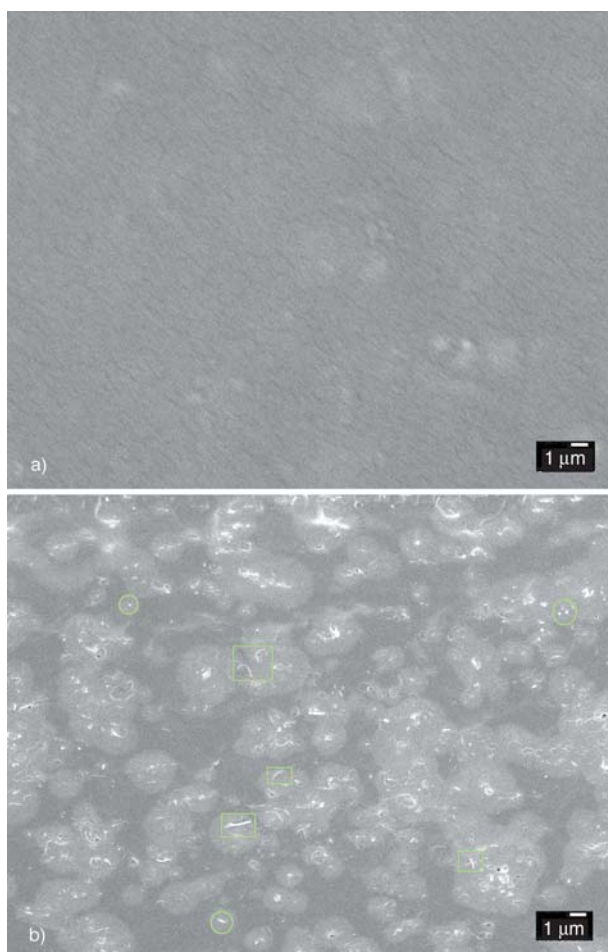


**Figure 2.** FE-SEM images of the fracture surfaces of a) CTS film and b) CTS/MMT/MWCNTs (1.0 wt% MMT, 1.0 wt% MWCNTs) nanocomposite film

weak and brittle. CTS chains could intercalate into layers of MMT and disperse MMT and MWCNTs uniformly according to Figures 1 and 2 and the previously reported literatures [2, 5, 20, 26]. The homogeneously dispersed MMT and MWCNTs act as bones of the CTS film, which may improve mechanical properties of the neat CTS film.

## 3.3. Mechanical properties

Figure 3a shows the effect of the content of incorporated MMT, MWCNTs, MMT and MWCNTs on Young's modulus of the nanocomposite films. As can be seen, the introduced functional additives impact Young's modulus of the CTS film markedly and differently. The Young's modulus increases gradually from 3378 to 4798 MPa with increasing MMT content from 0 to 5.0 wt%. The variation of Young's modulus with MWCNTs content exhibits an obviously different tendency. The Young's modulus firstly increases with increasing MWCNTs content from 0 to 2.0 wt%, and then decreases evidently with further increasing MWCNTs content to 5.0 wt%. For the CTS/MMT/MWCNTs nanocomposite film, the Young's modulus firstly increases greatly with increasing MMT and MWCNTs content, and then decreases slightly with further increasing their content. The highest Young's modulus of 5081 MPa is obtained when the contents of MMT and MWCNTs are 0.5 and 0.5 wt%, respectively. It can be concluded from Figure 3a that the incorporation of appropriate amount of MMT or MWCNTs could improve Young's modulus of the CTS film evidently. In addition, a synergistic effect of MMT and MWCNTs on Young's modulus of the CTS film is observed when the total content of MMT and MWCNTs is less than 2.0 wt%, which indicates that the introduction of two functional additives with different properties and structure (such as MMT and MWCNTs) may open a new approach for further improving mechanical properties of materials. The slight decrease of Young's modulus for the CTS/MMT/MWCNTs nanocomposite film with further increasing MMT and MWCNTs content is attributed to the negative effect of the further increased MWCNTs. The variation of tensile strength of the CTS/MMT, CTS/MWCNTs and CTS/MMT/MWCNTs nanocomposite films is similar to that of Young's modulus as shown in Figure 3b.
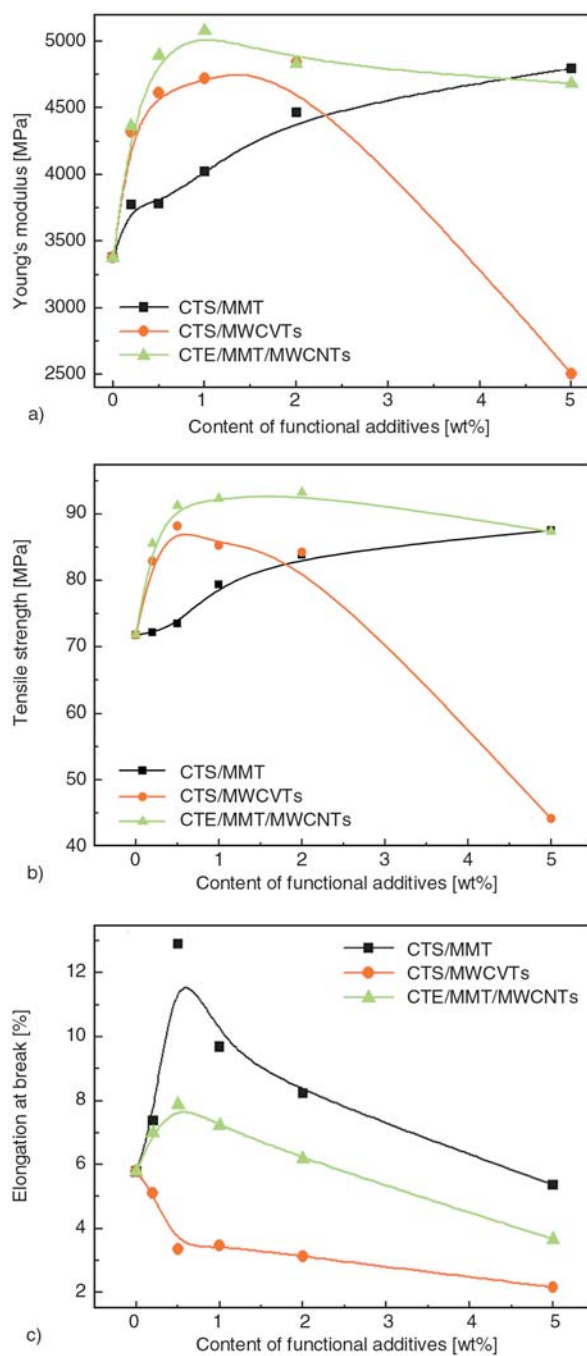
**Figure 3.** Variation of a) Young's modulus and b) elongation at break for the CTS/MMT, CTS/MWCNTs and CTS/MMT/MWCNTs nanocomposite films with content of MMT, MWCNTs, MMT and MWCNTs, respectively

Variation of elongation at break for the CTS/MMT, CTS/MWCNTs and CTS/MMT/MWCNTs nanocomposite films with content of MMT, MWCNTs, MMT and MWCNTs is shown in Figure 3c. The elongation at break of the CTS/MMT nanocomposite film increases from 5.78 to 12.91% with increasing MMT content from 0 to 0.5 wt%, and then decreases to 5.37% with further increasing

MMT content to 5.0 wt%. The introduction of MMT is often detrimental to the ductility of polymer materials. However, modified MMT could improve ductility of polymers as have been reported previously [28]. The key difference is the modification of MMT could enhance the interfacial interaction between MMT and the polymers. In this study, CTS acts as not only a polymer matrix, but also a modifier of MMT, which could intercalate into layers of MMT and enhance the interfacial interaction between CTS and MMT. Consequently, the elongation at break is improved. Unlike the positive effect of MWCNTs on Young's modulus and tensile strength of the CTS/MWCNTs nanocomposite film, the elongation at break of CTS/MWCNTs decreases gradually with increasing MWCNTs content. Similar phenomenon had also been observed by Wang *et al.* in the chitosan/carbon nanotube composites [2]. The introduction of MMT into the CTS/MWCNTs nanocomposite film could remedy the negative effect of MWCNTs on the elongation at break. The highest elongation at break is obtained when the contents of MMT and MWCNTs are 0.5 and 0.5 wt%, respectively.

## 3.4. Mechanism for the synergistic effect of MMT and MWCNTs

According to the results of Figure 3, the introduction of MMT and MWCNTs simultaneously could evidently improve mechanical properties of the neat CTS film owing to the synergistic effect of MMT and MWCNTs. Figure 4 schematically shows the synergistic effect of MMT and MWCNTs. The positively charged polymeric chains of CTS could intercalate into layers of MMT through a cation exchange process and cause the exfoliation of the weakly linked MMT sheets. The positively charged polymeric chains of CTS could adsorb onto the surface of MWCNTs and act as polymeric cationic surfactants in acidic medium. The positively charged polymeric chains of CTS repulse one another and are extended in acidic solution owing to the protonated –NH$_2$ groups, and then the homogeneous dispersion of MWCNTs is formed. Thus, there are two subassemblies in the acidic aqueous solution of CTS/MMT/MWCNTs: (1) exfoliated and homogeneously dispersed negative charged MMT sheets by positively charged polymeric chains of CTS; (2) homogeneously dispersed
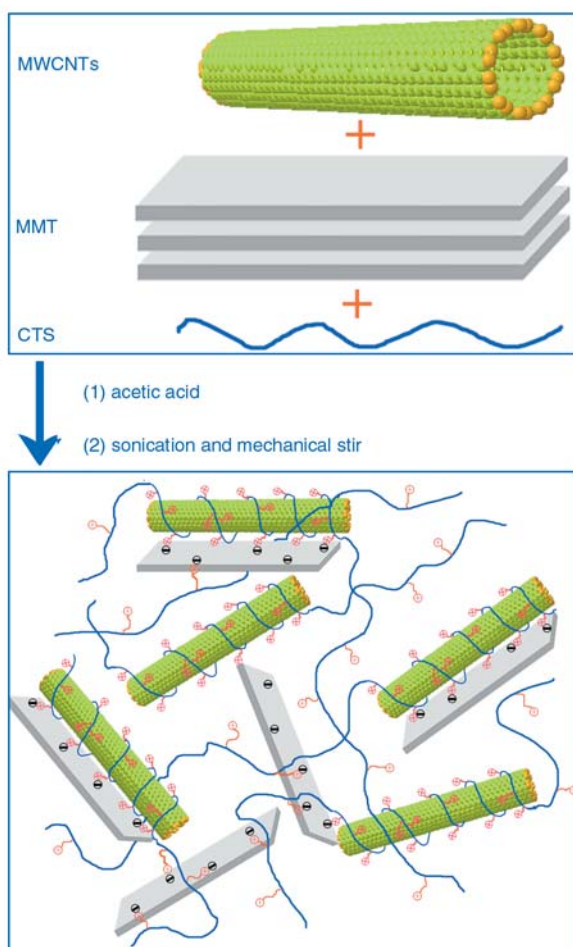
**Figure 4.** Schematic structure of the CTS/MMT/MWCNTs nanocomposite film

MWCNTs wrapped by positively charged polymeric chains of CTS. The $-NH_3^+$ groups on the chains of CTS adsorbed on the surface of MWCNTs could also interact with the negative charged MMT sheets and form the third MMT···CTS···MWCNTs subassembly which may be responsible for the synergistic effect of MMT and MWCNTs on mechanical properties of the neat CTS film.

## 4. Conclusions

The novel CTS/MMT/MWCNTs nanocomposite films were successfully prepared by the simple solution-evaporation method. The synergistic effect of MMT and MWCNTs on mechanical properties of the nanocomposite film is obviously observed. The Young's modulus of the neat CTS film is greatly improved by the introduction of MMT and MWCNTs simultaneously. The introduction of MMT into the CTS/MWCNTs nanocomposite film could remedy the negative effect of

MWCNTs on the elongation at break. The $-NH_3^+$ groups of CTS wrapped on the surface of MWCNTs could interact with the negative charged MMT sheets and form the MMT···CTS···MWCNTs subassembly which may be responsible for the synergistic effect of MMT and MWCNTs on mechanical properties of the neat CTS film. The introduction of two functional additives with different properties and structure for the improvement of material's properties may be applicable to other materials.

## References

[1] Tiwari A., Singh V.: Synthesis and characterization of electrical conducting chitosan-graft-polyaniline. Express Polymer Letters, **1**, 308–317 (2007).
DOI: 10.3144/expresspolymlett.2007.44
[2] Wang S-F., Shen L., Zhang W-D., Tong Y-J.: Preparation and mechanical properties of chitosan/carbon nanotubes composites. Biomacromolecules, **6**, 3067–3072 (2005).
DOI: 10.1021/bm050378v
[3] Zhang J. P., Wang Q., Wang A.: Synthesis and characterization of chitosan-*g*-poly(acrylic acid)/attapulgite superabsorbent composites. Carbohydrate Polymers, **68**, 367–374 (2007).
DOI: 10.1016/j.carbpol.2006.11.018
[4] Chen J. H., Liu Q. L., Fang J., Zhu A. M., Zhang Q. G.: Composite hybrid membrane of chitosan-silica in ervaporation separation of MeOH/DMC mixtures. Journal of Colloid and Interface Science, **316**, 580–588 (2007).
DOI: 10.1016/j.jcis.2007.09.022
[5] Darder M., Colilla M., Ruiz-Hitzky E.: Biopolymer-clay nanocomposites based on chitosan intercalated in montmorillonite. Chemistry of Materials, **15**, 3774–3780 (2003).
DOI: 10.1021/cm0343047
[6] Wang X. Y., Du Y. M., Luo J. W., Lin B. F., Kennedy J. F.: Chitosan/organic rectorite nanocomposite films: Structure, characteristic and drug delivery behaviour. Carbohydrate Polymers, **69**, 41-49 (2007).
DOI: 10.1016/j.carbpol.2006.08.025
[7] Lau C., Cooney M. J., Atanassov P.: Conductive macroporous composite chitosan-carbon nanotube scaffolds. Langmuir, **34**, 7004–7010 (2008).
DOI: 10.1021/la8005597
[8] Iijima S.: Helical microtubules of graphitic carbon. Nature, **354**, 56–58 (1991).
DOI: 10.1038/354056a0

[9] Qiao R., Ke P. C.: Lipid-carbon nanotube self-assembly in aqueous solution. Journal of the American Chemical Society, **128**, 13656–13657 (2006).
DOI: 10.1021/ja063977y

[10] Klink M., Ritter H.: Supramolecular gels based on multi-walled carbon nanotubes bearing covalently attached cyclodextrin and water-soluble guest polymers. Macromolecular Rapid Communications, **29**, 1208–1211 (2008).
DOI: 10.1002/marc.200800142

[11] Williams K. A., Veenhuizen P. T. M., de la Torre B. G., Eritja R., Dekker C.: Nanotechnology: Carbon nanotubes with DNA recognition. Nature, **420**, 761 (2002).
DOI: 10.1038/420761a

[12] Keren K., Berman R. S., Buchstab E., Sivan U., Braun E.: DNA-templated carbon nanotube field-effect transistor science. Science, **302**, 1380–1382 (2003).
DOI: 10.1126/science.1091022

[13] Dubois P., Alexandre M.: Performant clay/carbon nanotube polymer nanocomposites. Advanced Engineering Materials, **8**, 147–154 (2006).
DOI: 10.1002/adem.200500256

[14] Kim J. B., Premkumar T., Lee K., Geckeler K. E.: A facile approach to single-wall carbon nanotube/poly(allylamine) nanocomposites. Macromolecular Rapid Communications, **28**, 276–280 (2007).
DOI: 10.1002/marc.200600627

[15] Pradhan B., Setyowati K., Liu H. Y., Waldeck D. H., Chen J.: Carbon nanotube-polymer nanocomposite infrared sensor. Nano Letters, **8**, 1142–1146 (2008).
DOI: 10.1021/nl0732880

[16] Numata M., Asai M., Kaneko K., Bae A-H., Hasegawa T., Sakurai K.: Inclusion of cut and as-grown single-walled carbon nanotubes in the helical superstructure of schizophyllan and curdlan (β-1,3-glucans). Journal of the American Chemical Society, **127**, 5875–5884 (2005).
DOI: 10.1021/ja044168m

[17] Lu X., Imae T.: Dendrimer-mediated synthesis of water-dispersible carbon-nanotube-supported oxide nanoparticles. The Journal of Physical Chemistry C, **111**, 8459–8462 (2007).
DOI: 10.1021/jp0702999

[18] Tasis D., Tagmatarchis N., Bianco A., Prato M.: Chemistry of carbon nanotubes. Chemical Reviews, **106**, 1105–1136 (2006).
DOI: 10.1021/cr050569o

[19] Holzinger M., Abraham J., Whelan P., Graupner R., Ley L., Hennrich F.: Functionalization of single-walled carbon nanotubes with (R-)oxycarbonyl nitrenes. Journal of the American Chemical Society, **125**, 8566–8580 (2003).
DOI: 10.1021/ja029931w

[20] Zhang J. P., Wang Q., Wang L., Wang A. Q.: Manipulated dispersion of carbon nanotubes with derivatives of chitosan. Carbon, **45**, 1917–1920(2007).
DOI: 10.1016/j.carbon.2007.05.007

[21] Yang M. H., Jiang J. H., Yang Y. H., Chen X., Shen G., Yu R.: Carbon nanotube/cobalt hexacyanoferrate nanoparticle-biopolymer system for the fabrication of biosensors. Biosensors and Bioelectronics, **21**, 1791–1797 (2006).
DOI: 10.1016/j.bios.2005.09.004

[22] Li J., Liu Q., Liu Y., Liu S., Yao S.: DNA biosensor based on chitosan film doped with carbon nanotubes. Analytical Biochemistry, **346**, 107–114 (2005).
DOI: 10.1016/j.ab.2005.07.037

[23] Ray S. S., Okamoto M.: Polymer/layered silicate nanocomposites: A review from preparation to processing. Progress in Polymer Science, **28**, 1539–1641 (2003).
DOI: 10.1016/j.progpolymsci.2003.08.002

[24] Liang L., Liu J., Gong X. Y.: Thermosensitive poly(*N*-isopropylacrylamide)-clay nanocomposites with enhanced temperature response. Langmuir, **16**, 9895–9899 (2000).
DOI: 10.1021/la000270v

[25] Xia X. H., Yih J., D'Souza N. A., Hu Z. B.: Swelling and mechanical behavior of poly(*N*-isopropylacrylamide)/namontmorillonite layered silicates composite gels. Polymer, **44**, 3389–3393 (2003).
DOI: 10.1016/S0032-3861(03)00228-3

[26] Zhang J. P., Wang L., Wang A. Q.: Preparation and properties of chitosan-*g*-poly(acrylic acid)/montmorillonite superabsorbent nanocomposite via in situ intercalative polymerization. Industrial and Engineering Chemistry Research, **46**, 2497–2502 (2007).
DOI: 10.1021/ie061385i

[27] Eckel D. F., Balogh M. P., Fasulo P. D., Rodgers W. R.: Assessing organo-clay dispersion in polymer nanocomposites. Journal of Applied Polymer Science, **93**, 1110–1117 (2004).
DOI: 10.1002/app.20566

[28] Ray S. S., Bousmina M., Okamoto K.: Structure and properties of nanocomposites based on poly(butylene succinate-co-adipate) and organically modified montmorillonite. Macromolecular Materials and Engineering, **290**, 759–768 (2005).
DOI: 10.1002/mame.200500203

# Ethylene-octene copolymer (POE) toughened polyamide 6/polypropylene nanocomposites: Effect of POE maleation

*M. U. Wahit*[1*], *A. Hassan*[1], *Z. A. Mohd Ishak*[2], *T. Czigány*[3]

[1]Faculty of Chemical and Natural Resources Engineering, Universiti Teknologi Malaysia, 81310 Skudai, Johor, Malaysia
[2]School of Materials and Mineral Resources Engineering, Universiti Sains Malaysia, Engineering Campus, 14300 Nibong Tebal, Penang, Malaysia
[3]Department of Polymer Engineering, Faculty of Mechanical Engineering, Budapest University of Technology and Economics, H-1111 Budapest, Műegyetem rkp. 3, Hungary

**Abstract.** Ethylene-octene elastomer (POE) and ethylene-octene elastomer grafted maleic anhydride (POEgMAH) toughened nanocomposites of polyamide 6/polypropylene (PA6/PP) containing 4 wt% organophilic modified montmorillonite (MMT) were produced by melt compounding followed by injection moulding. The PA6/PP composition was kept constant (PA6/PP = 70/30 parts) while the elastomer (either POE or POEgMAH) content varied between 5 and 20 wt%. PP grafted maleic anhydride (PPgMAH) was used to compatibilize the blend system. The impact strength of the nanocomposite system was examined by the conventional Izod impact test at room temperature (RT). In addition, linear elastic fracture mechanics (LEFM) approach was used to study the fracture response of the notched three point bending type specimens at room temperature (RT) and –40°C. Fracture surfaces of the broken specimens were examined using scanning electron microscopy. The results show that while POEgMAH can remarkably improve the compatibility between PA6 and the elastomer thus increasing the toughness, the unmodified POE has less significant contribution to PA6/PP/organoclay toughness. Elastomer domains of POEgMAH show a finer and more uniform dispersion than that of POE in the PA6/PP/organoclay matrix. It is also observed that the toughness increased with the increasing elastomer concentration for both unmaleated and maleated POE.

**Keywords:** *nanocomposites, fracture toughness, impact strength, linear elastic fracture mechanics, ethylene-octene elastomer*

## 1. Introduction

Polymer-layered silicate nanocomposites have attracted increasing interest from both scientific and industrial perspectives because this new class of materials shows significant improvements in mechanical properties, barrier properties and thermal resistance at lower clay loading compared to pristine matrix [1]. In the last few years, much effort has been devoted to develop the thermoplastic nanocomposites based on blends of two or more polymeric materials, i.e. binary or ternary blends [2–6].

However, for any single thermoplastics nanocomposites system such as polyamide 6 (PA6) nanocomposites, incorporation of organoclay at high loading usually resulted in a severe embrittlement manifested in a drop of the impact strength and elongation at break [2, 7, 8]. For the thermoplastic blend nanocomposites system, Chow *et al.* [3] reported that PA6/PP nanocomposites exhibited

improvement in modulus and strength as compared to the pristine PA6/PP but at the expense of toughness. A similar observation has also been reported for micro-composites based on another blend system [5].

The most widely applied method to overcome this drawback is blending with elastomers such as maleated ethylene-propylene copolymer (EPRgMAH) [3, 7] and maleated styrene-ethylene-butadiene-styrene rubber (SEBSgMAH) [9–11]. According to González *et al.* [11], the addition of up to 6% of an organoclay to a 70/30 PA6/SEBSgMAH blend led to ternary compounds combining the stiffness improvement due to the inclusion of clay and the toughening effect of the rubber. It was shown that in the 70/30 blend with 3% organoclay, supertough behaviour of the nanocomposite was accomplished with a modulus increase of 44% with respect to the pure PA6 matrix.

However, to our knowledge not many papers had attempted to examine the fracture toughness of rubber toughened PA6/PP nanocomposites using linear elastic fracture mechanics (LEFM) approach. The objective of our study is to investigate the effectiveness of ethylene-octene elastomer (POE) and ethylene-octene elastomer grafted maleic anhydride (POEgMAH) as an impact modifier for PA6/PP/organoclay blends system using conventional Izod impact test and LEFM approach. POE, a relatively novel polyolefin elastomer, was developed by Dow Chemical Co. using a metallocene catalyst. Compared with EPR, POE typically exhibits easier mixing and better dispersion when blended with PP [7, 12–14]. In our previous work, POE was used as a toughening agent to form rubber-toughened PA6/PP nanocomposites [7, 14, 15]. The result showed that the addition of POE to the PA6/PP (70/30) nanocomposites improved the toughness of the nanocomposites but with limited success due to insufficient compatibility between PA6 and POE.

Conventionally, toughness has been characterized by the Izod impact test. However, the Izod impact test data cannot be used for design purposes, although they can be used for comparing the toughness between different polymer systems. With the objective to characterize toughness of polymer nanocomposites with greater accuracy, many researchers have adopted fracture mechanics approach in their studies [2, 16, 17].

Furthermore, the toughness evaluation of PA6/PP/elastomer nanocomposites, particularly fracture toughness, has not been systematically investigated. Only few studies can be found in the literature on the fracture behavior of PA6/PP/elastomer nanocomposites. The results from our previous work have shown that for PA6/PP blend with the 70/30 blend ratio, the toughness of the blends increased significantly while the strength and stiffness of PA6 was not much affected as compared to other blend ratio i.e. 60/40 and 50/50 [7]. This is the reason why in this study varying amount of unmaleated and maleated POE have been incorporated to 70/30 PA6/PP nanocomposites. Particular attention will also be paid to the fracture toughness of the nanocomposites system measured using LEFM.

## 2. Materials and sample preparation

The blends used in this work are described in Table 1. The PP (SM 240) was obtained from Titan PP Polymers, Johor Bahru, Malaysia. The melt flow index (MFI) and density were 25 g/10 min and 0.9 g/cm$^3$ respectively. The PA6 (Amilan CM 1017) was a commercial product of Toray Nylon

**Table 1.** PA6/PP (70/30) nanocomposites blend composition [wt%]

| Designation | Composition | PA6/PP (70/30) | PPgMA | Organoclay 1.30 TC | POE | POEgMAH |
|---|---|---|---|---|---|---|
| BC | PA6/PP/PPgMAH | 95 | 5 | | | |
| BC/F | PA6/PP/PPgMAH/1.30TC | 91 | 5 | 4 | | |
| BC/F/E5 | PA6/PP/PPgMAH/1.30TC/POE | 86 | 5 | 4 | 5 | |
| BC/F/E10 | PA6/PP/PPgMAH/1.30TC/POE | 81 | 5 | 4 | 10 | |
| BC/F/E15 | PA6/PP/PPgMAH/1.30TC/POE | 76 | 5 | 4 | 15 | |
| BC/F/E20 | PA6/PP/PPgMAH/1.30TC/POE | 71 | 5 | 4 | 20 | |
| BC/F/mE5 | PA6/PP/PPgMAH/1.30TC/POEgMAH | 86 | 5 | 4 | | 5 |
| BC/F/mE10 | PA6/PP/PPgMAH/1.30TC/POEgMAH | 81 | 5 | 4 | | 10 |
| BC/F/mE15 | PA6/PP/PPgMAH/1.30TC/POEgMAH | 76 | 5 | 4 | | 15 |
| BC/F/mE20 | PA6/PP/PPgMAH/1.30TC/POEgMAH | 71 | 5 | 4 | | 20 |

Resin AMILAN, Tokyo, Japan. The MFI at 230°C and 2.16 kg load and the density were 35 g/10 min and 1.14 g/cm³, respectively. The maleated PP (PPgMA) was Orevac CA 100 with ~ 1 wt% maleic anhydride (MA) produced by ATOFINA, Duteaux, France. The impact modifier, POE grade Engage 8150, was supplied by DuPont Dow Elastomers, Wilmington DE, USA. Its octene content and melt flow rate were 25 wt% and 0.5 g/10 min, respectively. Ethylene octane elastomer grafted maleic anhydride (POEgMAH) Fusabond NMN 493 D (medium MAH graft level) was a commercial product of Dupont, Wilmington DE, USA. Its melt flow index is 1.6 g/10 min. The organoclay (Nanomer 1.30TC) was a commercial product of Nanocor Inc., Arlington Heights IL, USA. It was a white powder containing montmorillonite (MMT) (70 wt%) intercalated by octadecylamine (30 wt%). Following pre-designed composition ratios, PA6, PP, PPgMAH, MMT and elastomer were dry blended in a tumble mixer, and then compounded by the simultaneous addition of all components to a Berstoff co-rotating twin screw extruder. The barrel temperature was maintained at 200, 220, 230 and 240°C from hopper to die, and the screw rotation speed was fixed at 50 rpm. Prior to blending, PA6 pellets were dehumidified using a dryer at 80°C for 8 h. The extruded materials were injection moulded into standard tensile, flexural and Izod impact specimens using a JSW Model NIOOB II injection-moulding machine with a barrel temperature of 210–240°C. Specimens were tested dry, as moulded.

## 2.1. Izod impact test

The notched Izod impact strength of the materials was measured with a Toyoseiki impact tester according to ASTM D256 (A). All specimens had a dimension of 62 mm×12.3 mm×3.2 mm. For each kind of blend, five specimens were tested and the average value is given.

## 2.2. Fracture toughness

The fracture toughness of the various nanocomposites systems was determined at high test speed. The notched three point bending bars were fractured by an instrumented impact pendulum (CEAST) equipped with DAS 800 advanced data acquisition unit at an impact velocity of $v = 3.7$ m/s, both at
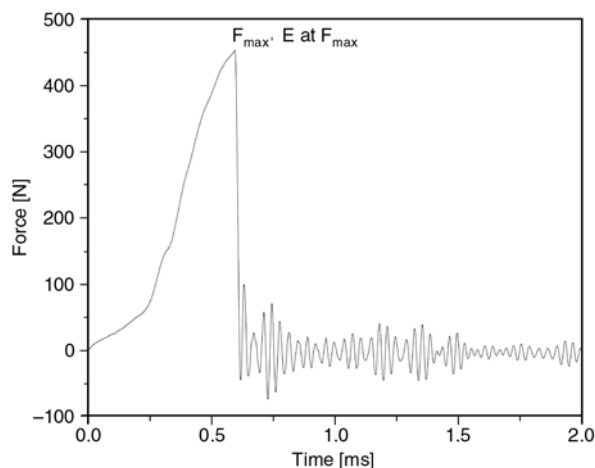


**Figure 1.** Characteristic force-time traces due to the impact of notched Charpy specimens

room temperature (RT) and –40°C. The notch was produced by saw and razor blade tapping. Impacting of the specimens occurred under the following conditions: mass of the striker: 2.19 kg; striker working range: 0.545 kN.

From the fractograms recorded as shown as an example in Figure 1, the maximum load ($F_{max}$), and the energy absorbed up to $F_{max}$ (energy required for fracture initiation, $E_{init}$) were analyzed. For $K_c$ (based on $F_{max}$) and $G_c$ (based on $E_{init}$) determination, the method adopted in ISO13586 was used [18].

## 3. Results and discussion

### 3.1. Effect of elastomer content

The Izod impact strength and fracture toughness, $K_c$ and fracture energy, $G_c$ of the neat PA6/PP blends and PA6/PP/organoclay nanocomposites as control materials are listed in Table 2. It is noted that the addition of 4 wt% organoclay has reduced the toughness of the nanocomposites. The Izod impact strength was reduced from 8.6 to 5.3 kJ/m², which is about 40%. Wang *et al.* [19] reported that the impact strength decreased from 115 J/m for the

**Table 2.** Mechanical properties of the neat PA6/PP (70/30) and the PA6/PP (70/30)/organoclay

| Properties | Testing condition | System | |
|---|---|---|---|
| | | BC | BC/F |
| Impact strength [kJ/m²] | RT | 8.6 | 5.3 |
| $K_c$ [MPa·m¹ᐟ²] | RT | 3.1 | 2.4 |
| $K_c$ [MPa·m¹ᐟ²] | –40°C | 2.7 | 2.0 |
| $G_c$ [kJ/m²] | RT | 8.0 | 5.6 |
| $G_c$ [kJ/m²] | –40°C | 3.5 | 3.3 |

neat PA6/PP to 17 J/m for PA6/PP filled with 5 wt% organoclay.

According to Stevenson [20], there are two main reasons why fillers have detrimental effects on the impact resistance. The first reason is that a significant volume fraction of the polymer, which can dissipate stress through the shear yielding or crazing mechanism, is replaced by the filler, which generally cannot deform and dissipate stress easily. The ability of the material to dissipate stress is therefore reduced. However, this is particularly true at high concentration of filler. The second reason is that certain fillers may hinder the local chain motions of the polymer molecules that enable them to shear yield, what can sharply decrease the impact resistance of the materials. It is also possible that polymer nanocomposites inherently contain incomplete dispersion of nanoparticles, which form aggregates that causes premature crack formation due to poor adhesion between nanparticles and matrix. The presence of exfoliated nanoparticles may also restrict molecular mobility of the surrounding matrix material, which in turn leads to the reduction of impact strength and toughness [21]. However, this drawback is believed to be overcome by the incorporation of a rubber phase.

In the subsequent steps, this research has been directed towards improving the toughness of PA6/PP nanocomposites by the incorporation of POE as an impact modifier. The notched Izod impact strength of the ternary blend nanocomposites is shown as a function of POE concentration in Figure 2. The effect of POE concentration on the Izod impact strength was measured at *RT*. A minor increment in impact strength was obtained with
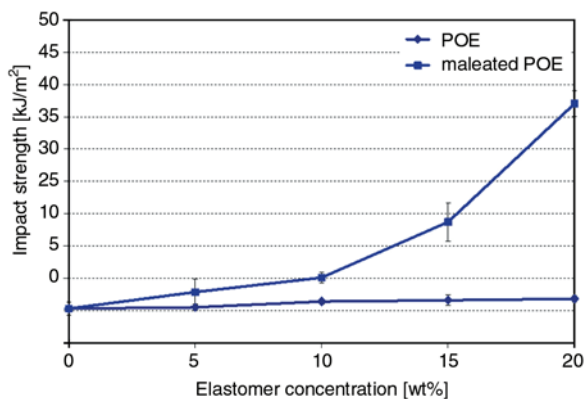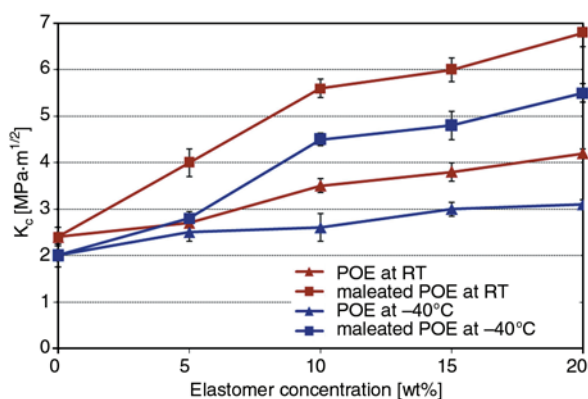


**Figure 3.** Effect of elastomer content on the $K_c$ of rubber-toughened PA6/PP nanocomposites at high test speed
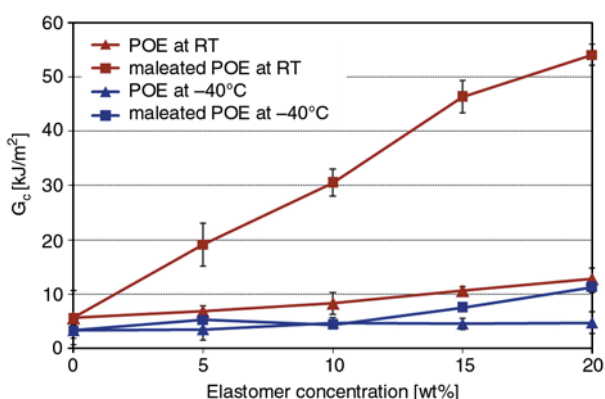


**Figure 4.** Effect of elastomer content on the $G_c$ of rubber-toughened PA6/PP nanocomposites at high test speed



**Figure 2.** Effect of elastomer concentration on the Izod impact strength of rubber-toughened PA6/PP nanocomposites

increasing POE concentration in the blends despite the fact that POE is incompatible with PA6.

The variation of $K_c$ and $G_c$ of all nanocomposites as a function of POE loading at two different temperatures are shown in Figures 3 and 4. As expected, $K_c$ and $G_c$ show a similar trend with Izod impact strength where it increases linearly with increasing POE loading. It is also observed in Figures 3 and 4 that the all nanocomposites exhibit higher value of $K_c$ and $G_c$ at RT than at –40°C.

The enhancement in the toughness could be explained as follows; when PPgMAH was added to PA6/PP, the interfacial adhesion between PA6 and PP was improved by forming PA6gPP copolymer [3, 14]. In addition to that, due to the structural similarity, there is a possible intermolecular attraction (physical entanglement) between PP and POE. As a result, the formation of PA6gPP and physical entanglement PP/POE contributed to the improvement of the compatibility between PA6 and POE. In addition, it is speculated that hydrogen bonding
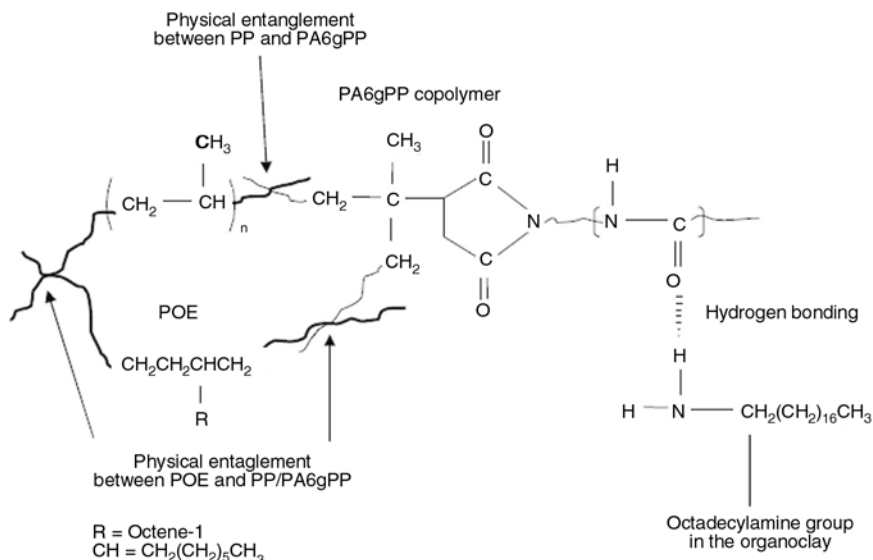
**Figure 5.** Interaction of POE and PA6gPP

could form between the amide group of the PA6gPP copolymer and the octadecylamine group of the organoclay intercalant. Figure 5 shows the proposed interaction between POE and PA6gPP copolymer nanocomposites.

Although the incorporation of POE elastomer did increase the toughness of the nanocomposites, the extent of toughening even at high POE content is well below that achieved without organoclay reinforcement. In other words, the addition of POE is not able to fully compensate the reduction in toughness caused by the organoclay. This limited improvement showed that the compatibilization of PA6/PP blends using PPgMAH is insufficient to ensure the compatibility of POE and PA6. In addition, the limited improvement of toughness properties may also be attributed to high polarity differences between POE and PA6, making this binary blend an immiscible system [3, 7, 14, 15, 22]. The problems of incompatibility can be overcome by the incorporation of either a block or graft copolymer having segments that may interact with each polymer component, or functionalized polymer that reacts with one or both polymers, leading to *in-situ* compatibilization during mixing process [23–25].

### 3.2. Effect of rubber functionality

Figure 2 shows the effect of rubber functionality on the impact strength of the nanocomposites. It is interesting to note that the impact strength of the

nanocomposites toughened by POEgMAH (10 wt%) increased around twice higher than that of pure PA6/PP blend and PA6/PP/organoclay. This indicates the effectiveness of POEgMAH as a toughening agent for PA6 as well as a compatibilizer for the PA6/PP blends. The increase in impact strength suggested better stress transfer across the interfaces in the nanocomposites and blends containing maleated rubber [26]. According to Yu *et al.* [23], if the rubber phase is highly dispersed, it acts as an effective stress concentrator and enhances both crazing and shear yielding in the matrix. Since both processes can dissipate large amounts of energy, there is a significant increase in the toughness of the blends.

Characteristic force-time traces registered during fracture of the notched three point bending specimens for the PA6/PP nanocomposites toughened by POE and maleated POE (10 wt%) are shown in Figure 6. Both samples fractured in brittle manner, hence the specimens broke immediately once $F_{max}$ was reached. However, from the fractograms, it is revealed that the Fmax value of the latter is higher compared to the former which leads to the higher $K_c$ value.

The effect of maleated POE loading on the Izod impact strength, $K_c$ and $G_c$ of the nanocomposites are shown in Figures 3 and 4. It can be seen that in all cases the Izod impact strength, $K_c$ and $G_c$ of the nanocomposites increase with the elastomer content. The significant enhancement of the Izod impact strength, $K_c$ and $G_c$ of the POEgMAH sys-
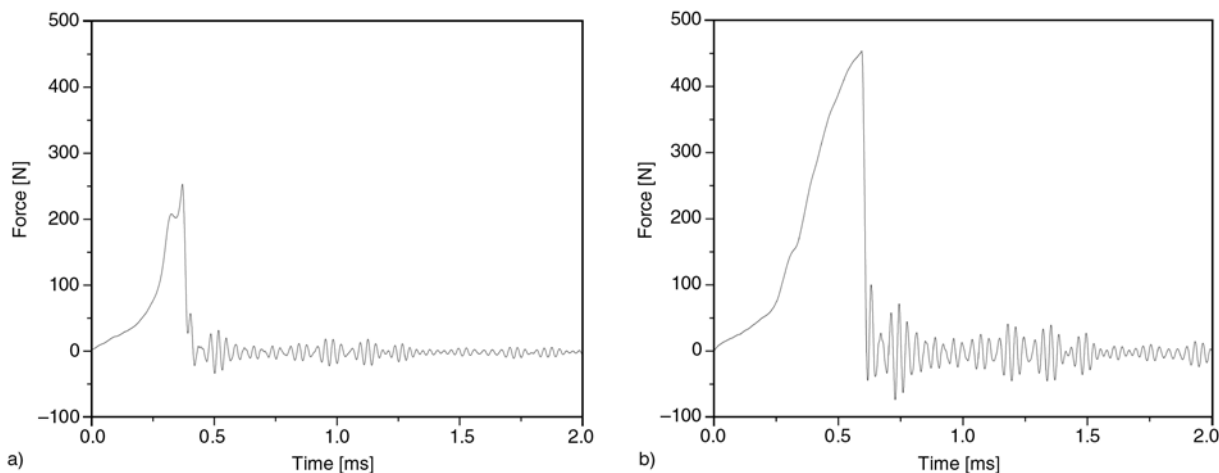
**Figure 6.** Comparison of *F–t* (*RT*) traces of impacted notched Charpy specimens of a) PA6/PP/organoclay/POE,
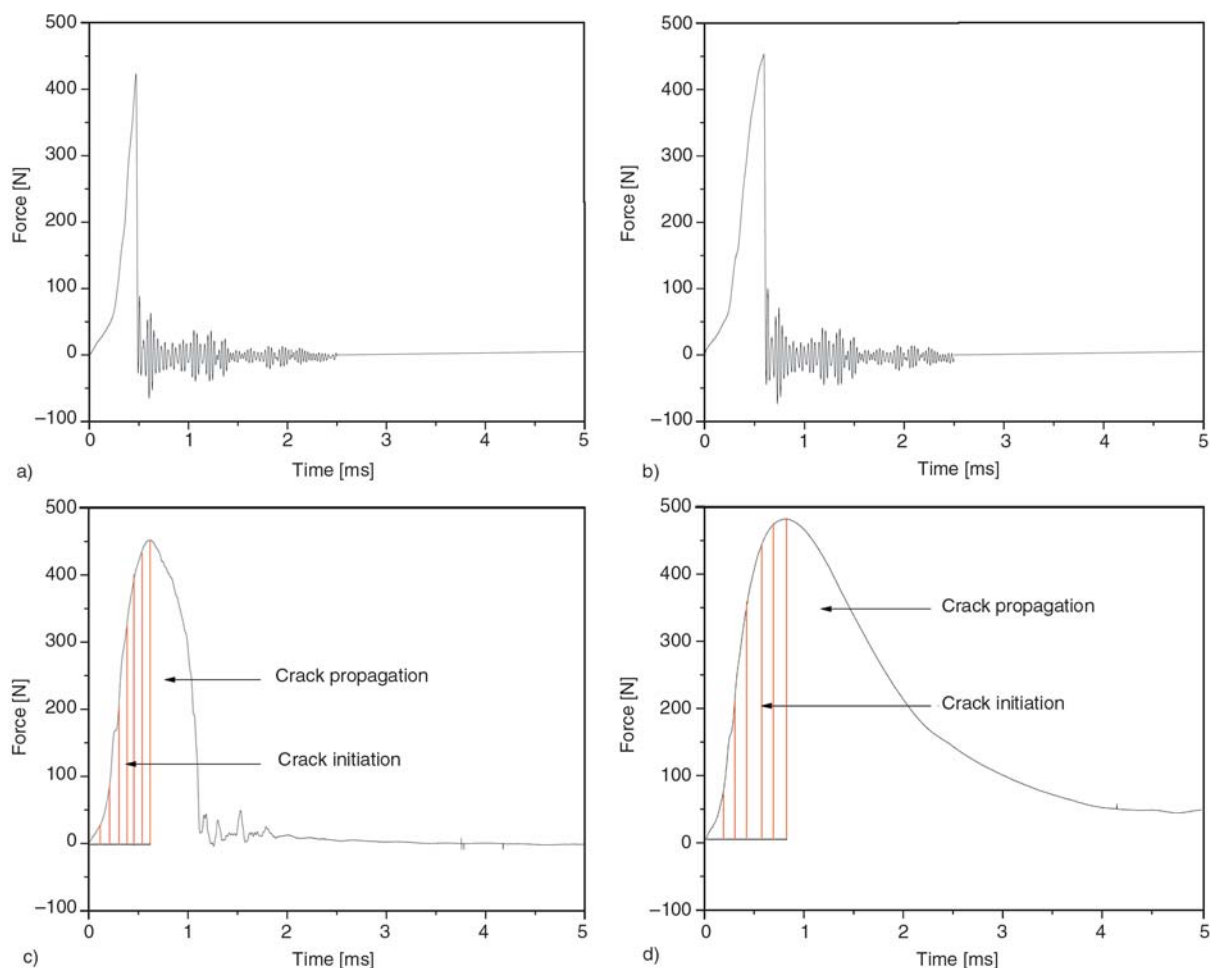b) PA6/PP/organoclay/POEgMAH



**Figure 7.** Comparison of *F–t* (*RT*) traces of impacted notched Charpy specimens of POEgMAH toughened
PA6/PP/organoclay with different POEgMAH concentration a) 5, b) 10, c) 15, d) 20 wt%

tem compared to POE system was observed. It was also found that the increment of the Izod impact strength is noteworthy for the nanocomposites with higher maleated POE content reaching a value of 37 kJ/m² , which is more than four times higher than

that of the PA6/PP blends. Figure 7 shows the *F–t* fractograms of the POEgMAH toughened PA6/PP nanocomposites with different concentrations of POEgMAH. It can be seen that the Fmax value increased as the POEgMAH concentration

increased. It is interesting to note that by comparing the *F–t* traces in Figure 7b and Figure 7c, the improvement in toughness of the nanocomposites becomes more apparent. The fractograms indicate that the nanocomposites failed in controlled fractured mode with considerable crack propagation (Figures 7c and 7d).

These phenomena were caused by the presence of the anhydride group of POEgMAH that reacts with the terminal amino group of PA6 during melt compounding and forms the PA6 grafted POE (PA6gPOE) copolymer subsequently as schematically shown in Figure 8. The formation of PA6gPOE will improve the interfacial bonding between PA6 and PP. Figure 9 shows the proposed interaction between the POEgMAH, PA6gPP, PP and organoclay. This behaviour confirms previously published results demonstrating that SEBS-gMAH is an efficient compatibilizer as well as impact modifier for PA6/PP blends [22]. Li *et al.* [27] in their work on nylon 11/POE have revealed that all nylon 11/POEgMAH blends showed higher impact strength than nylon11/POE. Yu *et al.* [23] obtained around five times improvement in the notched impact strength of PA6 with the incorporation of 20 wt% of maleated POE.

The elastomer functionality is also expected to have an important effect on the morphology of the blends, and this issue is examined here. Figure 10 presents the SEM micrograph taken from the cryogenically fractured surfaces of PA6/PP nanocomposites toughened with POE and POEgMAH. As shown in Figure 10a, it is observed that the separated spherical particles are mainly POE and the black pits correspond to sites where POE particles were extracted from the PA6/PP matrix. The immiscibility of POE and PA6 resulted in the phase separation of POE particles in the blends. The edges of the holes where POE have been extracted are quite smooth. This confirms that a weak interfacial adhesion is present between the two phases and reveals low compatibility between PA6 and POE. On the contrary, the SEM micrograph of PA6/PP/organoclay/POEgMAH as shown in Figure 10b presents the homogenous character of the morphology of the blends. Fewer particles are observed on the fracture surface of nanocomposites with maleated POE. The fracture surface is also characterized by a non-broken PA6/POEgMAH interface. Therefore, the
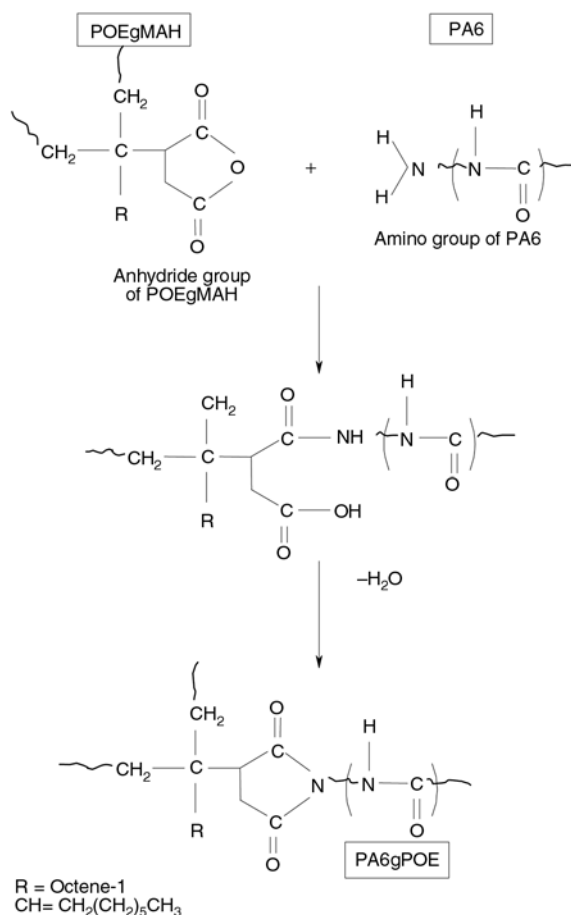


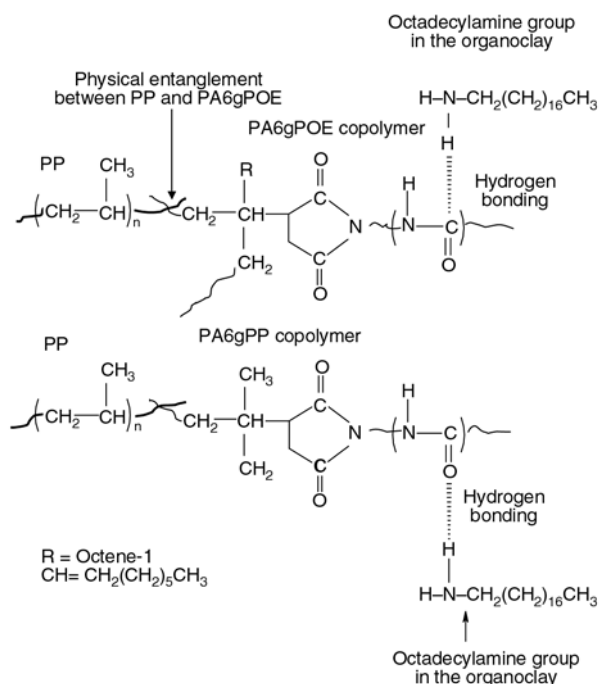**Figure 8.** Possible chemical reactions between PA6 and POEgMAH



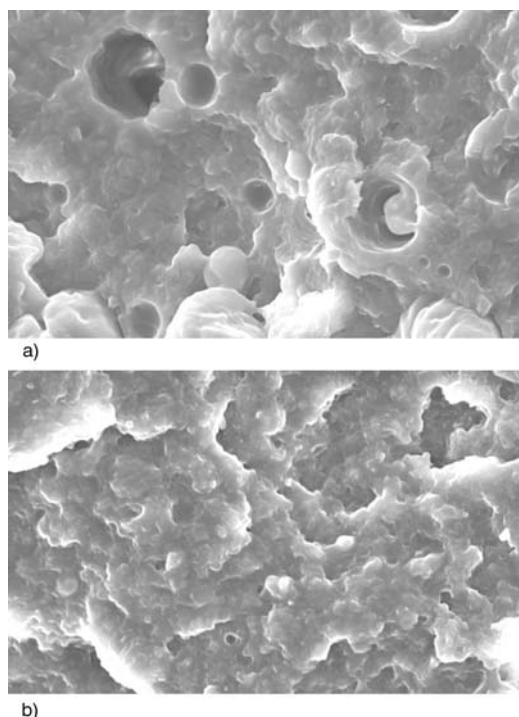**Figure 9.** Interaction of PA6gPOE, PA6gPP, PP and organoclay

**Figure 10.** SEM micrograph of cryogenically fractured surfaces of the PA6/PP/organoclay toughened by: a) POE, b) POEgMAH

phase boundary is almost indistinguishable in this blend.

From the measurement of a set of SEM micrographs on cryo-fractured surfaces, the size distribution of the POE domain is shown in Figure 11a. In comparison with maleated POE data in Figure 11b, the dispersed maleated POE phase exhibits a smaller size. The nanocomposites containing 10 wt% POEgMAH show a morphology of fine particles with an average diameter of 0.96 µm, which is relatively smaller than those observed in the nanocomposite blends of unmaleated POE (1.50 µm) of the same composition (see Table 3). Besides that, the maleated POE particles are also
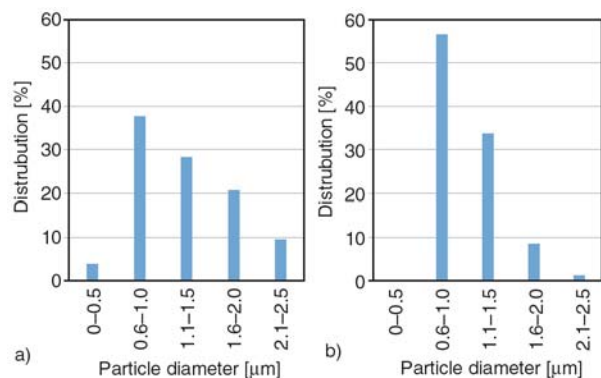


**Figure 11.** Histograms of elastomer particle size in PA6/PP/ organoclay a) POE, b) maleated POE

**Table 3.** The average of POE particle size in PA6/PP (70/30) nanocomposites with POE and POEgMAH

| Blend/Elastomer | Diameter range [µm] | Average particle diameter [µm] |
|---|---|---|
| BC/F/E10 | 0.50–2.30 | 1.50 |
| BC/F/mE10 | 0.65–2.00 | 0.96 |

more uniformly distributed as shown in Figure 11b. This conceptually suggested that the incorporation of POEgMAH makes the POE particles smaller and results in a finer dispersion of POE particles in the PA6/PP matrix due to the reduction of the interfacial tension of the blend. Similar findings have been reported for PA6/POEgMAH blends [26]. The enthalpy of the system that drove the POEgMAH grafted PA6 to the interface was reported to cause an increase in the interfacial area and a reduction in rubber particles size.

The SEM micrographs of the fracture surfaces taken after the impact test of the nanocomposites toughened with 20 wt% of POE and maleated POE are shown in Figure 12. It can be noted that the impact strength of the nanocomposites with POE is 6.8 kJ/m$^2$, while that of the nanocomposites with maleated POE is 37 kJ/m$^2$. It is evident that the morphologies of the fracture surfaces of the two blends are quite different. In case of the nanocom-
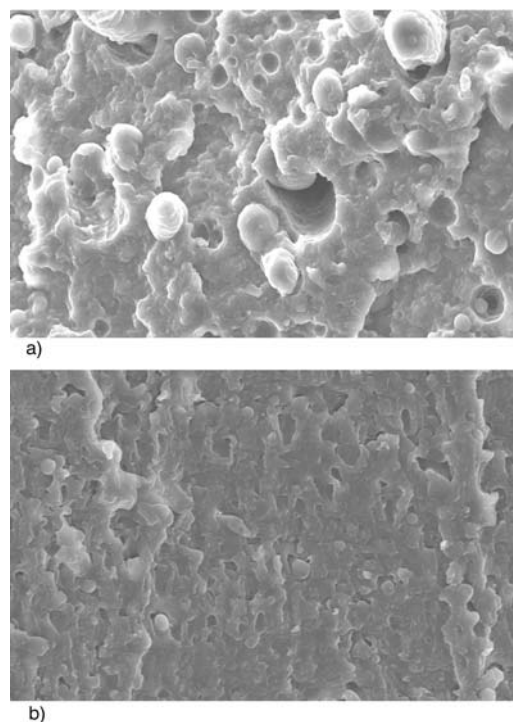


**Figure 12.** SEM micrograph of impact fracture surfaces of PA6/PP/organoclay with 20 wt% elastomer content a) POE, b) POEgMAH

posites containing POE, large holes, formed by the removing of the POE particles, are clearly observed. Moreover, it can be seen that the fracture surface is smooth, indicating that the matrix PA6/PP fractures in a brittle manner during impact. In case of nanocomposites containing maleated POE, the holes are slightly elongated or distorted and the outline of the holes is indistinct. The higher value of elongation at breakage and impact strength obtained for the maleated POE may arise as a consequence of this elongated phase morphology of the maleated POE in the PA6/PP matrix. The significant difference in impact strength between POE and maleated POE can be ascribed to the fact that the former nanocomposite fractures in brittle mode, whereas the latter one fractures in ductile mode.

In order to have efficient stress transfer between two phases, the rubber particles should be well dispersed so that they can act efficiently as impact modifier, and they should also be well bonded to the polymer matrix [27]. The anhydride group of the POEgMAH is able to react with the PA6 terminal group to form POEgPA6 copolymer that strongly tends to concentrate at PA6/PP interfaces during melt processing [22]. According to Liang and Li [28], when rubber was grafted with a suitable content of maleic anhydride (MAH), the rubber particles were dispersed uniformly in the continuous PA6 matrix and PP was encapsulated by thin layers of rubber (i.e. in a shell-core structure). When highly dispersed, the rubbery phase acts as an effective stress concentrator and enhances both crazing and shear yielding in the matrix. Since both processes can dissipate a large amount of energy, there is a significant increase in the toughness of nanocomposites toughened with POEgMAH [24].

Figure 13 shows a proposed schematic illustration of the organoclay distribution in the PA6/PP blends with POE and maleated POE. However, at this point, there is no experimental evidence to substantiate this scheme. In the unmaleated POE system, as PA6 has a higher polarity than POE and PP, organoclay was well exfoliated in the PA6 matrix verified by the XRD results in our previous work [7, 14, 15]. No migration of the organoclay is expected into the dispersed POE during melt mixing. According to Chow *et al.* [3] and Li *et al.* [27], this is due to the strong interfacial interaction such as hydrogen bonding among hydroxyl groups of the
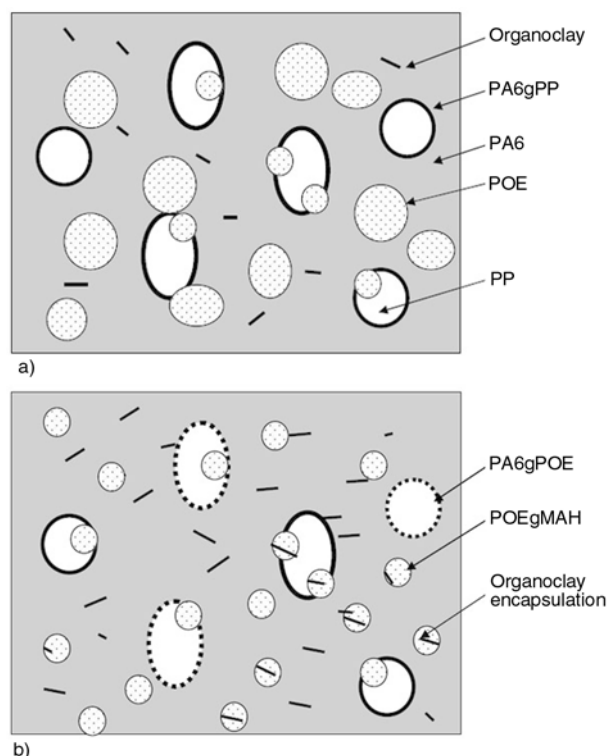


**Figure 13.** Schematic of the morphology of PA6/PP/PPgMAH/organoclay a) with POE, b) with POEgMAH

organoclay and PA6 phase, which hinders the silicate crystallites in the PA6 matrix from migrating to the dispersed POE phase. Furthermore, there was no specific interaction between organoclay and POE because POE is non-polar. As a result, the microstructure with the separation between organoclay and POE is expected as it can be seen in Figure 13a.

However, for the maleated POE system, the presence of polar functional group (maleic anhydride) has improved the miscibility and adhesion between POE and organoclay [26, 29]. When the adhesion between POE and organoclay is enhanced, the organoclay becomes encapsulated by the maleated POE, promoting the formation of core-shell inclusions as illustrated in Figure 13b. These two different morphologies resulted in significantly distinct toughness properties. The POE nanocomposite systems with encapsulated structure have higher toughness than those having a separated structure.

## 4. Conclusions

Based on this work performed on the fracture behaviour of the rubber toughened PA6/PP nano-

composites, the following conclusions can be drawn:

– The incorporation of organoclay has led to the expense Izod impact strength and the toughness ($K_c$ and $G_c$) of the pure PA6/PP blends.

– Toughness increased with the increasing of elastomer concentration in both unmaleated and maleated POE. However, the increment in toughness is very significant for the maleated POE system particularly at higher POEgMAH loading. For example, the blend containing 20 wt% POEgMAH exhibited six times improvement of Izod impact strength compared to the pure PA6/PP/organoclay.

– Significant changes in blend morphology and toughness were obtained when POEgMAH was applied. The POEgMAH average particles size were 0.96 µm; smaller compared to that of POE (1.50 µm) in PA6/PP/organoclay blends of the same composition, i.e. 10 wt% elastomer. A reduction in dispersed particle size and an increase in adhesion between the phases, brought about by the reaction between the amino group of PA6 and the anhydride group of POEgMAH during melt compounding succeed in forming PA6gPOE copolymer which was believed to be responsible for the toughness improvement of these blends.

## References

[1] Alexandre M., Dubois P.: Polymer-layered silicate nanocomposites: Preparation, properties and uses of new class of materials. Materials Science and Engineering, **28**, 1–63 (2000).
DOI: 10.1016/S0927-796X(00)00012-7

[2] Lauke B.: On the effect of particle size on fracture toughness of polymer composites. Composites Science and Technology, **68**, 3365–3372 (2008).
DOI: 10.1016/j.compscitech.2008.09.011

[3] Chow W. S., Mohd Ishak Z. A., Karger-Kocsis J., Apostolov A. A., Ishiaku U. S.: Compatibilizing effect of maleated polypropylene on the mechanical properties and morphology of injection molded polyamide 6/polypropylene/organoclay nanocomposites. Polymer, **44**, 7427–7440 (2003).
DOI: 10.1016/j.polymer.2003.09.006

[4] Chow W. S., Mohd Ishak Z. A.: Mechanical, morphological and rheological properties of polyamide 6/organo-montmorillonite nanocomposites. Express Polymer Letters, **1**, 77–84 (2007).
DOI: 10.3144/expresspolymlett.2007.14

[5] Harmia T., Friedrich K.: Fracture toughness and failure mechanisms in unreinforced and long-glass-fibre-reinforced PA66/PP blends. Composites Science and Technology, **53**, 423–420 (1995).
DOI: 10.1016/0266-3538(95)00031-3

[6] Kusmono, Mohd Ishak Z. A., Chow W. S., Takeichi T., Rochmadi: Enhancement of properties of PA6/PP nanocomposites via organic modification and compatibilization. Express Polymer Letters, **2**, 655–664 (2008).
DOI: 10.3144/expresspolymlett.2008.78

[7] Wahit M. U., Hassan A. Mohd Ishak Z. A., Rahmat A. R., Abu Bakar A.: Morphology, thermal, and Mechanical behavior of ethylene octene copolymer toughened polyamide 6/polypropylene nanocomposites. Journal of Thermoplastics Composites Materials, **19**, 545–567 (2006).
DOI: 10.1177/0892705706063927

[8] Chen B., Evans J. R. G.: Impact and tensile energies of fracture in polymer-clay nanocomposites. Polymer, **49**, 5113–5118 (2008).
DOI: 10.1016/j.polymer.2008.09.024

[9] González I., Eguiazábal J. I., Nazábal J.: Nanocomposites based on a polyamide 6/maleated styrene-butylene-co-ethylene-styrene blend: Effects of clay loading on morphology and mechanical properties. European Polymer Journal, **42**, 2905–2913 (2006).
DOI: 10.1016/j.eurpolymj.2006.07.014

[10] González I., Eguiazábal J. I., Nazábal J.: Rubber-toughened polyamide 6/clay nanocomposites. Composites Science and Technology, **66**, 1833–1843 (2006).
DOI: 10.1016/j.compscitech.2005.10.008

[11] González I., Eguiazábal J. I., Nazábal J.: Effects of the processing sequence and critical interparticle distance in PA6-clay/mSEBS nanocomposites. European Polymer Journal, **44**, 287–299 (2008).
DOI: 10.1016/j.eurpolymj.2007.11.027

[12] Bai S-L., Wang M.: Plastic damage mechanisms of polypropylene/polyamide 6/polyethylene octane elastomer blends under cyclic tension. Polymer, **44**, 6537–6547 (2003).
DOI: 10.1016/S0032-3861(03)00739-0

[13] Bai S-L., Wang G-T., Hiver J-M., G'Sell C.: Microstructures and mechanical properties of polypropylene/polyamide 5/polvethelene-octane elastomer blends. Polymer, **45**, 3063–3071 (2004).
DOI: 10.1016/j.polymer.2004.02.070

[14] Wahit M. U., Hassan A., Mohd Ishak Z. A., Abu Bakar A.: The effect of polyethylene-octene elastomer on the morphological and mechanical properties of polyamide 6/polypropylene nanocomposites. Polymer and Polymer Composites, **13**, 795–806 (2005).

[15] Wahit M. U., Hassan A., Rahmat A. R., Lim J. W., Mohd Ishak Z. A.: Effect of organoclay and ethylene-octene copolymer inclusion on the morphology and mechanical properties of polyamide/polypropylene blends. Journal of Reinforced Plastics and Composites, **25**, 933–954 (2006).
DOI: 10.1177/0731684406063529

[16] Cotterell B., Chia J. Y. H., Hbaieb K.: Fracture mechanisms and fracture toughness in semicrystalline polymer nanocomposites. Engineering Fracture Mechanics, **74**, 1054–1078 (2007).
DOI: 10.1016/j.engfracmech.2006.12.023

[17] Kwon S-C., Adachi T., Araki W., Yamaji A.: Effect of composing particles of two sizes on mechanical properties of spherical silica-particulate-reinforced epoxy composites. Composites Part B: Engineering, **39**, 740–746 (2008).
DOI: 10.1016/j.compositesb.2007.02.030

[18] ISO 13586: Plastics. Determination of fracture toughness ($G_{IC}$ and $K_{IC}$) – Linear elastic fracture mechanics (LEFM) approach (2000).

[19] Wang H., Zeng C., Elkovitch M., Lee L. J., Koeling K. W.: Processing and properties of polymer nano-composites. Polymer Engineering and Science, **41**, 2036–2044 (2001).
DOI: 10.1002/pen.10899

[20] Stevenson J. C.: Impact modifiers: Providing a boost to impact performance. Journal of Vinyl and Additive Technology, **1**, 41–45 (1995).

[21] Gam K. T., Miyamoto M., Nishimura R., Sue H. J.: Fracture behavior of core-shell rubber-modified clay-epoxy nanocomposites. Polymer Engineering and Science, **43**, 1635–1645 (2003).
DOI: 10.1002/pen.10137

[22] Ohlsson B., Hassander H., Törnell B.: Effect of the mixing procedure on the morphology and properties of compatibilized PP/PA blends. Polymer, **39**, 4715–4721 (1998).
DOI: 10.1016/S0032-3861(97)10291-9

[23] Yu Z-Z., Ke Y-C., Ou Y-C., Hu G-H.: Impact fracture morphology of nylon 6 toughened with a maleated polyethylene-octane elastomer. Journal of Applied Polymer Science, **76**, 1285–1295 (2000).
DOI: 10.1002/(SICI)1097-4628(20000523)76:8<1285:: AID-APP9>3.0.CO;2-U

[24] Yu Z-Z., Lei M., Ou Y-C., Hu G-H.: The role of interfacial modifier in toughening of nylon-6 with a core-shell toughened. Journal of Polymer Science Part B: Polymer Physic, **37**, 2664–2672 (1999).
DOI: 10.1002/(SICI)1099-0488(19990915)37:18< 2664::AID-POLB10>3.0.CO;2-O

[25] Yu Z-Z., Ou Y-C., Hu G-H.: Influence of interfacial adhesion on toughening of polyethylene-octane elastomer/nylon 6 blends. Journal of Applied Polymer Science, **69**, 1711–1718 (1998).
DOI: 10.1002/(SICI)1097-4628(19980829)69:9<1711:: AID-APP4>3.0.CO;2-E

[26] Premphet-Sirisinha K., Chalearmthitipa S.: Study on composition and characteristics of maleated ethylene-octane copolymer prepared by reactive extrusion on the morphology and properties of polyamide 6/ethylene-octane copolymer blends. Polymer Engineering and Science, **43**, 317–328 (2003).
DOI: 10.1002/pen.10027

[27] Li F. Q., Kim D. G., Wu D. Z., Lu K., Jin R. G.: Effect of maleic anhydride graft ratio on mechanical properties and morphology of nylon 11/ethylene-octane copolymer blends. Polymer Engineering and Science, **41**, 2155–2161 (2001).
DOI: 10.1002/pen.10910

[28] Liang J. Z., Li R. K. Y.: Rubber toughening in polypropylene: A review. Journal of Applied Polymer Science, **77**, 409–417 (2000).
DOI: 10.1002/(SICI)1097-4628(20000711)77:2<409:: AID-APP18>3.0.CO;2-N

[29] Long Y., Shanks R. A.: PP-elastomer-filler hybrids. I. Processing, microstructure, and mechanical properties. Journal of Applied Polymer Science, **61**, 1877–1885 (1996).
DOI: 10.1002/(SICI)1097-4628(19960912)61:11< 1877::AID-APP3>3.0.CO;2-G

# Tailoring of poly(vinyl alcohol) cryogels properties by salts addition

*S. Paţachia[1*], C. Florea[1], Chr. Friedrich[2], Y. Thomann[2]*

[1]Department of Chemistry, Transilvania University of Brasov, 29 Eroilor Street, 500036 Braşov, Romania
[2]Rheology Department, Albert Ludwigs University of Freiburg, 21st Stefan-Meier, 79104 Freiburg, Germany

**Abstract.** The present paper aims to study the possibility to modify the properties of poly(vinyl alcohol) (PVA) hydrogels prepared in the presence of different salt types ($Na_2SO_4$, NaCl and $NaNO_3$) in order to extend the nature of the salts already used in obtaining films or gels, to expand their concentration domains and to explain the increase of film strain, concomitantly with the increase of their crystallinity. The morphology of the PVA based hydrogels has been studied by Scanning Electronic Microscopy (SEM), the interaction between the PVA macromolecular chains and salts has been determined by Fourier Transform Infrared Spectroscopy (FTIR), while the mechanical properties of the cryogels have been investigated by oscillatory dynamic mechanical measurements. The gels swelling in water have been monitored by gravimetric method in order to evidence the alteration of the PVA cryogel properties such as crystallinity and porosity determined by the salt addition to the initial PVA aqueous solution. The data reported show that the ions present in the PVA solution influence the interaction between PVA-water and PVA-PVA chains; their influence on the salt-based PVA hydrogels follow the Hofmeister lyotropic series.

**Keywords:** *rheology, tailored-made polymers, poly(vinyl alcohol) cryogel, salts, Hofmeister series*

## 1. Introduction

PVA is a polymer with exceptional properties such as water solubility, biodegradability, biocompatibility, non-toxicity and non-carcinogenity that possesses the capability to form hydrogels by chemical or physical methods [1–6]. Its fields of applicability were widely broadened during the latest years due to the development of medicine and the increase of the needs in new biomaterials, to the introduction of new concepts in medication by creating the controlled drug release systems, to the environmental protection need, aiming at sustainable development by obtaining new ecological systems for water purification (membranes or absorbent materials), conductive systems for renewable energy sources, etc. [7–9]. PVA is a non-expensive and versatile

polymer, adaptable to various needs with minor modifications of the synthetic procedures [1, 10].
During the latest years many research groups focused their attention on the study of PVA films or gels obtained by the simple addition of salts to the aqueous PVA solution. Very interesting properties have been obtained. For example, the addition of NaCl to the PVA water solution and the freezing of the obtained solution at liquid nitrogen temperature led to the increase of the hydrogel crystallinity, and, as a consequence, to the increase of the rigidity modulus $G'$ [11]. The same increase of the $G'$ for PVA hydrogels obtained by freezing-thawing processes at –20°C/20°C has been evidenced by other researchers, corresponding to the relative swelling decrease [12]. PVA films prepared in the

presence of NaCl led to obtaining insoluble films, showing an unusual combination of properties: higher crystallinity and simultaneously, higher draw ratio [13, 14]. Moreover, high performance films have been obtained by casting PVA/$Na_2SO_4$ (up to 0.05 wt%)/$H_2O$ or PVA/$CH_3COONa$ (up to 0.1 wt%)/$H_2O$ solutions, and removing the salts used from the films through a washing process. Both films obtained are water resistant due to their high crystallinity, and they concomitantly have high drawability and mechanical resistance values [15]. Bhargav *et al*. obtained polymer electrolyte films for the solid state battery development by doping PVA gels with NaBr [16]. The PVA electrolyte film prepared in the presence of NaBr evidenced a lower crystallinity value than the value corresponding to the neat films. Obtaining PVA films doped with $BaCl_2$ has been reported by Bhajantri *et al*. [17]. A complex formation between $Ba^{2+}$ ions and OH groups of PVA is considered to be responsible for the PVA film crystallinity increase. The dc and ac conductivities of the $BaCl_2$ doped PVA films have been increased along with the increase of the doping agent concentration.

PVA hydrogels in contact with micro-molecular inorganic salts have also been studied, aiming at elucidating the osmotic properties of the cryogels during a long-lasting exposure to aqueous media, at establishing the gels' behaviour in contact with physiological liquids or at designing electrolyte sensors based on PVA hydrogel materials, which exhibit an intelligent behaviour in the presence of electrolyte solutions [18–24]. It has been reported that PVA hydrogels collapse when they come into contact with NaCl, KCl, CsCl, $Na_3PO_4$ and $Na_2SO_4$ solutions; the gel's shrinking depends on the salt nature and concentration. The osmotic stability of the PVA hydrogels and the fact that they maintain their porous morphology during ageing have been evidenced. All these properties make the PVA cryogels a suitable material for cell immobilization and sensors design.

In this framework, our paper comes to extend the nature of the studied salts used for the PVA cryogel preparation ($Na_2SO_4 \cdot 10H_2O$, NaCl and $NaNO_3$) and to expand the concentration domains of the salts (25 wt% with respect to PVA). The salt-based PVA hydrogels obtained have been characterized by visual methods, SEM, FTIR, rheological and gravimetric measurements. The solid content,

equilibrium water content (*EWC*) of the gels, the collapse kinetic when in contact with 0.5M $Na_2SO_4 \cdot 10H_2O$ solution, shrinking equilibrium, and the mechanism of water diffusion from the gels during their collapse have all been investigated. The analyses performed aimed at correlating the morphological alteration of the salt-based gels prepared with the nature of the salt used depending on its kosmotropic or chaotropic character.

This procedure enables us to obtain PVA cryogels with tailored properties by using very simple methods.

## 2. Experimental

### 2.1. Materials

The PVA used for this work was purchased in powder form, with industrial grades, from the Chemical Plant Râşnov (Romania) and it was used without any further purification. The polymer has a polymerization degree of 900, a saponification degree of 98% and a molecular weight of 48 600 g/mol. $Na_2SO_4 \cdot 10H_2O$ and $NaNO_3$ were purchased from Reactivul Bucureşti (Romania), while NaCl was procured from Fluka (Germany). All the salts used during the current study had analytical reagent grades.

### 2.2. Preparation of aqueous solutions

a) A 12 wt% PVA aqueous solution was prepared in distilled water at 80°C under continuous magnetic stirring for 3 hours in a dust-free environment. The PVA solution obtained was chilled until it reached the room temperature, and it was filtered and divided in four equal parts. One part of the PVA solution was stored as obtained, and it was used for the neat PVA hydrogel preparation. The other three parts of the PVA solution prepared were split into equal volumes and further used for the preparation of the salt-based PVA solutions.

b) 0.5M sodium sulphate solution was prepared with distilled water, at ambient temperature, using $Na_2SO_4$ solid state with analytical grade purchased from Reactivul Bucureşti.

### 2.3. Preparation of salt-based PVA solution

In order to prepare salt-based PVA solutions, the same volumes of the previously synthesized PVA

solution were mixed with 25 wt% (based on the PVA weight) of NaCl, $Na_2SO_4 \cdot 10H_2O$ and respectively $NaNO_3$ under continuously magnetically stirring at 80°C for 1 hour. After the complete dissolution of the salt into the PVA solution, three different salt-based PVA solutions have been obtained; the solutions were cooled until reaching the room temperature and filtered before further usage.

## 2.4. Synthesis of salt-based PVA hydrogels

20 ml from each PVA/$H_2O$ obtained and respectively PVA/salt/$H_2O$ solutions were cast in 10 cm diameter Petri dishes. The cast solutions were submitted to a 12 hours freezing at –20°C and a 12 hours thawing at room temperature (22°C). The submission of the samples to the freezing-thawing cycle has been performed thrice, until the solutions were converted to white and opaque hydrogels that exhibit good mechanical resistance.

At the end of the last thawing cycle, the obtained PVA hydrogels containing salts were soaked in distilled water in order to remove the salts used during the preparation process and the polymer that was not crosslinked during the freezing and thawing process; the procedure of distilled water exchanging for the PVA/$H_2O$ and PVA/salt/$H_2O$ hydrogels has been repeated every 24 hours for 7 days.

All the PVA hydrogels obtained were immersed in excess of distilled water in order to reach the swelling equilibrium for another 7 days.

## 2.5. Methods
### 2.5.1. Gravimetry

The monitoring of PVA/$H_2O$ and PVA/salt/$H_2O$ sample mass variation as a result of losing water during the immersion in electrolyte solution has been done gravimetrically, by using a Kern ABS/ABJ balance which has a precision of $10^{-4}$ g.

Samples weighing approximately 0.50–0.75 g were immersed in 100 ml solution of $Na_2SO_4$, taken out of the solution at a previously predetermined time, gently blotted on filter paper for salt excess removal and weighed.

The percentage of water retained by the analyzed hydrogels at time t after their immersion into the $Na_2SO_4 \cdot 10H_2O$ 0.5M electrolyte solution has been calculated on the basis of the Equation (1):

$$\Delta m_{ret} \, [\%] = \frac{m_t - m_x}{m_x} \cdot 100 \qquad (1)$$

where $m_t$ represents the mass of the hydrogel at time $t$ after its immersion into the electrolyte solution, and $m_x$ is the mass of the dry gel [18].

### 2.5.2. Scanning Electron Microscopy

The characterization of PVA/$H_2O$ and PVA/salt/$H_2O$ hydrogels was performed by using an Environmental Scanning Electron Microscope. Metal sample coating was done with a Polaron SC 7640 ion sputter coating instrument, at a 1.5 kV voltage.

### 2.5.3. Fourier Transform Infrared (FT-IR) spectroscopy

The neat PVA sample and the PVA hydrogels that reached the shrinking equilibrium in the presence of different aqueous salt solutions were subjected to FTIR spectroscopy in the range of 4000 and 600 cm$^{-1}$, using a Perkin-Elmer spectrophotometer. Prior to the measurement execution, the PVA/$H_2O$ and PVA/salt/$H_2O$ hydrogels have been vacuum dried overnight until no weight change has been evidenced.

### 2.5.4. Rheometry

The rheological experiments were performed using a Paar Physica UDS200 rheometer. The geometry used was a 25 mm diameter steel plate. All rheometry measurements were carried out using a disc shape sample with a diameter of 25 mm and an average thickness of 1.5 mm. The storage and loss modulus characteristic to the different studied hydrogels as well as their viscosity were determined at a constant temperature of 25°C.

## 3. Results and discussion

The visual observation of the PVA cryogels obtained in the presence of different salts led to the conclusion that the gels' transparency could be tailored by modifying the nature of the salt added to the PVA solution (Figure 1). The transparency of the gel is a very important property for the PVA based cryogels used for ocular medical devices or sensor design. Transparent PVA cryogels have
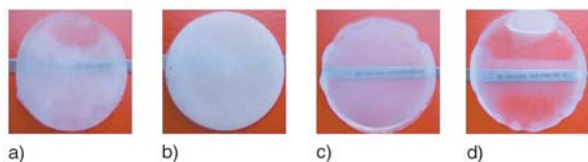
**Figure 1.** Visual aspect of the PVA cryogels obtained in the presence of different salts, after their washing. a) PVA/H$_2$O, b) PVA/Na$_2$SO$_4$/H$_2$O, c) PVA/NaCl/H$_2$O, d) PVA/NaNO$_3$/H$_2$O

already been obtained using dimethyl sulfoxide (DMSO) as solvent [25], but DMSO is a toxic volatile solvent. The modification of the gel thickness represents another procedure used to obtain transparent PVA gels, but this method has limited applicability by the decrease in membrane mechanical resistance.

Using different salts in obtaining cryogel and removing them by washing with distilled water is a very easy method for tailoring PVA cryogel membrane transparency that does not involve toxic substances and keeps the needed membrane dimensions, and, as a consequence, their mechanical resistance.

As depicted in Figure 1, PVA/Na$_2$SO$_4$/H$_2$O cryogels are opaque, exhibiting a more heterogeneous structure when comparing with the PVA/H$_2$O cryogel. PVA/NaCl/H$_2$O cryogels are more translucent, while the PVA/NaNO$_3$/H$_2$O cryogels have a higher transparency than the neat PVA gel, evidencing a homogeneous structure.

As it is already known, PVA cryogels are obtained by polymer crystallization, crystallites playing the role of the crosslinking agent [26]. Differences in cryogel transparency could be correlated to obtaining different gel morphology, due to the influence of the salts on the solution characteristics, and due to the specific interactions between the ions coming from the salts dissociation, water molecules and PVA chains.

SEM images evidenced higher morphological differences between the cryogels obtained in the presence of different salts, as it is illustrated in Figure 2. The addition of Na$_2$SO$_4$ to the initial PVA solution determined the formation of a cryogel with a more compact structure with less interconnected pores, by comparison with the structure of the neat PVA cryogel. On the other hand, the addition of NaCl and NaNO$_3$ respectively, determined the increase in gel porosity. In the presence of NaCl, a gel with
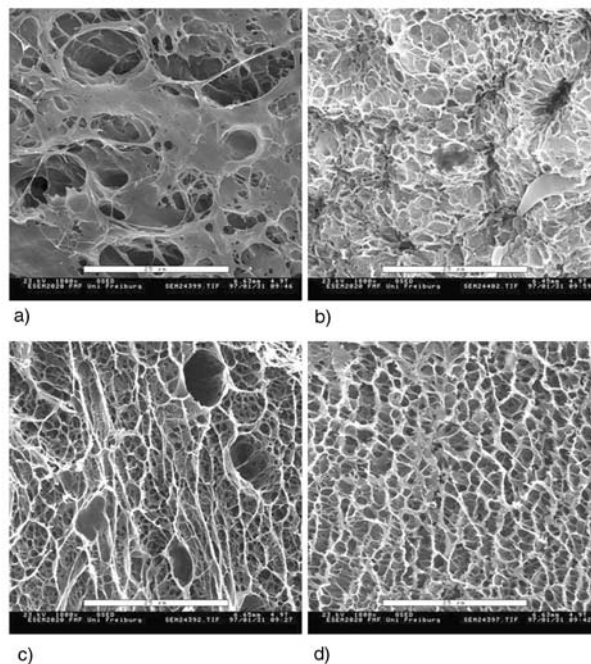


**Figure 2.** SEM images of PVA hydrogels obtained, for a magnification of 1800×. a) PVA/H$_2$O, b) PVA/Na$_2$SO$_4$/H$_2$O, c) PVA/NaCl/H$_2$O, d) PVA/NaNO$_3$/H$_2$O

a very large distribution of the pore dimensions and shapes has been obtained. Some elongated structures could be observed in the SEM image recorded for this hydrogel. NaNO$_3$ presence during the PVA cryogel formation determined the obtaining of a gel with small pores that have a uniform size and shape distribution.

The FTIR spectroscopy has been used for the characterization of the interaction between the PVA macromolecular chains and salts. The spectra of all the prepared PVA hydrogels are shown in Figure 3, where the major absorption bands related to the hydroxyl and acetate groups are evidenced. The
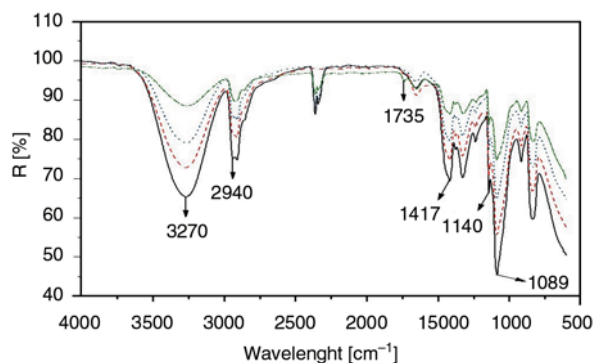


**Figure 3.** FTIR spectra characteristic to the PVA and PVA/salts cryogels: (—) PVA, (– – –) PVA+Na$_2$SO$_4$, (• • •) PVA+NaCl and (– • – • –) PVA+NaNO$_3$

absorption band obtained in the range of 3600 and 3200 cm$^{-1}$ is linked to the –OH groups involved in the intramolecular and intermolecular hydrogen bonds. The absorption band shown on the FTIR spectra in the range of 2840 to 3200 cm$^{-1}$ corresponds to the C–H bond from alkyl groups, and the band between 1700 and 1750 cm$^{-1}$ is characteristic to the stretching C=O from the acetate groups remained in the PVA during its obtaining. No new absorption bands or band shifting are present on the FTIR spectra of the cryogels, showing that no chemical interactions between PVA and the used salts occurred.

The FTIR analysis enabled us to obtain information concerning the cryogel crystallinity based on the band intensity ratio of 1141 cm$^{-1}$:1096 cm$^{-1}$ [27].

The ratio of absorption bands intensities (height) of the 1141 and 1096 cm$^{-1}$ band has been determined for the neat PVA hydrogels as well as for the PVA/salt hydrogels prepared. The addition of salt to the PVA solution during the hydrogel sample preparation caused an increase of the PVA/salt/H$_2$O crystallinity. This result is in agreement with other literature reports [13–15, 17, 28] and could be correlated to the cryoscopy, determined by the presence of the salts in the aqueous solution of PVA. The decrease of the solution freezing point determines an increase in the period of macromolecules staying in the liquid phase, and, as a consequence, they could move, reorganize themselves and interact for a longer period, leading to higher crystalline domains. By comparing the hydrogel crystallinity as a function of the salt nature, it could be observed that the PVA/Na$_2$SO$_4$/H$_2$O hydrogels have the highest value of crystallinity (0.544), being followed by the PVA/NaCl/H$_2$O hydrogels (0.530); the lowest crystallinity value obtained belongs to PVA/NaNO$_3$/H$_2$O hydrogels (0.496). This hierarchy could be also correlated with the position of the used salts in the Hofmeister series [29–31]. Higher interaction between the macromolecular chains could occur due to the capacity of the sulphate ions of the kosmotropic type to take out the water from the polymeric gel (salting-out effect). In the particular case of PVA, this means an increase in H bonding generation. The lowest value of the crystallinity determined for the PVA/NaNO$_3$/H$_2$O hydrogels could be explained by the chaotropic character of NO$_3^-$ ions. The NaNO$_3$ based PVA hydrogels lower interaction with water molecules

**Table 1.** Content of solid matter and equilibrium water content determined for PVA/H$_2$O and PVA/salt/H$_2$O hydrogels

| Crt. Nr. | Hydrogel type | CS [%] | EWC |
|----------|---------------|--------|-----|
| 1 | PVA/H$_2$O | 8.16 | 0.9184 |
| 2 | PVA/Na$_2$SO$_4$/H$_2$O | 10.52 | 0.8948 |
| 3 | PVA/NaCl/H$_2$O | 8.26 | 0.9173 |
| 4 | PVA/NaNO$_3$/H$_2$O | 8.10 | 0.9189 |

allow them to interact with OH groups of PVA, determining the decrease of the polymer-polymer chain interaction, and, as a consequence, a lower polymer crystallinity value is obtained.

The interaction between the PVA chains, determined by the addition of Na$_2$SO$_4$ to the initial PVA aqueous solution, is so strong that, after the salt release from the cryogel matrix, the swelling degree of the salt-based cryogel will never reach the swelling degree of the neat PVA cryogel.

This aspect can be evidenced by the gel solid content (CS) and the equilibrium water content (EWC) determined after the reaching of their swelling equilibrium (Table 1). The concentration in solid matter for each of the prepared hydrogels has been determined after the complete removal of the salt from the hydrogels prepared in the presence of salts, using Equation (2):

$$CS\,[\%] = \frac{m_x}{m_{we}} \cdot 100 \qquad (2)$$

where $m_{we}$ represents the equilibrium mass of the swollen hydrogel in water and $m_x$ represents the mass of the dried gel (xerogel) [18].

For all the prepared hydrogels the content of water at their equilibrium state (EWC) has also been determined as the ratio between the mass of the water contained by the hydrogel at the swelling equilibrium and the mass of the xerogel. The EWC values have been calculated in order to compare the water content of the prepared cryogels at their equilibrium state with the EWC value of the human body cells. For all the PVA based hydrogels prepared, the EWC values are higher than the cell EWC value (0.6) [32], evidencing the suitability of these cryogels to be used in the biomaterial field.

The highest CS value and the lowest EWC value obtained for the PVA cryogels prepared in the presence of Na$_2$SO$_4$ are in total agreement with the SEM analysis results. The relative small variation of the CS and EWC determined for the prepared

PVA and PVA salt-based cryogels follows the same rule as the gel transparency, SEM images and crystallinity modification.

The cryogel transparency increase (following the order: Na$_2$SO$_4$, NaCl and NaNO$_3$) corresponds to the decrease in the cryogel crystallinity, their compactness decrease, the decrease of the solid content and the EWC increase.

Taking into account that the mechanical properties of the gels are closely related to the gel's crystallinity (crosslinking), the mechanical behaviour of the PVA/H$_2$O and PVA/salt/H$_2$O hydrogels has been studied by oscillatory dynamic mechanical measurements. Figure 4 presents the frequency dependency of both storage ($G'$) and loss ($G''$) moduli for the neat and salt-based PVA hydrogels prepared by freezing and thawing techniques, at a constant strain of 1%.

The frequency sweep experiments evidenced that both the storage modulus $G'$ and the loss modulus $G''$ are not dependent on the frequency variation between 0.1 and 10 Hz. The comparative analysis of $G'$ and $G''$ values obtained by using the rheological experiments evidences that $G'$ is considerably higher than $G''$, showing the solid-like behaviour of the studied gels in agreement with the existence of a network structure.

Both moduli, $G'$ and $G''$, are highly dependent on the hydrogel type studied. As depicted in Figure 4a), the PVA/Na$_2$SO$_4$/H$_2$O hydrogels have the highest storage modulus, which evidence a higher crosslinking density comparing to all the other hydrogels analyzed, due to the higher interaction of the polymer chains as consequence of salting out phenomenon. The comparative analysis of the storage modulus specific to PVA/NaCl/H$_2$O and PVA/NaNO$_3$/H$_2$O hydrogels evidences minor differences between the crosslinking densities.
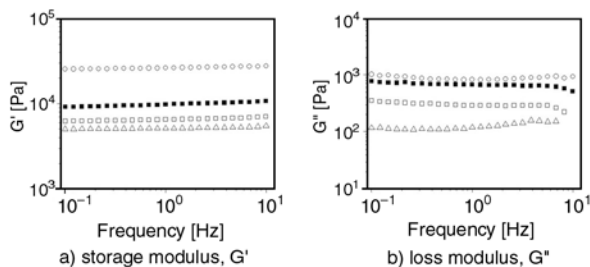


**Figure 4.** Modulus dependency as a function of the frequency, at 1% deformation (■) PVA, (o) PVA+Na$_2$SO$_4$, (Δ) PVA+NaCl and (□) PVA+NaNO$_3$
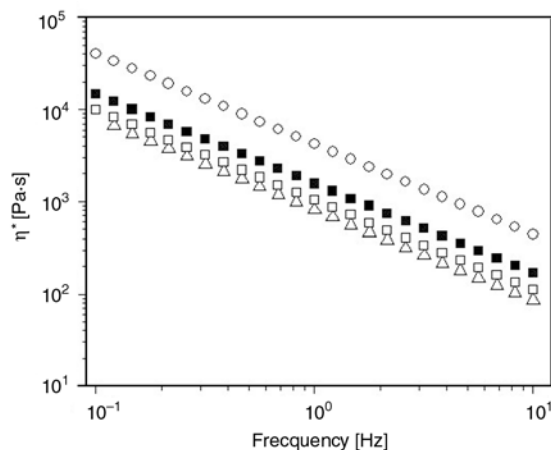


**Figure 5.** Viscosity dependency of different types of PVA hydrogels on the frequency (■) PVA, (o) PVA+Na$_2$SO$_4$, (Δ) PVA+NaCl and (□) PVA+NaNO$_3$

The viscosity dependency of neat and salt-based PVA hydrogels on the frequency sweep is depicted in Figure 5. The graphical representation illustrates that the viscosity is decreasing proportionally to the frequency increase for all the analyzed samples.

These rheological results obtained are in agreement with the Hofmeister series and with our above-mentioned data, obtained by gravimetrical, SEM and FTIR measurements.

Figure 6 shows the strain dependence of the storage modulus at a constant frequency of 1 Hz for different types of synthesized hydrogels. At low strain amplitudes, the storage modulus $G'$ is not dependent on the strain variation; this behaviour indicates that the deformations imposed to the network structure of all the studied types of hydrogels are
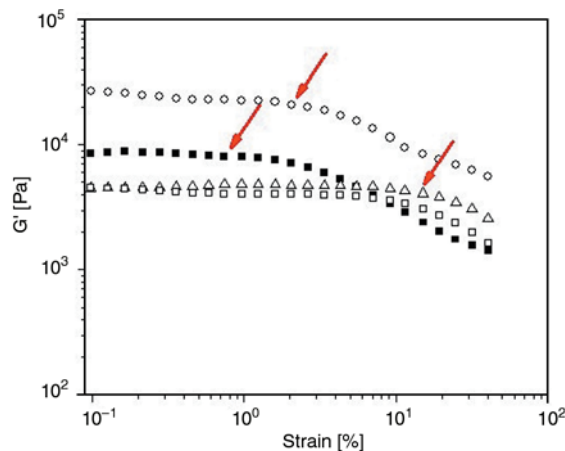


**Figure 6.** Storage modulus $G'$ variation as function of strain amplitude, at 1 Hz constant frequency (■) PVA, (o) PVA+Na$_2$SO$_4$, (Δ) PVA+NaCl and (□) PVA+NaNO$_3$

entirely reversible. Contrary, at high values of strain amplitude, the $G'$ of the studied samples is decreasing with the increase of strain amplitude, indicating that the deformation is no longer reversible.

From the rheological measurement obtained, it can be observed that the domain of reversibility for the gel deformation is higher if more chaotropic salts are used (such as NaCl and $NaNO_3$) and lower if kosmotropic salts are used ($Na_2SO_4$). Furthermore, it is obvious that all the salts determine the increase of the domain of elastic behaviour for the salt-based PVA cryogels in comparison to the domain of elastic behaviour specific to the neat PVA cryogel. Usually, a higher crystallization degree results in a more rigid structure. In this case, the formation of more compact structures in the presence of salts could be due to crystallization, polymer chain interaction in the amorphous phase as well as to chain entanglement repartition between the crystalline domains. A higher kosmotropic effect leads to stronger amorphous phase chain interaction, and, consequently, lower elasticity. The more chaotropic the salts, the lower the interaction in the amorphous phase, leading to more elastic gel behaviour.

To compare the rheological behaviour of the PVA hydrogels prepared in the presence of different salts, the values of the sample storage modulus, $G'_{sample}$, have been normalized by the storage modulus characteristic for the PVA/$H_2O$ hydrogel.

The normalized storage modulus has been calculated using the Equation (3):

$$\Delta G = \frac{G'_{sample}}{G'_{PVA\ hydrogel}} \qquad (3)$$

where $G'_{sample}$ represents the storage modulus of the analyzed neat or salts based PVA hydrogels, and $G'_{PVA\ hydrogel}$ represents the value of the storage modulus characteristic of the PVA/$H_2O$ hydrogelic matrix.

The normalized storage modulus at 1% deformation for the various types of hydrogels studied by rheological measurements at a constant frequency of 1 Hz is illustrated in Figure 7.

As shown in the Figure 7, the PVA/$Na_2SO_4$/$H_2O$ hydrogel has a higher normalized storage modulus than the neat PVA hydrogel; this is due to the increase in the interaction between the polymeric chains, both in the crystalline and amorphous
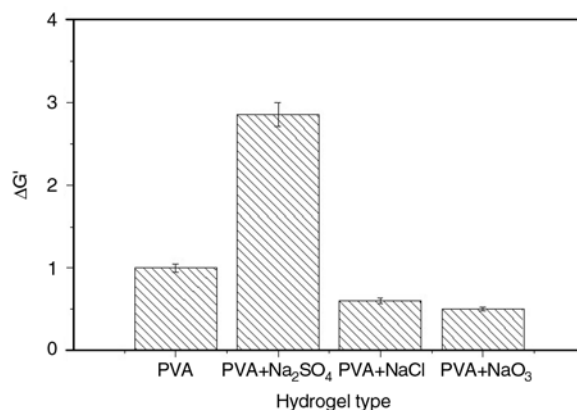


**Figure 7.** Normalized storage modulus $\Delta G'$ variation depending on the PVA hydrogel type ($\nu = 1$ Hz and $\gamma = 1\%$)

phases, determined by the capacity of the kosmotrope sulphate ions to make the water structure. The hierarchy of the normalized $G'$ variation with the salts' nature is in agreement with the lyotropic Hofmeister series and our above mentioned results. But, comparing the $\Delta G'$ values of the salt-based PVA hydrogels and simple PVA hydrogel, we can say that higher values of $\Delta G'$ are expected for all the hydrogels prepared in the presence of salts due to their higher crystallinity. In the case of NaCl and $NaNO_3$ use, the graphical representation shows that $\Delta G'$ values are lower than the value corresponding to the PVA hydrogel. This aspect evidences that the crystallinity degree controls the mechanical characteristics of the gel, the repartition of the crystallites as well as the chain interaction in the amorphous phase. It is possible that a higher interaction between the polymer chains occurs due the fast elimination of the water molecules from the network of the gels, as a result of the stronger kosmotropic character manifested by the added salt; the higher polymer chain interaction leads to a higher number of entanglements of polymeric chains entrapped between the former growing up crystallites. This fact contributes to the increase of the $G'$ maintaining the same value for the elasticity of the gel. In the presence of the more chaotropic ions, only a part of the water molecules are structured around them, the other part interacting with the polymer chains. The lower gel's collapse facilitates the crystallite growth and chain entanglements are avoided. In this manner, the effect of the smaller increase of the gel's crystallinity could be balanced by the water molecules retained into the gel. The first factor, crystallinity, determines the
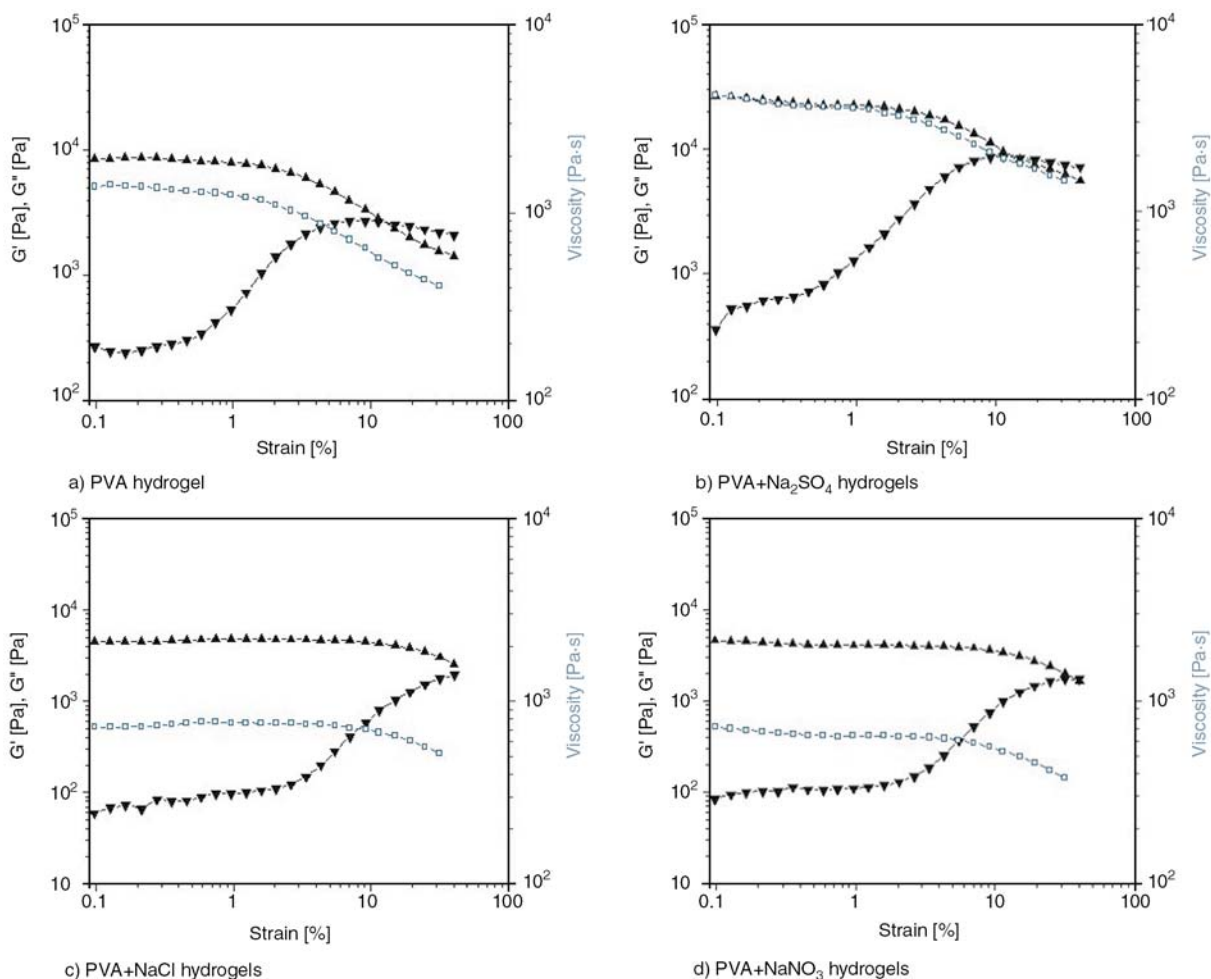
**Figure 8.** Rheological parameters variation as a function of strain (▲) storage modulus $G'$, (▼) loss modulus $G''$ and
(□) viscosity η

increase of $G'$, while the second factor, the water molecules, determines the $G'$ value decrease due to the plastifying character exhibited by the water. The stronger the chaotropic ions, the lower the $G'$ value of the gels.

This aspect has been followed by the determination of the critical modulus $G'_x$ and critical strain $\gamma_x$ values from the junction point of the two curves that characterise the $G'$ and the $G''$ variation as function of the strain amplitude (Figure 8).

Regardless of the nature of the hydrogels studied, at lower strain amplitudes, the loss modulus values are lower than the storage modulus values, in total agreement with the existence of a network structure. The graphical representation in Figure 8 shows that, for small strain values, the storage modulus of the neat and salt-based PVA hydrogels is not dependent on the strain amplitude. This behaviour evidences that the deformation imposed on the network structure is entirely reversible. The

increase of the strain amplitude applied above the critical value induces the liquid like behaviour of the gels that means irreversible deformation, evidenced by the decrease of the storage modulus and the increase of the loss modulus.

In Figure 9 the dependence of $G'_x$ and $\gamma_x$ on the salt nature is plotted.

The graphical representation illustrates that the $G'_x$ values corresponding to the neat PVA cryogel and to the cryogels prepared in the presence of chaotropic salts are very close, while the $G'_x$ value of the gel prepared in the presence of kosmotropic ions is significantly higher. The interesting part is the influence of the chaotropic salts on the elasticity domain of the gels: stronger chaotropic ions extend the elasticity domain even if the gel crystallinity increased. This could be an explanation and a validation for the behaviour of the PVA/NaCl/H$_2$O hydrogels that exhibit a simultaneous increase in crystallinity and drawability.
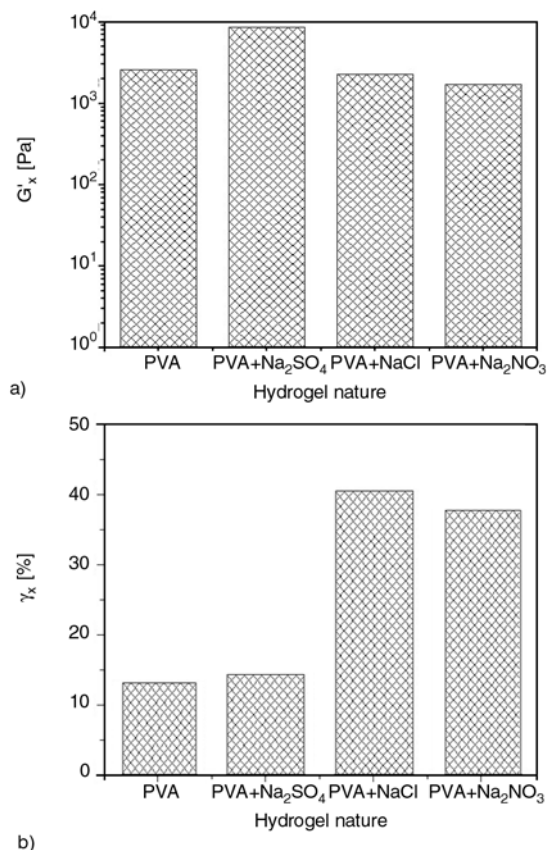
a)



b)

**Figure 9.** The variation of the critical modulus and the critical deformation as a function of the PVA hydrogel nature

This aspect could also be related to the hydrogel morphology: a higher porosity of the gel leads to a higher water content at swelling equilibrium. The rheological properties of the gels are influenced by their water content as well as by their crosslinking degree (crystallinity). NaCl and NaNO$_3$ use for hydrogel preparation leads to an increase in gel porosity, an increase of water content, and, consequently, a decrease in the $\Delta G'$ by comparison with the neat PVA hydrogel.

The alteration of the PVA cryogel crystallinity and porosity determined by the salt addition to the initial PVA aqueous solution influences the mechanical active behaviour of cryogels when in contact with electrolyte solutions.

In order to evidence this influence, the behaviour of PVA/H$_2$O and PVA/salt/H$_2$O hydrogels in the presence of sodium sulphate aqueous solution has been studied using a gravimetric method.

Figure 10 depicts the variation in time of the amount of water retained by the different types of analyzed cryogels as result of their contact with the 0.5M salt solution.
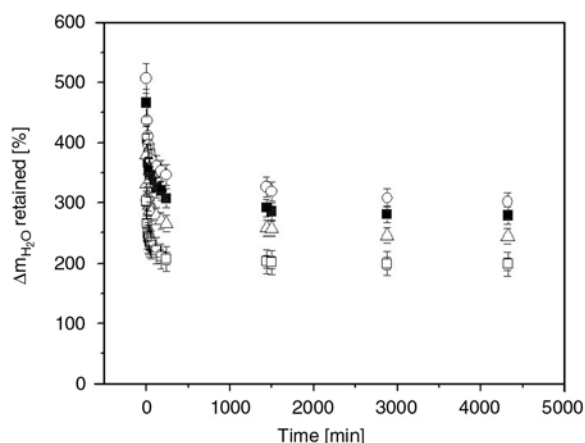


**Figure 10.** The variation of water retained percentage as function of time and he nature of the hydrogel during immersion in 0.5M Na$_2$SO$_4$·10H$_2$O, (■) PVA, (o) PVA/Na$_2$SO4/H$_2$O, (Δ) PVA/NaCl/H$_2$O and (□) PVA/NaNO$_3$//H$_2$O

The contact with the Na$_2$SO$_4$ aqueous solution of the different types of hydrogels prepared determines their collapse. It is obvious that the percentage of the water retained by the neat PVA hydrogel as well as by the PVA hydrogels prepared in the salt presence is significantly decreasing on the first interval of analysis (0 to 500 minutes), due to the elimination of water initially absorbed by the samples studied during the swelling process. After approximately 1500 minutes of contact between the sodium sulphate solution and the hydrogels, the changing of the sample mass is not significant as a result of reaching the shrinking equilibrium; a plateau is reached, as depicted in the graphical representation in Figure 10.

It can be observed that the highest collapse is obtained for the PVA/NaNO$_3$/H$_2$O cryogels, while the lowest is evidenced for the PVA/Na$_2$SO$_4$/H$_2$O cryogels. This behaviour is in agreement with the above-mentioned cryogel characteristics. PVA/NaNO$_3$/H$_2$O cryogels, with a very porous structure, having a higher contact surface with the salt solution, and being less crystalline, exhibit a stronger collapse. PVA/Na$_2$SO$_4$/H$_2$O cryogels exhibit a lower collapse because they are more compact and have a higher crystallinity.

The mechanism of water diffusion from the cryogels during their shrinking process and the rate of the water release from their network structure are also dependent on the cryogels' morphology; the waters diffusion mechanism could be tailored by using different salts for the PVA cryogel preparation.

The mechanism of water diffusion during the shrinking process in $Na_2SO_4$ aqueous solution has been analyzed using the Equation (4):

$$1 - \frac{M_t}{M_{we}} = k \cdot t^n \qquad (4)$$

where $M_t$ represents the weight of the samples at the time $t$ after their immersion into the electrolyte aqueous solution, $M_{we}$ is the mass of the hydrogels at its swelling equilibrium, $k$ represents the constant that characterized the three dimensional, reticulated hydrogel network, and the $n$ parameter is the exponential coefficient that describes the type of the water diffusion mechanism [33–36].

Linear dependencies $(\ln(1 - M_t/M_e) = b + a \cdot \ln t)$ have been obtained in double logarithmic coordinates for all the samples collapsed, as it could be seen in Figure 11.

The fitting parameters corresponding to the water diffusion from the hydrogel matrix are depicted in the table displayed below (Table 2).

The calculation of the kinetic slopes allowed determining the $n$ values, which characterize the mechanism of water diffusion from the studied polymeric network. The values obtained for the $n$ parameter, in the range of 0.20 to 0.25, evidenced a non-Fickian diffusion of water from all the hydrogel types studied (PVA/$H_2O$ and PVA/salt/$H_2O$), during their immersion into an aqueous solution of $Na_2SO_4$. As it is illustrated in Table 2 the slopes of the curves are dependent on the studied hydrogel type.

The low values for the $n$ parameter have been obtained due to the lower concentration of the start-
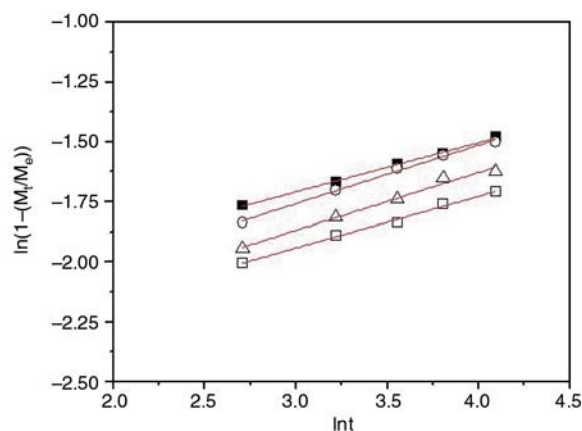
**Table 2.** Fitting parameters of water diffusion from PVA/$H_2O$ and PVA/salt/$H_2O$ hydrogels in the presence of 0.5M $Na_2SO_4 \cdot 10H_2O$

| Crt. Nr. | Hydrogel type | a | b | R² |
|---|---|---|---|---|
| 1 | PVA/$H_2O$ | 0.2050 | –2.3234 | 0.9972 |
| 2 | PVA/$Na_2SO_4$/$H_2O$ | 0.2441 | –2.4896 | 0.9942 |
| 3 | PVA/NaCl/$H_2O$ | 0.2406 | –2.5905 | 0.9841 |
| 4 | PVA/$NaNO_3$/$H_2O$ | 0.2147 | –2.5860 | 0.9926 |

ing PVA solution. As we reported in other papers [37], the crystallinity of the cryogels is highly influenced by the initial PVA solution concentration. All the salts used for the preparation of the salt-based PVA cryogels determined their crystallinity increase, and, therefore, the increase of the $n$ values, describing the water diffusion from more rigid (crystalline) structures. From this point of view, the hierarchy of the salts is the same, determined by checking their influence on the other properties of the cryogels.

In agreement with the former results, the rate of the water release is higher for the gels having higher crystallinity due to the lower interaction of the polymer chains with the water molecules, and it decreases for lower crystalline cryogels, due to the higher interaction of the water molecules with the polymer OH groups that are not involved in the crystallization process.

The order of the water release rates follows the same rule found for the other properties:
PVA/$Na_2SO_4$/$H_2O$ (1.83%/min) > PVA/$H_2O$ (1.82%/min) > PVA/NaCl/$H_2O$ (1.30%/min) > PVA/$NaNO_3$/$H_2O$ (0.98 %/min).

# 4. Conclusions

PVA cryogels are ecological materials, biodegradable, biocompatible, non-toxic and non-carcinogenic, with very large domains of application. Any method that could be helpful in the PVA cryogels properties tailoring is important because it could enlarge its application fields.

The salts addition to the PVA aqueous solution, before submitting it to the repeated freezing-thawing cycles for the cryogels obtaining, is one of the simplest methods that allow the modification of the hydrogel properties.

The data reported in this paper show that the ions present in the PVA solution influence the interac-

**Figure 11.** Dynamic kinetic variation of water diffusion from different types of hydrogels in the presence of 0.5M $Na_2SO_4 \cdot 10H_2O$, (■) PVA, (o) PVA+$Na_2SO_4$, (△) PVA+NaCl and (□) PVA+$NaNO_3$

tion between PVA-water and PVA-PVA chains, leading to the obtaining of cryogels with different crystallinity and porosity. The ion influence follows the Hofmeister lyotropic series: kosmotropic anions determine higher cryogels crystallinity and compactity while chaotropic anions determine higher amorphous and more porous cryogels obtaining. As consequence, the cryogel properties such as: transparency, EWC, capacity to collapse in the presence of electrolytes solutions, the collapse rate, the collapse mechanism, and rheological properties could be modified by adding different salts to the initial PVA solution.

## Acknowledgements

## References

[1] Paţachia S.: Blends based on poly(vinyl alcohol) and the products based on this polymer. in: 'Handbook of polymer blends and composites' (eds.: Vasile C., Kulshreshtha A. K.) Rapra Technology, Shawbury, 288–365 (2003).

[2] Hennink W. E., van Nostrum C. F.: Novel crosslinking methods to design hydrogels. Advanced Drug Delivery Reviews, **54**, 13–36 (2002).
DOI: 10.1016/S0169-409X(01)00240-X

[3] Peppas N. A., Bures P., Leobandung W., Ichikawa H.: Hydrogels in pharmaceutical formulations. European Journal of Pharmaceutics and Biopharmaceutics, **50**, 27–46 (2000).
DOI: 10.1016/S0939-6411(00)00090-4

[4] Ratner B., Hoffman A. S., Schoen F. J., Lemons J. E.: Biomaterials science: An introduction to materials in medicine. Elsevier Academic Press, San Diego (2004).

[5] Hassan C. M., Peppas N. A.: Structure and applications of poly(vinyl alcohol) hydrogels produced by conventional crosslinking or by freezing-thawing methods. Advances in Polymer Science, **153**, 37–65 (2000).
DOI: 10.1007/3-540-46414-X

[6] Hoffman A. S.: Hydrogels for biomedical applications. Annals of the New York Academy of Science, **944**, 62–73 (2001).

[7] Werner B., Bu H. T., Kjonisken A-L., Sande S. A., Nyström B.: Characterization of gelation of aqueous pectin via the ugi multicomponent condensation reaction. Polymer Bulletin, **56**, 579–589 (2006).
DOI: 10.1007/s00289-006-0522-6

[8] de Jong S. J., De Smedt S. C., Demeester J. M., van Nostrum C. F., Kettenes-van den Bosch J. J., Hennink W. E.: Biodegradable hydrogels based on stereocomplex formation between lactic acid oligomers grafted to dextran. Journal of Controlled Release, **72**, 47–56 (2001).
DOI: 10.1016/S0168-3659(01)00261-9

[9] dos Reis E. F., Campos F. S., Lage A. P., Leite R. C., Heneine I. G., Vasconcelos W. L., Lobato Z. I. P., Mansur H. S.: Synthesis and characterization of poly (vinyl alcohol) hydrogels and hybrids for rMPB70 protein adsorption. Materials Research, **9**, 185–191 (2006).
DOI: 10.1590/S1516-14392006000200014

[10] Paţachia S., Valente A. J. M., Papancea A., Lobo V. M. M. V: Poly(vinyl alcohol) [PVA]-based polymer membranes: Synthesis and applications. in 'Organic and Physical chemistry using chemical kinetics' (eds.: Medvedevskikh Y. G., Valente A., Howell R. A., Zaikov G. E.) Nova Publishers, New York, 103–166 (2007).

[11] Nuget M. J. D., Hanley A., Tomkins P. T., Higginbotham C. L.: Investigation of a novel freeze-thaw process for the production of drug delivery hydrogels. Journal of Materials Science: Materials in Medicine, **16**, 1149–1158 (2005).
DOI: 10.1007/s10856-005-4722-7

[12] Lozinsky V. I., Domotenko L. V., Zumbov A. L., Simenel I. A.: Study of cryostructuration of polymer systems. XII. Poly(vinyl alcohol) cryogels: Influence of low-molecular electrolytes. Journal of Applied Polymer Science, **61**, 1991–1998 (1996).
DOI: 10.1002/(SICI)1097-4628(19960912)61:11< 1991::AID-APP13>3.0.CO;2-2

[13] Iwaseya M., Katsuyama N., Yamaura K., Dai L-X.: Effect of degree saponification on the properties of films obtained from PVA/NaCl/$H_2O$ systems. Journal of Materials Science, **41**, 1979–1982 (2006).
DOI: 10.1007/s10853-006-3082-0

[14] Yamaura K., Naitoh M.: Preparation of high performance films from poly(vinyl alcohol)/NaCl/$H_2O$ systems. Journal of Materials Science, **37**, 705–708 (2002).

[15] Iwaseya M., Watanabe M., Yamaura K., Dai L-X., Noguchi H.: High performance films obtained from PVA/$Na_2SO_4$/$H_2O$ and PVA/$CH_3COOONa$/$H_2O$ systems. Journal of Materials Science, **40**, 5695–5698 (2005).
DOI: 10.1007/s10853-005-1429-6

[16] Bhargav P. B., Mohan V. M., Sharma A. K., Rao V.: Structural and electrical studies of sodium iodide doped poly(vinyl alcohol) polymer electrolyte films for their application in electrochemical cells. Ionics, **13**, 173–178 (2007).
DOI: 10.1007/s11581-007-0102-2

[17] Bhajantri S. F., Ravindachary V., Harisha A., Ranganathaiah C., Kumaraswamy G. N.: Effect of barium chloride doping on PVA microstructure: Positron annihilation study. Applied Physics A: Materials Science and Processing, **87**, 797–805 (2007).
DOI: 10.1007/s00339-007-3923-y

[18] Paţachia S., Valente A. J. M., Baciu C.: Effect of non-associated electrolyte solutions on the behaviour of poly(vinyl alcohol)-based hydrogels. European Polymer Journal, **43**, 460–467 (2007).
DOI: 10.1016/j.eurpolymj.2006.11.009

[19] Lozinsky V. I., Zubov A. L., Titova E. F.: Swelling behavior of poly(vinyl alcohol) cryogels employed as matrices for cell immobilization. Enzyme and Microbial Technology, **18**, 561–569 (1996).
DOI: 10.1016/0141-0229(95)00148-4

[20] Lozinsky V. I., Plieva F. M.: Poly(vinyl alcohol) cryogels employed as matrices for cell immobilization. 3. Overview of recent research and developments. Enzyme and Microbial Technology, **23**, 227–242 (1998).
DOI: 10.1016/S0141-0229(98)00036-2

[21] Paţachia S., Baciu Florea C.: Poly(vinyl alcohol) hydrogels interaction with electrolytes in aqueous solution. Revue Roumaine de Chimie, **52**, 1145–1149 (2007).

[22] Paţachia S., Florea C.: Poly(vinyl alcohol) cryogels: Investigations on their behaviour in aqueous electrolytes solutions. in 'Recent advances in research on biodegradable polymers and sustainable composites' (eds.: Jimenez A., Zaikov G.E.) Vol 3, 70–78, Nova Publisher, New York (2008).

[23] Kim J. J., Park K.: Smart hydrogels for bioseparation. Bioseparation, **7**, 177–187 (1999).

[24] De S. K., Aluru N. L., Johnson B., Crone W. C., Beebe D. J., Moore J.: Equilibrium swelling and kinetics of pH-responsive hydrogels: Models, experiments, and simulations. Journal of Microelectromechanical Systems, **11**, 544–555 (2002).
DOI: 10.1109/JMEMS.2002.803281

[25] Cha W-I., Hyon S. H., Ikada Y.: Transparent poly(vinyl alcohol) hydrogel with high water content and high strength. Die Makromolekulare Chemie, **193**, 1913–1925 (2003).
DOI: 10.1002/macp.1992.021930812

[26] Hassan C. M., Peppas N. A.: Cellular PVA hydrogels produced by freezing/thawing. Journal of Applied Polymer Science, **76**, 2075–2079 (2000).
DOI: 10.1002/(SICI)1097-4628(20000628)76:14<2075::AID-APP11>3.0.CO;2-V

[27] Mansur H. S., Sadahira C. M., Souza A. N., Mansur A. A. P.: FTIR spectroscopy characterization of poly(vinyl alcohol) hydrogel with different hydrolysis degree and chemically crosslinked with glutaraldehyde. Material Science and Engineering C: Biomimetic and Supramolecular Systems, **28**, 539–548 (2008).
DOI: 10.1016/j.msec.2007.10.088

[28] Shaheen S. M., Ukai K., Dai L., Yamaura K.: Properties of hydrogels of atactic poly(vinyl alcohol)/NaCl/H₂O system and their application to drug delivery. Polymer International, **51**, 1390–1397 (2002).
DOI: 10.1002/pi.1061

[29] Zhang Y., Cremer P. S.: Interactions between macromolecules and ions: The Hofmeister series. Current Opinion in Chemical Biology, **10**, 658–663 (2006).
DOI: 10.1016/j.cbpa.2006.09.020

[30] Gurau M. C., Lim S-M., Castellana E. T., Albertorio F., Kataoka S., Cremer P. S.: On the mechanism of the Hofmeister effect. Journal of the American Chemical Society, **126**, 10522–10523 (2004).
DOI: 10.1021/ja047715c

[31] Omta A. W., Kropman M. F., Woutersen S., Bakker H. J.: Influence of ions on the hydrogel-bond structure in liquid water. Journal of Chemical Physics, **119**, 12457–12461 (2003).
DOI: 10.1063/1.1623746

[32] Saraydin D., Çaldiran Y.: In vitro dynamic swelling behaviors of polyhydroxamic acid hydrogels in the simulated physiological body fluids. Polymer Bulletin, **46**, 91–98 (2001).
DOI: 10.1007/s002890170093

[33] Ahmad B., Bashir S., Nisa S., Huglin M. B.: Chemically crosslinked N-vynil-2-pyrrolidone/2-hydroxyethyl methacrylate (VP/HEMA) copolymer for controlled release of cyclic oligopeptide. Turkish Journal of Chemistry, **23**, 279–285 (2004).

[34] Peppas N. A., Khare A. R.: Preparation, structure and diffusional behavior of hydrogels in controlled release. Advance Drug Delivery Reviews, **11**, 1–35 (1993).
DOI: 10.1016/0169-409X(93)90025-Y

[35] Kim B., La Flamme K., Peppas N. A.: Dynamic swelling behavior of pH-sensitive anionic hydrogels used for protein delivery. Journal of Applied Polymer Science, **89**, 1606–1613 (2003).
DOI: 10.1002/app.12337

[36] Ji S., Ding J.: The wetting process of a dry polymeric hydrogel. Polymer Journal, **34**, 267–270 (2002).
DOI: 10.1295/polymj.34.267

[37] Paţachia S., Rînja M., Friedrich Chr.: Correlation between poly(vinyl alcohol) cryogel swelling capacity and synthesis parameters. in 'Recent advances in research on biodegradable polymers and sustainable composites' (eds.: Jimenez A., Zaikov G. E.) Vol 3, 130–138, Nova Publisher, New York (2008).